UNIVERSITÀ
DEGLI STUDI
DI PADOVA

DIPARTIMENTO DI SCIENZE CHIMICHE

SCUOLA DI DOTTORATO IN SCIENZE MOLECOLARI

Indirizzo Scienze Chimiche

XXIV Ciclo

Polymer Supported Heterogenous Catalysts for Direct Synthesis of Hydrogen Peroxide in Absence of Selectivity Enhances

Direttore della Scuola: Ch.mo Prof. Antonino Polimeno

Supervisore: Prof. Marco Zecca

Dottorando: Stefano Sterchele

“So some things in life are bad,
they can really make you mad,
and other things just make you swear and curse.
When you're chewing on life's gristle,
don't grumble, give a whistle.
And this will help things turn out for the best.
And...
Always look on the bright side of life,
always look on the bright side of life.

If life seems jolly rotten,
there's something you have forgotten,
and that's to laugh and smile and dance and sing.
When you're feeling in the dumps,
do not be silly chumps.
Just purse your lips and whistle, that's the thing.
And... Always look on the bright side of life.
And... Always look on the bright side of life...”

by Monty Python's Life of Brian

“La Natura non regala niente”

by C.B.

Acknowledgements

First, I would like to thank my supervisor, Prof. Marco Zecca, for his continuous support on my Ph.D. work and for taking care of my scientific growth, aiming on both the increase of my researcher skills and on my preparation in chemistry.

A fundamental contribution, regarding the part of the work dedicated to catalytic tests, came from the strict collaboration with Dott. Pierdomenico Biasi and Akademi Professor Tapio Salmi, from the Åbo Akademi in Turku, Finland, to who I'm especially grateful.

I'm very grateful to Dott. Paolo Centomo, for his significant contribution to the Ph.D. Project.

Abstract

The research program developed during the Ph.D. School is focused on the study of metal catalysts supported on cross-linked functional polymers (CFPs) for the direct synthesis of hydrogen peroxide.

In the last twenty years this compound has become a commodity with a constant increasing demand because of its strong oxidant properties and the formation of water as the reduction byproduct. In particular, H_2O_2 is widely employed as environmentally-friendly bleaching and cleaning agent.

The best alternative to the current process, in particular for the small-scale production, is certainly the synthesis of H_2O_2 from the elements (direct synthesis). This is generally carried out with a heterogeneous catalyst under triphase condition. For safety reasons, the hydrogen-oxygen mixtures, according to the wide explosion range, are properly diluted with an inert gas, usually nitrogen or carbon dioxide.

The catalyst is generally composed by one or more nanostructured noble metals, supported on an inorganic solid, carbon or organic materials. It is well known in literature that the presence in solution of additives, like halides (bromide and chloride) and mineral acids, dramatically improves the catalytic performances, in particular the selectivity towards H_2O_2. However, the use of these additives presents some process drawbacks, such as corrosion, leaching of catalyst, etc, which do not allow the straightforward use of the H_2O_2 solutions obtained from the direct synthesis. It is therefore mandatory a further step of purification to remove the additives. As a consequence, in order to evaluate the effective performance of the catalysts,the research activity during this PhD thesis aim at the investigation of catalytic systems free of selectivity enhancers. In particular, their presence has been avoided not only in the reaction mixture, but also during the preparation of the catalysts.

In the frame of this PhD Thesis, a few sets of mono- and bimetallic catalysts, supported on the commercially available macroreticular resin, Laxness Lewatit K2621, have been studied in detail. This work has been performed in a research group with a long

standing experience in the investigation of polymer-based metal catalysts for industrially relevant reactions and, for a few months, in the Laboratory of Industrial Chemistry and Reaction Engineering of Akademi Prof. Tapio Salmi (Department of Chemical Engineering, Process Chemistry Centre, Åbo Akademi University, Turku, Finland) for the detailed study of the catalysts performances.

The research program is based on the synthesis, the characterisation and the investigation of the catalytic behaviour of the catalysts, obtained by carefully controlling a few essential parameters during the synthesis, such as the nature of the precursor, the reducing agent and the experimental conditions. These three key-points remarkably affect the features of metal nanoparticles (size distribution, difective structure, etc...) and, hence, the behaviour of the catalysts. In particular, the use of tetraaminepalladium (II) sulfate as the metal precursor and the reductive treatment with hydrogen under mild condition lead to a catalyst with noteworthy catalytic performances, specially a remarkable selectivity (70%).

The investigation has also included four libraries of bimetallic materials, Au/Pd and Pt/Pd catalysts based on K2621, obtained as followed:

- by keeping constant the content of palladium (1 wt.%) and changing the one of the second metal (0.1, 0.25, 0.5, 1 wt.% of Pt or Au);

- by treating the material with two different reduction protocols (formaldehyde under reflux temperature and hydrogen (5 bar) under 60°C).

The catalytic results clearly show that the addition of platinum and gold to palladium improves the catalytic performances, although apparently with different mechanisms. The best catalysts are consistent with the empiric trends so far reported in literature.

Finally a new class of mesoporous cross-linked polymers, featured by high surface area at the dry state, has been studied. This non-commercial polymer, quite promising as catalytic support, has been investigated in details and used for the preparation of palladium nanoparticles. This material, in view of its peculiar morphology, shows unique catalytic properties, exhibiting simultaneously a modest activity and a remarkable (70 – 80) and constant H_2O_2 selectivity: this unique features makes this catalyst a good candidate for a mechanistic study of the direct synthesis of hydrogen peroxide.

Riassunto

Il programma di ricerca sviluppato durante il triennio della Scuola di Dottorato si focalizza sullo studio di catalizzatori metallici supportati su polimeri reticolati funzionali per la sintesi diretta di perossido di idrogeno.

Questa sostanza, diventata negli ultimi anni una *commodity* con un mercato in costante crescita, è massicciamente utilizzata come forte ossidante e, in particolare, come sbiancante , in quanto è compatibile con l'ambiente.

Il processo di sintesi di H_2O_2 che in prospettiva può diventare alternativo all'attuale per produzioni su piccola scala è la sintesi a partire dagli elementi (sintesi diretta). Questa reazione viene normalmente condotta con un catalizzatore eterogeneo in condizioni trifasiche. Inoltre le miscele idrogeno-ossigeno vengono debitamente diluite con un gas inerte, a causa dell'ampio intervallo di esplosività dei due gas.

Il catalizzatore è normalmente costituito da uno o più metalli nobili nanostrutturati, supportati su un solido inorganico, carbone o matrici organiche. È noto in letteratura che l'uso di additivi in soluzione, come alogenuri (bromuri e cloruri) e di acidi minerali, migliora drasticamente le prestazioni catalitiche, in particolare la selettività verso H_2O_2. Queste stesse sostanze sono però indesiderate, in quanto non consentono l'uso diretto della soluzione di H_2O_2 ottenuta, se non previa rimozione degli additivi e in aggiunta creano problemi dal punto di vista impiantistico (corrosione, *leaching*, ecc). L'intero studio è stato concepito con lo scopo di indagare i sistemi catalitici, in modo da evitare qualsiasi interferenza dovuta a questi additivi, evitandone quindi la presenza, non solo durante le prove catalitiche, ma anche in fase di sintesi, attraverso l'accurata scelta dei precursori metallici.

In questo triennio, sono stati studiati alcuni materiali mono- e bimetallici supportati su una resina macroreticolare commerciale, Laxness Lewatit K2621. Il lavoro è stato svolto nell'ambito di un gruppo di ricerca già attivo da anni nello studio di catalizzatori metallici supportati su polimeri per reazioni di interesse industriale e per alcuni mesi presso i laboratori di ricerca del Prof. Tapio Salmi (Department of Chemical Engineering, Process Chemistry Centre, Laboratory of Industrial Chemistry and Reaction Engineering

Åbo Akademi University, Turku, Finland) per la realizzazione delle prove catalitiche. L'indagine si è incentrata sulla sintesi, sulla caratterizzazione e sullo studio delle prestazioni catalitiche di materiali preparati variando alcuni importanti parametri di sintesi, quali il tipo di precursore, l'agente riducente e le condizioni sperimentali. Questi hanno una grande ripercussione sulle caratteristiche delle nanoparticelle metalliche (distribuzione dimensionale, difettività, ecc), le quali incidono a loro volta pesantemente sulle proprietà catalitiche. In particolar modo, l'uso di un complesso tetraamminico di palladio (II) e la riduzione in condizioni blande con idrogeno impartiscono al materiale notevoli proprietà catalitiche, caratterizzate da una rimarchevole selettività (70%), inedita in letteratura.

Lo studio ha preso in considerazione anche quattro librerie di catalizzatori bimetallici Au/Pd a Pt/Pd supportate sulla stessa resina usata in precedenza, ottenute sia mantenendo fissa la quantità in peso di palladio e variando quella del secondo metallo, che utilizzando due distinti protocolli di riduzione. I risultati catalitici portano a supporre che platino e oro aumentino le prestazioni catalitiche con meccanismi tra loro molto differenti. Inoltre, la composizione dei migliori catalizzatori bimetallici preparati nell'ambito di questo lavoro di Tesi risulta in linea con le indagini fenomenologiche riportate in letteratura.

Durante il periodo di dottorato, è stato preparato e studiato un polimero reticolato non commerciale ad elevata porosità e successivamente utilizzato come supporto per il catalizzatore. Il materiale risultante ha mostrato peculiari proprietà catalitiche esibisce una bassa conversione di idrogeno ma un'elevata selettività in H_2O_2 con valori nell'intervallo tra 70 e 80%. Queste caratteristiche lo pongono come un buon candidato per uno studio meccanicistico più approfondito della reazione.

Contents

CHAPTER 1

1. Introduction

Hydrogen peroxide is a strong and clean oxidizing agent with many applications as bleaching in pulp and paper industry, waste-water treatment, chemical synthesis and electronics. The current world wide production is about 2.2 millions of tons/year and its demand increases with a rate of about 4 % for year [1]. It is considered a very attractive oxidant to be used in green oxidations, considering that H_2O is its only by-product. Also for atom economy principles H_2O_2 is interesting for its very high content of active oxygen (about 47%), lower than only the molecular oxygen [2][3] (Table 1.1) .

Table 1.1: Oxidizing agents and their characteristics

Oxidant	% of active oxygen	Oxidation by-product
H_2O_2	47,1	H_2O
tBuOOH	17,8	tBuOH
HNO_3	25,0	NO_x, N_2O, N_2
N_2O	36,4	N_2
NaClO	21,6	NaCl
$NaClO_2$	35,6	NaCl
NaBrO	13,4	NaBr
$KHSO_3$	10,5	$KHSO_4$
$NaIO_4$	29,9	NaI
PhIO	7,3	PhI

Due to its standard potentials of oxidation are $E^o = 1.763$ V at pH 0 and $E^o = 0.878$ V at pH 14, hydrogen peroxide is both a strong oxidant agent able to oxidize a large typology of organic and inorganic substrates and a reducing agents be able to reduce the strongest and polluting oxidizing agents like $KMnO_4$, $K_2Cr_2O_7$, NaClO, and Cl_2. It can also form a series of crystalline peroxo-hydrate bonding to metals, oxoacid salts and nitrogen

compounds and also a host of peroxidic compounds, largely used in organic synthesis. Some typical reaction of H_2O_2 are listed in Table 1.2.

Table 1.2: The main reactions of hydrogen peroxide

1	Decomposition	$2\ H_2O_2 \rightarrow 2\ H_2O + O_2$
2	Oxidation	$H_2O_2 + M \rightarrow MO + H_2O$ es. $CN^- + H_2O_2 \rightarrow OCN^- + 2H_2O$
3	Addiction	$H_2O_2 + A \rightarrow A\text{-}H_2O_2$ es. $2\ Ph_3PO + H_2O_2 \rightarrow (Ph_3PO)_2 \cdot H_2O_2$
4	Reduction	$H_2O_2 + R \rightarrow RH_2 + O_2$ es. $Cl_2 + H_2O_2 + 2\ OH^- \rightarrow 2\ Cl^- + 2\ H_2O + {}^1O_2{}^* (\rightarrow h\nu)$
5	Substitution	$H_2O_2 + RX \rightarrow ROOH + HX$ es. $PhC(O)OH + H_2O_2 \rightarrow PhC(O)OOH + H_2O$

Hydrogen peroxide was discovered by the French chemist Louis Jacques Thenard [4] in 1818, who treated barium peroxide with sulfuric acid and removed excess water by evaporation under reduced pressure (Equation 1.1).

$$BaO_2(s) + H_2SO_4(aq) \rightarrow BaSO_4(s) + H_2O_2(aq) \qquad (1.1)$$

Since then a large number of different processes was developed for the H_2O_2 production, based on either electrochemistry (for instance the electrolysis of $(NH_4)_2SO_4$ or H_2SO_4 and the cathodic reduction of molecular oxygen),or redox reactions (for instance the oxidation of isopropanol or methylbenzyl alcohol and the autoxidation of organic compounds).

Over 95% of the current industrial production of H_2O_2 is carried out via Riedl-Pfleiderer process, a two steps route which involves the hydrogenation of an alkyl-anthraquinone (AQ) using Ni or Pd catalyst followed by an oxidation with air (Fig. 1.1). The hydrogen peroxide stream is then purified and concentrated [1].

The main advantages of this process is that it avoids direct contact between H_2 and O_2, and the continuous production at moderate temperature (40 – 60 °C). However, there are many disadvantages such as an extensive use of organic solvents, large amounts of by-products (mainly over-reduced anthraquinone), and the necessity of several steps of separation and concentration, requiring a rather large energy input. This makes the process economically viable only in large scale plants (Table 1.3).

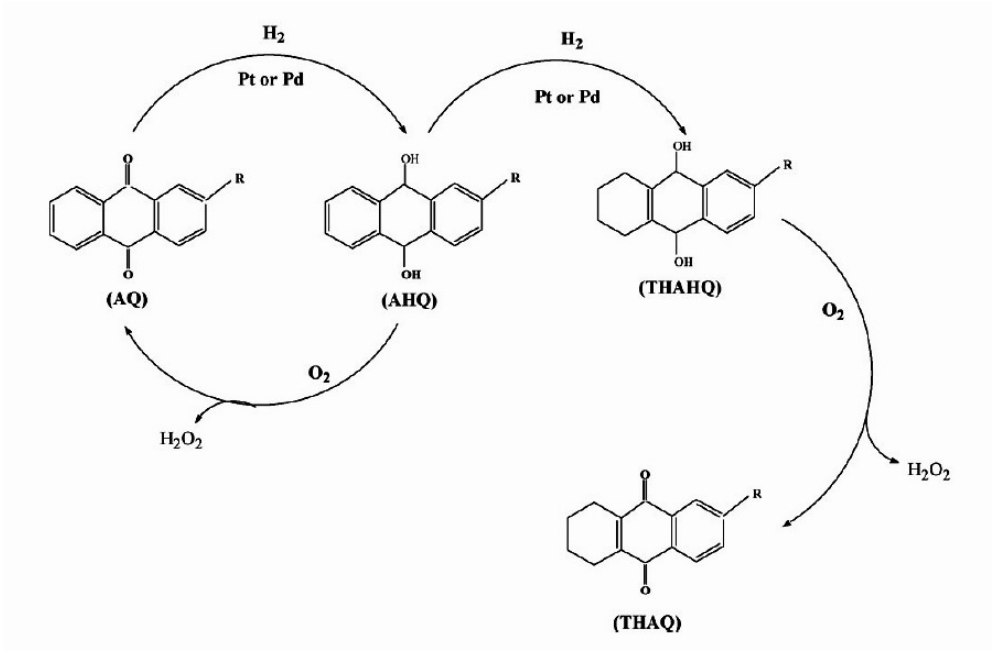

Figure 1.1: Scheme of the Riedl-Pfleiderer process

Known since the beginning of the 20th century, the direct synthesis of hydrogen peroxide (DS) [5] has only become a real promising alternative to the anthraquinone route over the last years [1][6]. It seems a simple reaction, but actually it is rather complex. Together with the formation of H_2O_2, there are several side reactions that seriously affect the selectivity of the process, i.e. the formation of water, the decomposition of hydrogen peroxide, and the reduction of hydrogen peroxide (Fig. 1.2).

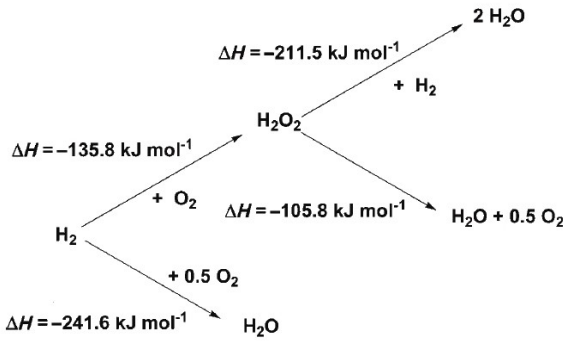

Figure 2: The reaction scheme

Furthermore, the process is highly complicated due to the existence of three phases: gas (H_2 and O_2), liquid (solvent) and solid (catalyst), which usually involves important mass transfer limitations (see Table 1.3).

Table 1.3: Pro's and con's of Riedl-Pfleiderer vs. DS process [1].

Anthraquinone Autoxidation		**Direct Synthesis**	
PROs	**CONs**	**PROs**	**CONs**
Well-established technology	Economically advantageous process only for large scale plants	Small scale plants	Low concentration of H_2O_2
Solution with high concentration of H_2O_2 without pollutants	Constant regeneration of alchylanthraquinone	*in situ* production	Low H_2O_2 selectivity
	High costs of transport and storage due to the risk on the handle solutions with high concentration of H_2O_2	No cost or risk due to the transport and storage of H_2O_2 solutions	Diffusive problems of hydrogen and oxygen in the reaction medium
	Few world wide producers		Careful control of H_2/O_2 ratio

The most important aspects of the direct synthesis of hydrogen peroxide are illustrated in this first part of introduction. The catalysts and their supports reported in the literature have been summarized just as the promoters employed to stabilize the hydrogen peroxide formed or enhance the selectivity of this product. In the second part the focus of the discussion is the use of cross-linked functional polymers as catalyst support in the direct synthesis of hydrogen peroxide.

1.1 Catalyst

All catalysts described in the literature are based on noble metals supported on different substrates. Palladium, gold, silver and platinum are the most commonly employed metals. Of these, Pd, Pd/Pt and Pd/Au are generally the best, usually in a supported form. In some papers it is shown that colloidal Pd is also very active for H_2O_2 synthesis under ambient conditions [7][8]. Landon *et al.* [9] obtained selectivities up to 90% by using a 0.6 wt. % Pd/sulfonated carbon catalyst in a low reaction temperature (1-2 °C). At higher temperatures, selectivity to H_2O_2 decreases dramatically, which was attributed mainly to its decomposition. Li *et al.* [10] also compared the performance of various metals on a Y zeolite at low temperature, and found Pd to have the best productivity

(284 $molH_2O_2 \cdot mol_{Pd}^{-1} \cdot h^{-1}$), followed by Pt (16 $molH_2O_2 \cdot mol_{Pt}^{-1} \cdot h^{-1}$), and Au (14 $molH_2O_2 \cdot mol_{Au}^{-1} \cdot h^{-1}$). Other metals such as Ag, Cu, Rh and Ru showed very low productivities due to much higher activity toward the reaction of decomposition.

Olivera *et al.* [11] predicted that Au could be more active than Pd or Pt for H_2O_2 synthesis, based on a theoretical study of the energetics of the reactions involved. Li *et al.* [12] tested different zeolite supported Au catalysts (2 °C, 37 bar) and achieved 16.5 $molH_2O_2 \cdot mol_{Au}^{-1} \cdot h^{-1}$ with an uncalcined catalyst and 13.7 $molH_2O_2 \cdot mol_{Au}^{-1} \cdot h^{-1}$ with a calcined catalyst (both 4.3 wt.% Au/Y zeolite). However, uncalcined catalysts were proved unstable and with remarkable leaching of Au during use, so they could not be successfully reused.

Hutchings and his coworkers [9][13][14] focused on the combination of Au and Pd to improve the production rate and selectivity to hydrogen peroxide in reactions at low temperature (2 °C) and short residence times (30 minutes). Landon *et al.* [9] reported a production of H_2O_2 using a 5 wt.% Pd-Au(1:1)/alumina catalyst (12.3 $molH_2O_2 \cdot mol_{Pd+Au}^{-1} \cdot h^{-1}$) significantly higher than with either the 5 wt.% Au-only (6.0 $molH_2O_2 \cdot mol_{Au}^{-1} \cdot h^{-1}$) or the 5 wt.% Pd-only (0.79 $molH_2O_2 \cdot mol_{Pd}^{-1} \cdot h^{-1}$) catalysts. They proposed that Pd acts as a promoter for the Au catalyst, and that the catalyst was comprised of Pd-Au alloys rather than of the two metals separately or an another form of aggregation. Edwards *et al.* [13] extended this study and tested a range of Pd, Au and Pd-Au catalysts supported on different materials, and observed the highest yields for Pd-Au catalysts supported on carbon and silica: 304.0 and 298.5 $molH_2O_2 \cdot mol_{Pd+Au}^{-1} \cdot h^{-1}$, respectively. Li *et al.* [14] showed that the enhancement effect of replacing some of the Au with Pd in a zeolite supported catalyst is much more marked than that observed with titania, silica or iron oxide as supports. They found the best catalyst composition to be 2.5 wt.% Au/1.8 wt.% Pd (343.2 $molH_2O_2 \cdot mol_{Pd+Au}^{-1} \cdot h^{-1}$).

In turn, Li *et al.* [14] s studied the addition of different metals on a zeolite supported Au catalyst, and also obtained the best results with the Au-Pd catalyst. The addition of Ru or Rh had no marked effect, but the addition of Pt has a marked enhancement in the yield of hydrogen peroxide, which is consistent with the suitability of Pt for H_2O_2 production reported elsewhere [15][16].

Other bimetallic catalysts such as Pd-Ag or Pd-Pt have also been studied. Liu *et al.* [15] analyzed the effect of adding Pt to a Pd/silica catalyst and found that the addition of only 5 atom% Pt to a catalyst that contained 0.5 wt. % Pd resulted in a 2.5-fold increase in the rate of peroxide formation with only a small decrease in selectivity, whilst the

addition of more Pt did cause a decrease in the selectivity. This fact was also confirmed by Bernardotto *et al.* [17], who showed that the addition of 0.1 wt. % Pt to a zirconia supported Pd catalyst enhanced the yield of H_2O_2 with respect to the monometallic catalyst at room conditions (119.1 vs. 97.4 $molH_2O_2 \cdot mol_{Pd+Pt}^{-1} \cdot h^{-1}$), whilst the best results for a combination of Pd and Au were obtained with much higher amounts of Au (1.2 wt. %, 80.9 $molH_2O_2 \cdot mol_{Pd+Au}^{-1} \cdot h^{-1}$).
Also the organic supports are a valid alternative to the inorganic ones (see below).

1.1.1 Oxidation state

The effect of palladium oxidation state on the catalytic activity has also been widely discussed in the literature, although the results are sometimes contradictory. Hâncu *et al.* [18] explored the use of both Pd^0 and Pd^{II} catalysts in the direct synthesis of hydrogen peroxide in supercritical CO_2 as the solvent. They took advantage of the rapid reaction between cyclohexene and hydrogen peroxide to avoid H_2O_2 decomposition, and so used cyclohexene oxide formation to indirectly measure H_2O_2, and found that Pd^0 catalysts are significantly superior in activity in the generation of H_2O_2 after 3 hours of reaction at room temperature and high pressure (170 bar). This was later confirmed by Burch *et al.*, who reported [19] that reduced catalysts showed improved hydrogen conversion and hydrogen peroxide selectivity when compared to their unreduced counterparts. Liu *et al.* [20] also concluded that Pd^0 is the active phase in the direct formation of H_2O_2 when they observed that the PdO/SiO_2 catalyst showed some activity only after a short period under a N_2/H_2 flow, which presumably was enough to reduce part of the PdO as indicated by a change in the color of the slurry from brown to gray. The apparent rate of H_2O_2 formation then was about 1/3 of that of the fully reduced catalyst (26.2 vs 69.6 $molH_2O_2 \cdot mol_{Pd}^{-1} \cdot h^{-1}$). A different conclusion was reached by Melada *et al.* [21], who tested a preactivation process consisting in particle surface oxidation: a zirconia supported Pd catalyst was reduced in situ by passing a pure hydrogen flow into the reaction medium (0.03 M H_2SO_4 in methanol) followed by pure oxygen. After removing excess oxygen, a $H_2/air/N_2$ mixture was fed and H_2O_2 synthesis started. They observed that surface oxidation induced very high catalytic activity on 2.5 wt.% Pd/ZrO_2 with the maximum productivity over 55.3 $mmolH_2O_2 \cdot mol_{Pd}^{-1} \cdot h^{-1}$ working at 20°C and atmospheric pressure. Furthermore, they changed the $H_2/air/N_2$ mixture for an undiluted H_2/O_2 mixture with oxygen in large excess ($H_2:O_2$ = 4:96) and noted that the

productivity was lower at the beginning of the reaction, but increased notably after long reaction times (up to 58.5 mmolH_2O_2·mol_{Pd}^{-1}·h^{-1} after 5 h). Besides, water production rate was 50 times lower than in air, which corresponds to a significantly higher selectivity towards H_2O_2 (around 40 %) that remained extremely stable for several hours.

1.1.2 Support

Acidic supports such as carbon, silica, zirconia and zeolites generally give better results due to the higher stability of hydrogen peroxide in an acidic environment. Another acidic support, titania, also proved suitable for H_2O_2 synthesis, [22] with formation rates usually three times higher than the corresponding alumina supported catalyst. Other supports such as alumina [9][19][23][24] and iron oxide [25] have also been successfully employed in hydrogen peroxide synthesis, although productivities are lower than those obtained with acidic supports. This was confirmed by Edwards et al., who showed that the support has a great influence [26] on the productivity. A range of Pd-Au supporting materials prepared by impregnation are compared and the order of reactivity found was C > TiO_2 > SiO_2 > Al_2O_3 > Fe_2O_3. A common factor in all these studies is the fact that calcined catalysts are more stable, and therefore can be reused several times.

Ntainjua *et al.* [27] identified the isoelectric point of the support as the major parameter affecting the selectivity towards H_2O_2. In their experiments, supports with low isoelectric points such as carbon and silica give the highest rates of synthesis. This is intimately related to the acidic promoters in the system, as will be discussed later.

The addition of different dopants to the supporting material has also been investigated. Melada *et al.* [21] successfully tested different Pd catalysts supported on SO_4^{2-}, Cl^-, F^- and Br^- doped zirconia for hydrogen peroxide synthesis under mild conditions (20 °C, 1 bar). Using a doped support generally improved the production rate and selectivity towards H_2O_2, although it also depended on the solvent of choice. Recently, this group [28] has also reported the benefits of support sulfonation for ceria and zirconia supported Au-Pd catalysts. They also compared the performance of Pd and Pd-Au supported on sulfonated zirconia after a redox pre-treatment, and reported that H_2O_2 productivity increases from 71.3 for the monometallic catalyst to 135.2 molH_2O_2·mol_{Pd}^{-1}·h^{-1} for the bimetallic catalyst after 3 hours of reaction at 20 °C and 1 bar, while selectivity increased from 50 to 61 %. It is noteworthy the increase of the kinetic

constant of H_2O_2 formation, as well as the decrease of the kinetic constant associated with direct water formation, which explains the increase in selectivity with respect to the monometallic catalyst. Sulfonic acid functionalized silica has also been successfully used for H_2O_2 synthesis [29], showing significantly higher selectivity, yield and final concentration of peroxide than the not functionalized silica-supported catalysts used for comparison. The authors also found that the functionalization did not affect the hydrogenation reaction of H_2O_2, but it greatly inhibited the decomposition reaction, therefore increasing the selectivity. Blanco-Brieva *et al.* [30] recently reported remarkable results when carrying out the synthesis reaction at high pressure (95 bar) in a methanolic medium using a palladium catalyst supported on sulfonic acid-functionalized silica, achieving a productivity of 1857 $molH_2O_2 \cdot mol_{Pd}^{-1} \cdot h^{-1}$ and H_2O_2 concentrations up to 8 wt. %.

Functional resins have also been reported as suitable supports for H_2O_2 synthesis. Blanco-Brieva *et al.* [31] reported that the grafting of Pd^{II} ions into macroporous acidic resins produced highly effective catalysts, obtaining hydrogen peroxide production rates close to 1105 $molH_2O_2 \cdot mol_{Pd}^{-1} \cdot h^{-1}$, using a 12 ppm of HBr in 96:4 MeOH:H_2O mixture as reaction medium at 40 °C and 100 bar. This high performance was attributed to the ability of the sulfonic acid groups of the resin to interact with and stabilize the Pd^{II} ions without further reduction to Pd^0. However, they did not study in depth the state of Pd^{II} at the end or during the catalytic reaction, or the catalyst reusability. Burato *et al.* [32] confirmed the catalytic potential of the previously described catalyst, even under milder conditions (20 bar and -10 °C), but found that its color turned gray already after the first run, which suggested at least a reduction of Pd^{II} to Pd^0, as they confirmed by TEM analysis. Furthermore, they tested the catalyst after pre-reduction of Pd^{II} to Pd^0, and found it to be remarkably more active and stable, increasing the molar yield from 35 to 46 %. In a previous paper Burato *et al.* [33] showed the presence of polymer-bound acidic groups in the support appears to have a positive influence on catalytic performance but the support acidity is not essential for catalytic success.

1.2 Promoters

As explained above, supported noble metals such as Pd and Au are the most typically employed catalysts for direct synthesis of hydrogen peroxide. However, their major drawback is the fact that they are also active for the combustion of hydrogen to water and the decomposition of hydrogen peroxide. This can be controlled to some extent with the addition of promoters, which fall into two categories: halides, that could act as catalysts poisons retarding water production and increasing hydrogen peroxide selectivity; and acids, that could retard base-catalysed decomposition of hydrogen peroxide. It is worth noting that these promoters has been reported to produce a loss in catalytic activity for some Au-Pd catalysts. However, the use of promoters is generally considered crucial [13], especially for monometallic Pd catalysts.

1.2.1 Halides

Pospelova *et al.* [34] early reported the beneficial effect of adding a mineral acid such as HCl in order to inhibit the decomposition of the peroxide. Nowadays, chlorides and bromides are the most commonly employed halides. They have been found to cause a drastic decrease in the activity of Pd catalysts related to the side reactions responsible for H_2O_2 consumption, increasing the selectivity toward hydrogen peroxide. This could be due to the blockage of high energy sites of the catalyst [35], responsible for the dissociative chemisorption of O_2 and/or re-adsorption of H_2O_2 [28]. This is consistent with previous results by Dissanayake and Lunsford [8], who used Raman spectroscopy to determine that only diatomic oxygen is responsible for the formation of H_2O_2 on palladium. The optimization of the amount of halide is usually referred to its concentration, although some authors have suggested that it should be more related to the ratio between halide and Pd in the catalyst [30]. Landon *et al.* [9] studied the effect of the addition of HBr ($1.8 \cdot 10^{-5}$M) and found that hydrogen conversion at a given temperature decreased compared to a similar reaction without Br^- present, and selectivity to H_2O_2 remained high at temperatures up to 20 °C. This is consistent with a poisoning of the active sites responsible for water production. Liu *et al.* [36] thoroughly studied the role of Cl^- anions in the direct formation of H_2O_2 over a silica supported Pd catalyst in a H_2SO_4 / ethanol system. The kinetic data obtained suggested that Cl^- had a positive effect on the net formation of peroxide, firstly

inhibiting hydrogen combustion and secondly limiting the reduction and decomposition of H_2O_2. Choudhary *et al.* [37] studied the hydrogenation of H_2O_2 employed a Pd/C catalyst in aqueous acidic medium containing different halide anions. The inhibiting action gradually increased from F^- to I^- and they suggested that the electronegativity of the anion directly influenced this effect on the H_2O_2 hydrogenation. However, I^- caused a complete catalyst deactivation due to poisoning.

Therefore, in the presence of Cl^- and especially Br^-, the reduction of H_2O_2 is appreciably inhibited with increasing halide anion concentration. It was also found that this hydrogenation is zero-order with respect to the H_2O_2 concentration, and its activation energy is higher in the presence of Br^- than C. Ntainjua *et al.* [38] studied the effect of a bromide pretreatment on Au-Pd catalysts supported on MgO and C. Whereas the MgO based catalysts showed a remarkable enhancement in H_2O_2 productivity (97 vs 202 $molH_2O_2 \cdot mol_{Pd+Au}^{-1} \cdot h^{-1}$) with a pretreatment of 0.044 wt % Br^- (molar ratio Br/Au+Pd = 0.015), no significant effect was observed for the C based catalysts (265 vs 287 $molH_2O_2 \cdot mol_{Pd+Au}^{-1} \cdot h^{-1}$). This effect was attributed to the nature of the Au-Pd particles present on the catalyst: the carbon based catalyst presented homogeneous Au–Pd alloy nanoparticles (very active in direct synthesis), whereas the MgO supported catalyst has Au–Pd alloys with a Pd-rich surface and a Au-rich core (with much lower activity).

1.2.2 Acids

Ntainjua *et al.* [27] have suggested that the role of acid is intimately related to the catalyst support, particularly to its isoelectric point, which controls the degree of surface charging. They observed that supports with low isoelectric points, such as carbon and silica, provide the highest productivities for Pd-only and Pd-Au supported catalysts. Specifically, for a Pd-Au/C catalyst, they observed a maximum in activity at $pH \approx 2$. Apparently, the crucial parameter is pH rather than acid concentration [39]. Hydrogen halides are a common choice as promoters, as they combine the function of the acidic proton with the effect of the anion described above, and so HCl and HBr are usually employed [6][30][36][40]. Sulphuric acid is also often used as promoter [15][28].

Han and Lunsford [40] studied the role of HCl and H_2SO_4 as promoters. The system H_2SO_4 / ethanol gave better results than HCl /ethanol, reaching 204 $molH_2O_2 \cdot mol_{Pd}^{-1} \cdot h^{-1}$ after 7 hours at atmospheric pressure and 10 °C over a Pd/silica. By contrast, they

observed no net formation of peroxide in a H_2SO_4 / water system. They also suggested that one of the roles of protons is to prevent hydrogenation or reduction of H_2O_2, rather than the base-catalyzed decomposition of H_2O_2 as stated by other authors [9].

Ishihara *et al.* [22] studied the dependence of H_2O_2 formation rate with pH in reaction mixture used H_2SO_4 or NaOH to control pH. As expected, no peroxide formation was found under very basic conditions, and the optimum condition for peroxide synthesis over an Au/silica catalyst was found around pH 7.

Phosphoric acid is also found in the literature as a suitable acid promoter [19]. Choudhary *et al.* [37] compared the role of phosphoric acid with that of different acids such as sulphuric acid, nitric acid and hydrogen halides in the hydrogenation of H_2O_2. They highlighted the fact that H_3PO_4 is less corrosive and the phosphate anions act as H_2O_2 stabilizer. Moreover, metal leaching from the catalyst was only observed at the highest concentrations of H_3PO_4 (>0.3M), whereas appreciable metal leaching was observed in the presence of HCl, HBr and HNO_3. Acid pretreatment of the support has been reported to have significant effect on the productivity of H_2O_2 for Au-Pd catalysts, as reported by Edwards *et al.* [41]. They found that the acid pretreatment of a carbon support prior to the addition of the active metals led to an important increase in selectivity and the complete suppression of the hydrogenation reaction. The beneficial effect of the acid pretreatment was attributed to an enhancement of the gold dispersion in the bimetallic alloy particles that generates smaller Au-Pd nanoparticles. This modified dimensional distribution of nanoparticles showed a double effect: the increase of the activity for the synthesis and the switch off of the active sites for H_2O_2 hydrogenation, therefore increasing the selectivity. However, they did not observe this suppression of the hydrogenation reaction for acid pretreated TiO_2 supports, although the pretreatment still produced a significant enhancement in catalyst performance [42].

1.3 Solvent

The most common solvent, and the first option for a liquid reaction medium, is water. It provides the safest conditions, is non toxic, non flammable, and highly miscible with hydrogen peroxide. In fact, aqueous reaction media are popular in the literature. However, its main drawback is the low solubility of the reacting gases (hydrogen and oxygen) [1][6], which strongly limits mass transfer and thus the rate of peroxide production. This problem was early reported by Krishnan *et al.* [43], who compared the

performance of different organic media (methanol, ethanol, isopropanol, dioxane and acetone) with Pd supported on phosphate viologen phosphonate catalysts working at room temperature and atmospheric pressure. They observed almost no H_2O_2 formation after 6 hours in a water / H_2SO_4 system, whereas the organic solvent / H_2SO_4 systems yielded up to 200 mM H_2O_2 in the same time, especially methanol and acetone. However, when HCl was used as acid promoter instead of H_2SO_4 the production of hydrogen peroxide was found in the aqueous medium (150 mM after 6 hours). This suggested a strong halide effect. Interestingly, this effect did not appear to affect organic solvents. They attributed the differences between water and organic solvents to the liquid film mass transfer at the gas-liquid interface, being rate determining. Burch *et al.* [19] studied the effect of the addition to the reaction mixture of different organic compounds, with different polarities and miscibilities in water. Some compounds, such as toluene and hexane, which are known to increase the solubility of H_2 and O_2 in water, were found to increase the conversion but gave very low selectivities towards H_2O_2. This behavior probably was due to their immiscibility with water and therefore a deficient contact with the catalyst. Others organic substances, such as triethanolamine, which is a strong binding ligand for transition metals, completely suppressed the reaction. Alcohols in general were found to be the best solvent or co-solvents for H_2O_2 production, since they are miscible with water and able to dissolve the promoters. Particularly, it was found that ethanol was more effective at higher concentrations, giving 34 % selectivity with a 75/25 ethanol/water mixture. Considering the effectiveness of alcohols as co-solvents, some authors have described successful results in pure ethanol [15][40] and methanol [28][32][33], although water/methanol mixtures are also commonly employed as solvents for direct synthesis of H_2O_2 [44]. Edwards *et al.* [26] studied the effect of water/methanol ratio using a 2.5 wt.% Au/2.5 wt. % Pd/TiO_2, short reaction times (30 minutes) and low temperatures (2°C) without the addition of halide or acid promoters. They found the optimal water/methanol ratio at 20:80 (reaching 249 mol $H_2O_2 \cdot mol_{Pd+Au}^{-1} \cdot h^{-1}$), attributed to an enhanced solubility of the reaction gases in the solvent. Li *et al.* [14] c compared the results obtained in water, water/methanol and water/acetone solvents for both 2.5 wt.% Au/Y-zeolite and 2.5 wt.% Au/2.5 wt.% Pd/Y-zeolite supported catalysts in short reaction times (30 minutes) and room temperature (20°C). The bimetallic catalyst in water/acetone mixture gave the best productivity (140 $molH_2O_2 \cdot mol_{Pd+Au}^{-1} \cdot h^{-1}$ vs 97 $molH_2O_2 \cdot mol_{Pd+Au}^{-1} \cdot h^{-1}$ and 33 $molH_2O_2 \cdot mol_{Pd+Au}^{-1} \cdot h^{-1}$ using water/methanol and only water respectively).

Recently Piccinini *et al.* [44] studied the influence of reaction conditions on the direct synthesis of hydrogen peroxide, like H_2/O_2 molar ratio, total pressure, solvent and its mass, temperature, etc. They found that 2.5 wt.% Au/2.5 wt.% Pd/C catalysts have a optimal water concentration in methanol at 8 wt.% in which the best H_2O_2 productivity is showed. However under this condition they found the hydrogenation of H_2O_2 is active, differently from water/methanol in 20:80 ratio.

Supercritical carbon dioxide has also been successfully employed as solvent for H_2O_2 direct synthesis. It is considered a "green solvent", since it is relatively non toxic, non flammable, and inexpensive A wide range of reactions can be carried out using $scCO_2$ technology, including hydrogenations, Friedel-Krafts alkylations, hydroformylations, etherifications and estherifications [45][46]. In particular hydrogenations are clean, fast and more selective. Of particular relevance to hydrogenation and oxidation reactions is the fact that H_2 and O_2 are completely miscible with supercritical CO_2 (T_c= 31°C and P_c= 74 bar), and even under subcritical conditions (this situation is commonly called CO_2 expanded solvents) their solubility is much higher than in organic solvents or water, so the mass transport limitations associated with conventional solvents are avoided or greatly diminished. Moreover, the solubility of H_2O_2 in $scCO_2$ is low, which facilitates its separation from the solvent and minimizes the chances for product degradation through prolonged contact with the catalyst. The acidic character of CO_2 also helps the stabilization of aqueous hydrogen peroxide, eliminating the need for acidic promoters. Beckman and co-workers [47] first achieved the direct synthesis of H_2O_2 in $scCO_2$ with a Pd-catalyzed hydrogenation followed by the oxidation of a fluorinated (hence CO_2-philic) anthraquinones. Later, they developed CO_2 soluble Pd catalysts [47], obtaining 30-40% yield after 3 hours when using a Pd^{II} catalyst (22°C, 170 bar). They also found the activity of the reduced catalyst to be approximately twice that of the unreduced catalyst. However, the synthesis of the CO_2-soluble palladium catalyst was tedious and expensive, and they also studied the use of a regular Pd supported catalyst and a very small amount of water [48], but the difficulty of accurately measuring the concentration of H_2O_2 formed remained.

2. NANOPARTICLES

The study of the synthesis and the proprieties of metal nanoparticles [49][50][51] is an attractive field which has been continuously developing for 20-25 years with important fall-out into material science, chemical industry and life science. This subject, widely present in the open literature and the patents, spreads into many fields such as the analysis of spectroscopic and magnetic properties of quantum semiconductors [52][53] [54], the photochemistry applied to the nanostructured materials [55], the synthesis and the catalysis with nanoparticles stabilized by polymers or ligands [56][57][58], the spectroscopic analysis of nanoparticles in gas phase [59], the investigations of metals or ceramics with nanocrystalline domains [60].

The nanoparticles, a class of "chemical objects" intermediate between the bulk and the single molecule, can be isolated as aggregates of atoms of sizes between 1 and 50 nm, often referred to also as either "colloids" or "clusters" if they show a regular and controlled structure. To prevent agglomeration, these nanosized bodies must be stabilized by molecular compounds (ligands) or a whole plethora of protecting agents [61]. These materials show specific physical and chemical properties, due to the size in the nanometer-scale, also called "quantum size" [62]. This behavior is exhibited when the particle, containing only a few hundreds of atoms, dramatically modifies its electric and electronic properties, due to the decrease of the state density in both the valence and the conduction bands. Further reduction will end up in a situation where the bands turn into more or less discrete energy levels [63] (Figura 1.3).

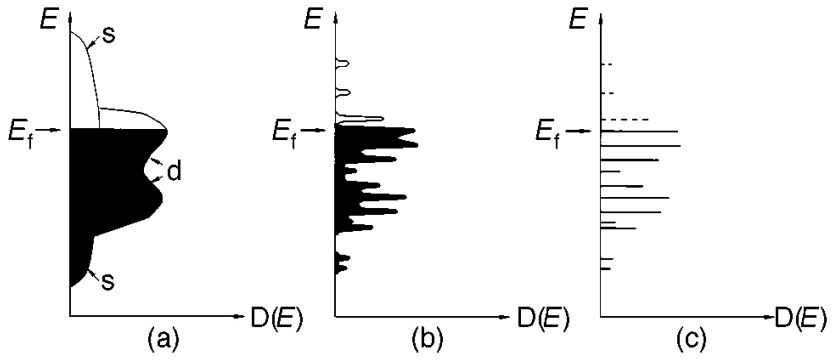

Figure 1.3: Density of the electronic bands.

An intrinsic feature of the reduced size (and very fascinating for the applications) is the increase of the proportion surface atoms. In 1.5 nm particles the surface atoms dominate

with ca. 70% of the total number of atoms. Differently from inner atoms, surface atoms are less coordinatively and electronically unsaturated. The ensuing excess surface energy makes these nanoparticles thermodynamically unstable. Moreover, for the same reason the surface atoms are particularly reactive, which explains why they readily bind solvent molecules in liquid phase or undergo partial or total oxidation of surface when they are exposed to air.

The percentage or fractional proportion of the surface atoms of a cluster (also called its dispersion) may be estimated geometrically on the basis of the dimension and the shape of the particle [64][65]. If the the structure of the cluster is a regular polyhedron composed by n closed shells surrounding a single central atom and overlay one to another, it is possible to determine the total number of atoms of the particle and of each shell, including the n-th outermost one. The equation 2.1 calculates the number of atoms that must be added to a full-shell nanocluster with n shells to complete an additional (n+1)-th one [66].

$$N_m = 10n^2 + 2 \qquad \text{(eq. 2.1)}$$

where N_m is the number of metal atoms for each shell and n is the number of the shell [67]. These full-shells nanoparticles, also called "magic number clusters", contain 13, 55, 147, 309... atoms of metal (Figure 1.4).

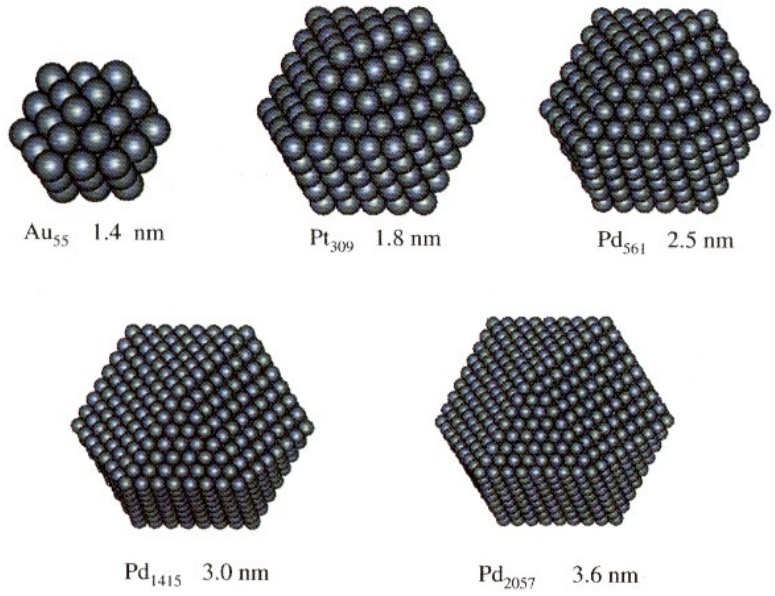

Figure 1.4: "Magic number clusters"

2.1 Methods of synthesis

There are essentially two approaches for the preparation of nanoparticles, shown in Figure 1.5. On the one side there are the so-called "top down methods", e.g. by the mechanical grinding of bulk metals and subsequent stabilization of the resulting nanosized metal particles by the addition of colloidal protecting agents [68]. On the other sider there are the so-called "bottom up methods", i.e. the wet chemical nanoparticle preparation rely basically on the following methods [69][70]:

- chemical reduction of metal salts including electrochemical routes;
- thermolysis, including photolytic, radiolytic and sonochemical routes;
- controlled decomposition of pre-formed metastable organometallics.

After the decomposition of the metal precursor (through one of three previous approaches), the free metal atoms form the more or less structured aggregates, generally called nanoparticles. Whatever the method, the aggregation of the nanoparticles must be prevented, so that the nanosized systems result to be kinetically stable, though not thermodynamically. Generally these systems are also referred to as Stabilized Metal Nanoparticles (SMN).

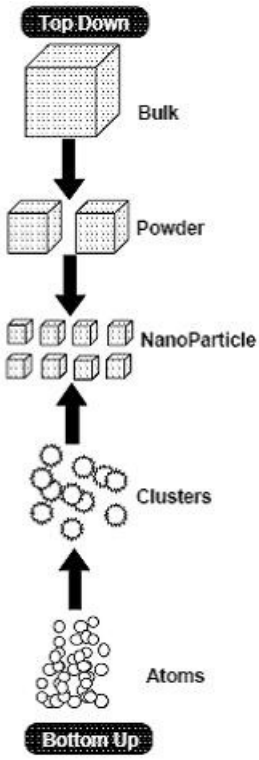

Figure 1.5: Two approaches to prepare the metal aggregates

2.2 Model of formation of the nanoparticles

Turkevich who established the first reproducible standard and reproducible procedure for the preparation of metal colloids [71] also proposed a mechanism for the stepwise formation of nanoclusters based on the process of nucleation, growth, and agglomeration [72][73].

The initial step of nucleation involves the reduction of metal precursor, obtaining the zero-valent atoms, and the successive collisions with further metal species in solution (either atoms or "sub-cluster") gives rise irreversibly to a first stable "seed" nucleus of 13 metal atoms, i.e. possible smallest full-shell cluster [61] (see the previous paragraph).

Another important contribute was given by LaMer *et al.* [73], who proposed that the concentration of metal atoms in solution must be high enough to reach "supersaturation" and that the nucleation from supersaturated solutions occurs suddenly. Moreover, they stated that monodispersity of nanoparticles is a consequence of carefully separating the nucleation step from the subsequent growth stage [61]. For metal aggregates, the nucleation is the result of a complicated interplay of factors such as the difference between the redox potentials of the metal salt and the reducing agent, and the reaction conditions including the rate of addition, the reaction temperature, and even the stirring rate [61]. Only if the nucleation is complete before the growth step begins, a monodisperse sample is achieved, i.e. short nucleation times are the prerequisite for monodisperse particle formation. According to the proposed mechanism, the nucleation process quickly consumes enough of the metal atoms formed initially to decrease their concentration below a critical threshold. No new metal cluster nuclei are created in the subsequent diffusion-controlled growth stage during which the remaining metal atoms are taken up by the nuclei already in existence [61]. If nucleation and growth do overlap, the duration of the growth period will differ between various nucleation sites, resulting in a broad particle size distribution.

Subsequent to nucleation event, the particle growth depends exclusively on the balance of two factors, the specific surface energy of the metal vs. the entropy loss. If the former is significantly higher, the growing particles tend to undergo "Ostwald ripening" [74] or coalescence, i.e. an unwanted mechanism ending in size broadening hence polydispersity. Were the process stopped quickly at this stage, the resulting particles would be polydispersed – sometimes with two distinct particle sizes. In practice, the most effective way to separate nucleation from growth is the quick "injection" of strong

reducing agents, such as hydrides, in the solution of metal precursor.

Another very important contribution to the understanding of mechanistic aspects on the formation of the nanoparticles produced by reduction of metal precursor was made recently by Finke *et al.* [75]. They established the four-step, double autocatalytic mechanism by which transition metal organometallic or metal-salt precursors self-assemble into zero-valent precious metal nanoclusters under reductive conditions. Essentially, this concept replaces the generally accepted three-step mechanism of nanoparticle nucleation, autocatalytic growth, and bimolecular agglomeration by the four steps of particle formation depicted in Figure 1.6 [61]. This mechanism was demonstrated in a systematic kinetic investigation on the reduction of the low-valent complex [Pt(COD)$PtCl_2$] with hydrogen in presence of tributylamine, Bu_3N, and (1,8-bis(dimethylamino)naphthalene) as ‘‘proton sponge’’. As shown in Figure 1.6, the reaction begins with a slow, continuous reduction step (A-B) in which the metal atoms form a nucleus. This is followed by fast autocatalytic surface growth (A + B → 2B), and then by bimolecular agglomeration (B + B → C), and finally by an unprecedented step of autocatalytic agglomeration between small (B) and a larger (bulk metal like) clusters (C). This final step is represented in Figure 1.6 as (B + C → 1.5 C) [61].

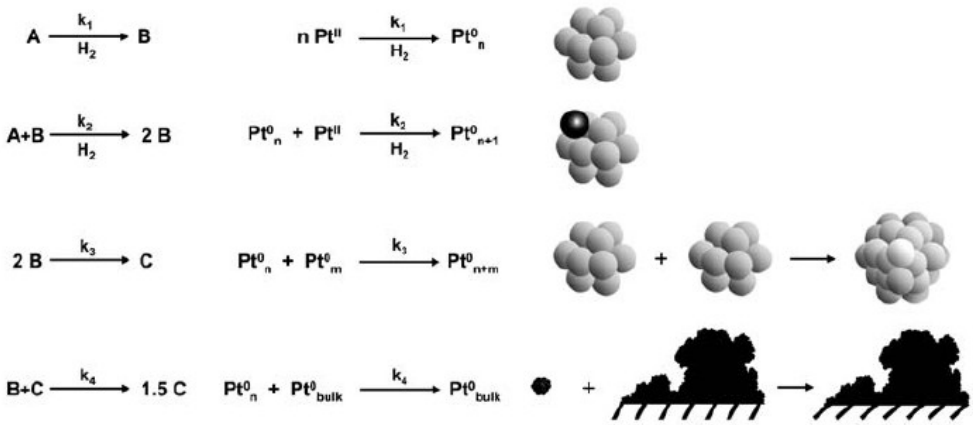

Figure 1.6: Four-step model proposed by Finke *et al.*[75]

2.2.1 Bimetallic nanoparticles

Mono- or bimetallic nanoparticles have attracted a great interest in scientific research and industrial applications such as catalysis, owing to their unique large surface-to-volume ratios and quantum-size effects [76][77]. Bimetallic nanoparticles composed of

two different metals are more promising than monometallic nanoparticles from both the scientific and technological point of view [78]. These have shown novel catalytic behaviors due to the synergistic effect based on the effect of second metal element added. This effect of the second metal can be often explained in terms of an ensemble and/or a ligand effect in catalysis [79].

Also the preparations of bimetallic nanoparticles can be classified into two categories: physical and chemical techniques. Generally, the chemical methods have the advantage to be able to easily control the primary structures of nanoparticles, such as size, shape, and composition. Such methods for monometallic nanoparticles can be applied with few adjustments to the preparation of bimetallic nanoparticles and are usually classified into three categories [79].:

- simultaneous reduction (or co-reduction);
- successive reduction for two kinds of metal precursors;
- ‘‘self-organization’’ of bimetallic nanoparticle by physically mixing two kinds of already-prepared monometallic nanoparticles with or without after-treatments.

These approaches often give different size and structure such as alloy or core/shell to the resulting bimetallic nanoparticles. Various typical structure models of bimetallic nanoparticles are shown in Figure 1.7. The precise control of size, its distribution, shape, composition, and crystal structure of bimetallic nanoparticles is crucial in the field of catalysis.

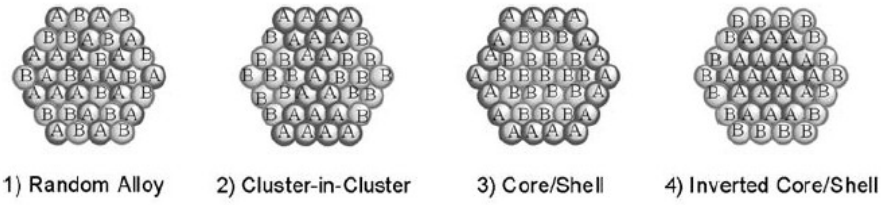

Figure 1.7: The four simplest micro-structure of bimetallic nanoclusters [79].

2.1.3 Reducing Agents

The wet-chemical preparation of SMN from reduction of suitable metal precursor/s offers advantages such as the reproducibility and the size control [59][61][79].

A large number of reducing agents are used. Each one can be a suitable chemical tool for a fine control of the features of nanoparticles obtained. Some are easily and widely

used for the reduction of precious metal precursors, such as molecular hydrogen [80] [81], formaldehyde [81], formates [81], alcohols and polyols [81][82]. Other reducing agents are also effective, such as boron hydrides [81][83], aluminum hydrides [81] or hydrazine [81], but must be handled with exceeding care due to toxicity or safety issues (or both) and are less commonly employed.

2.1.4 Stabilization of nanoparticles

The specific surface areas of metal nanoparticles are huge so that they are thermodynamically unstable, having an excess surface free energy in comparison with the lattice energy. The protective agents are essential to stabilize the metal nanoparticles (usually positively charged). To accomplish this they must make repulsive forces to prevail over the attractive ones [71]. It is important to achieve sufficient inter-particle separation and it can be helpful to use sterically demanding substituents. The mode of stabilization can be classified essentially on the type of protecting shell [66]:

- electrostatic [71];
- steric (using polymers, as poly(N-vinyl-2-pyrrolidone) [84]);
- ligand (P, N, S donors) [85] [86]
- electrosteric [87][88]
- solvent, e.g., THF [89] [90] or long chain alcohols [91][92][93].

Heterogeneous supports can also prevent the agglomeration of metal nanoclusters and can be considered as stabilizers under this respect. Additionally, they can also regulate particle size, especially when the metal aggregates are prepared by precipitation. Many preparative routes have been described for loading metal nanoclusters mainly onto/into various inorganic supports [94][95][96], but also organic matrix [83][97][98], which can provide to control their morphology and behavior. Composite materials, with no additional stabilizers in their preparative, have potential applications in many areas like surface-enhanced Raman scattering, photonic crystals, catalysis, and in chemical sensors. The main prerequisites for materials to be used as supports or exo-templates for nanoclusters are:

– inertness and neutral chemical properties;

– a large surface area;

– pore sizes optimized for the nanoclusters to be ‘‘hosted’’ or encapsulated.

All these features are present in the cross-linked functional polymers (see later), and make them a promising and suitable organic supports for catalysis [83].

3. CROSS-LINKED FUNCTIONAL POLYMERS (CFPs)

Cross-linked functional polymers (CFPs), called also commonly functional resins [99] [100], are useful in a wide range of chemical applications, including solid-phase synthesis [101][102][103], chromatography [104][105][106][107] and the controlled release of drugs [108]. Other important uses include CFPs supported reagents [109] and catalysts [83], ion-exchange resins [110], molecular imprinting [111][112][113], and molecular sensors [114].

CFPs have considered for many years promising support in metal catalysis, since when Haag and Whitehurst [115] proposed to use this type of supports as macro-ligand for metal species as active homogeneous catalyst and an important patent of Wöllner and Neier, Bergbau Chemie [116] suggested in the same years to use CFPs as support for Pd^0 (or metallic palladium) in order to have a Pd^0/resin catalyst. These materials started shortly after to be used in the one-pot synthesis of methyl isobutyl ketone (MIBK) from acetone and molecular hydrogen [117].

A cross-linked functional polymer is an isotropic organic matrix, made up of macromolecular chains interconnected by covalent bonds or strong hydrogen bonds, or physically entangled one with another. These materials are usually prepared from the radical co-polymerization of vinyl monomers and of divinyl co-monomer as cross-linking agent. These polymeric chains can bear dangling groups that may be chosen from a variety of candidates. The choice of suitable monomers and the functional group is a key factor for a well-defined morphology, chemical and physical proprieties of the resulting material.

The most representative CFPs are classified in microporous (gel-type resins) and macroporous ones (macroreticular resins). Figure 1.8 hows how the two types of materials behave when a proper solvent is used as the swelling medium.

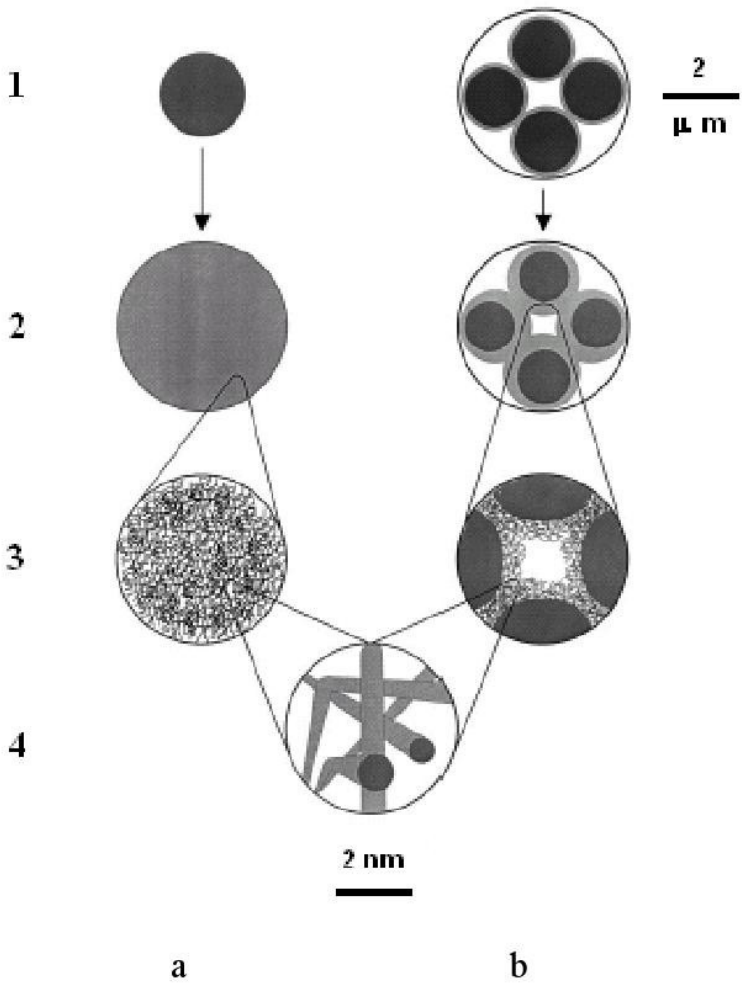

Figure 1.8: Scheme of the morphology on micro- and nano-scale of gel-type (a) and macroreticular (b) resin.

For macroreticular resins, a detectable porosity (macro-porosity) is present already in the dry state (Figure 1.8, image 1-b) that can be observed with SEM microscopy and estimated with techniques based on gas physisorption. This porosity is usually in the order of hundreds of nanometers. In the swollen state, a remarkable nano-porosity can be also observed. It is mainly produced by the the swelling of external layers, more or less thin, of the dense nodules that form the macroreticular resin architecture [118] (Figure 1.8, image 2/3-b).

Unlike the macroreticular resins, gel-type ones don't exhibit any porosity in the dry state (Figure 1.8, image 1-a), but a narrow tunable nano-porosity can be found in the swollen state (Figure 1.8, image 3-a). The nano-pore modulation is essentially obtained by control of cross-linking degree [119][120][121][122].

The proportion of the cross-linking agent in the monomers mixture is the key factor differentiating these two type of resin. For styrene/divinylbenzene (PS/DVB) resins the

presence of a 1 - 5 wt.% of DVB produces a gel-type matrix, whereas a mixture with 5 – 60 wt.% of DVB and the presence of diluents allows to prepare a macroreticular material [118]. The cross-links in macroreticular resins are much less equally distributed than in gel-type ones, because the tetrafunctional divinyl monomers are much more reactive than the bifunctional mono-vinyl ones. At the beginning of the polymerization process an insoluble microgel is quickly formed due to the preferential reaction of divinyl monomers. It is rich in unreacted double bonds, tends to expel the unconverted monomers and the diluent, if any is present. This phenomenon, thermodynamically favored, is known as syneresis and brings about the early separation of the solid polymer from the polymerization mixture. This is the reason why the macroreticular resins are formed by dense and inaccessible nodules (Figure 3, image 1-3b). The analysis of a ground PS/DVB macroreticular resin showed the presence of agglomerates of nodules, mainly in the size range of 20 - 80 nm, distributed in a relatively lightly cross-linked matrix [118]. If the polymerization is carried with a non-solvent diluent, the structure of the macroreticular resin is formed by voluminous agglomerates of microspheres (100-200 nm) each showing smaller nuclei, mainly in the range of dimension 10 - 30 nm and more or less clustered together, which gives the agglomerates a typical cauliflower-like morphology. The relatively little cross-linked matrix which surrounds the nodules presents an extensive mesoporosity (5-15 nm), which is mainly responsible for the high surface area of these polymers. There can also be a second population of larger mesopores (20-50 nm) in between the microspheres and a population of macropores (50-1000 nm) located between the agglomerates [123]. The choice and the amount of the diluent(s) used in the monomers mixture is fundamental to module the pore size control and its distribution, i.e. for example increasing the permanent porosity in the nanometer scale (generally $1<d<20$ nm) [124]..

These two classes of cross-linked polymers show a different behavior when the polymer is in swollen state: whereas gel-type resins usually absorb substantial amounts of solvent and their volume remarkably increases, macroreticular ones swell much less, since this phenomenon involves only the accessible part of the polymer.

Both types of material are universally used in the presence of liquid (i.e. in the swollen state, *vide infra*): more or less consistent part of the polymer is converted into something like a “pseudo-solution” of interconnected polymer chains (Figure 1.8, image 4). The absorption of the liquid is driven by the osmotic pressure of the pseudo-solution

and makes the polymer framework to expand. This sets up the elastic counter-forces, because the chains in the cross-linked framework cannot be separated and the polymer cannot be dissolved (Figure 1.9). The swelling of the polymer chains is therefore primarily due to a positive entropic effect and enthalpic contributions can inhibit or enhance the degree of swelling. This depends on the nature of solvent, the cross-linking degree of matrix and the lipophilic or hydrophilic nature of monomers. The condition of "pseudo-solution" of the resin particles in the swollen state is proved, at least for some systems, by relatively high rotational mobility of probe molecules dissolved in the liquid medium [122][125] and by the remarkable translational mobility of the solvent molecules confined inside the swollen matrix [126]. The combined use of EPR spectroscopy to measure of the mobility of a radical probe (generally a nitroxide radical) bound to a swollen matrix (spin-labelling) or dissolved in the swelling medium (spin probing)[122], and ISEC (Inverse Size-Exclusion Chromatography) allowed to show that the viscosity of the solution within both resin frameworks is essentially higher than to the pure solvent. In particular for gel-type resin, the viscosity is the main parameter which controls the diffusion inside the swollen matrix [122]: in fact a decrease of rotational mobility is observed increasing the cross-linking degree and the polymer chains density. For macroreticular resin the inner diffusion is mainly favored by its permanent porosity and can also be fast [118].

Furthermore the ISEC technique is useful to measure not only the swelling propriety of CFP (expressed in ml/g), but also the distribution of the average chain concentration (in nm/nm^3), an important parameter to estimate the heterogeneity of porosity in the swollen state.

On this basis, the control of porosity is a strong tool which affects the inner accessibility of resin particles and a fundamental feature for many applications , such as the liquid phase processes (catalysis, selective adsorption, etc) and the template controlled synthesis (TCS approach) of nanocluster inside the CFPs [127][128][129][130].

3.1 General aspects of CFPs

The chemical functionalization of the resins allows to control some of their properties, such as the swelling degree in different solvents [118][131]. Two approaches are possible for the preparation of a functional polymer: the polymerization or co-polymerization of monomers which have a suitable substituted group or the chemical modification of pre-

formed polymers [118].

The polymerization (or the co-polymerization) of monomeric precursors can be carried out in many ways. One of the most common one is the radical polyaddition, (chemically or photochemically initiated), but cationic or anionic polymerization are also used sometimes.

In rare cases it is been necessary the use of metallorganic species as polymerization catalyst (in particular metal-alkyl complexes with a low electronic density at the metal centre) to better control the process. The relative reactivity of monomers can be used to prepare a block co-polymer or to control the composition of the polymer matrix [132] on micro- and nanometric scale.

Suspension polymerization [133][134] is particularly useful for producing cross-linked polymer beads in the size range 10-1000 μm, for applications such as packed column chromatography and solid-phase synthesis. A typical oil-in-water (O/W) procedure involves the suspension in water of an immiscible oil phase containig the dissolved monomer(s), often with the addition of a porogen in the case of highly cross-linked macroporous resins [105][106]. The suspension is polymerized under vigorously stirring to directly form spherical particles and the initiator is preferentially soluble in the monomer phase [135][136]. Each monomer droplet may be considered as a "microbulk" polymerization reactor with efficient heat transfer to the surrounding aqueous continuous phase. Water-soluble monomers may be polymerized via water-in-oil (W/O or "inverse") suspension polymerization techniques, where the monomer, or often a concentrated aqueous solution of the monomer, is polymerized in an immiscible apolar hydrocarbon medium [137][138].

In both cases surfactants are usually added to inhibit droplet coalescence. Recently, the scope of suspension polymerization has been broadened by the development of multi-stage templated techniques, which allow the formation of large, mono-disperse, macroporous beads by consecutive swelling processes [139].

An alternative way for the preparation of crosslinked functional polymers is the chemical modification of an organic matrix already synthesized. This approach is the most used in organic chemistry and allows to use as starting materials microporous or macroporous resin with known chemical-physical features (cross-linked degrees, porosity, ...). The physical proprieties of these matrix don't usually change in the functionalization process, but it is necessary a careful choice of the reagents and the reaction condition, also to avoid by-products formation. The final distribution of

functional groups obtained from a post- functionalization process could be different from an analogue matrix obtained from direct polymerization of related monomers. In fact, the chemical modifications of the pre-formed matrix strongly depends on the diffusion of reagents into the framework and the post- functionalization reactions take place only in the accessible portion of organic matrix. Additionally the functionalization degree can depend also from the presence of other substituents already anchored to the polymer chain and from the swelling ability of solvent.

An another possible route is the post-polymerization between monomers provided with functionality of interest and residual double bond of polymer matrix [140].

An important factor to evaluate for the industrial application is the mechanical propriety of material. The gel-type resins show a relatively high inner diffusion, but due to the low cross-linking gives the texture of these materials makes them difficult to handle. The macroreticular ones are mechanically more resistant, but also more fragile. Moreover, the materials can be stressed by frequent swelling and drying cycles which eventually lead to the formation of cracks and production of fines.

3.1.1 Cation-exchange resins as catalytic supports

Resins based on styrene/divinylbenzene are of great interest, and cation-exchange resins functionalized with sulfonic acid groups also play an important role as heterogeneous acid catalysts [118]. Depending on the reaction conditions, the functional groups (sulfonic groups) may be uniformly introduced into the resin or, when the modification reaction is diffusion controlled, functionalization can start at the surface of the polymer particle and then move inwards, initially into the pores and finally into the matrix [118]. Sulfonation, an electrophilic aromatic substitution, is reversible and the equilibrium position is controlled by the temperature. As the consequence starting from 120-130°C (and in presence of water), these resins can release sulfuric acid in the medium (Figure 1.9).

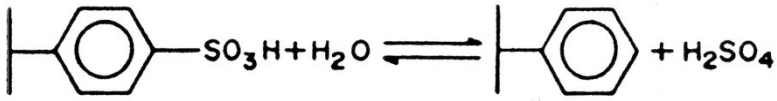

Figure 1.9: Sulfonation/desulfonation equilibrium of a phenyl group of a PS/DVB matrix

However many important reactions of academic and industrial interest are carried out

under mild condition, below the limit of thermal stability of sulfonated polystyrene/divinylbenzene. Moreover some commercially available sulfonic resins thermally stable up to 180°C due to a chemical modification of the matrix (i.e. chlorination of the aromatic rings)[118].
Not only the sulfonic groups in the organic framework can be used as acidic catalytic sites, but also as anchors to suitable metal precursors or complex (see later).

3.2 Metal catalysts supported on CFPs

Metal supported catalysts are dramatically important in the modern industrial chemistry [141][142]. They are featured by two components [83][98]: the former is a organic or inorganic support with specific structural and chemical features, the latter are metal nanostructured clusters, in which the zero-valent metal is typically able of electronic activation of reagents (Figure 1.10).

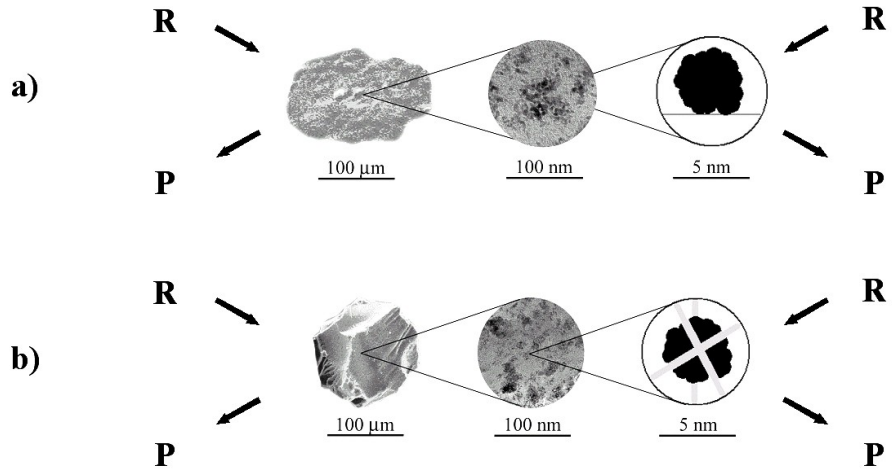

Figure 1.10: Traditional vs. CFPs supported catalysts

The traditional supports, with the exception of amorphous carbon, have typically an inorganic nature and their basic role is to disperse and stabilize the metal nanostructured systems (Figure 1.10, a). However it is well known that the support can also play a chemically active role in the control of reactivity and selectivity (see for example [143]). The reagents involved in the metal catalyzed reaction, must enter the cavities of the support. This can sometimes produce a "molecular sieving" (dimensional selectivity) and also introduce them into a reaction micro-environment which can be much different

in comparison with the "bulk" mixture. In this spatially confined reactor (Figure 1.10, b) the kinetic and thermodynamic data of the catalyzed reaction can also be significantly different [131]. This makes these materials highly innovative, for their potential action as promoters or co-catalysts. and very promising due to the ease of tuning and designing their chemical and morphological properties on the molecular scale, which could lead to also the preparation of bifunctional catalysts, very useful for multistage reactions.

In last decade the research group I have been working with has studied in a systematic way the CFPs as efficient supports for innovative metal catalysts [131] to be applied in the field of Fine and Specialty Chemicals [144].

These cross-linked polymers can have functional groups suitable to anchoring the metal precursor, which can be introduced during the polymerization or with a post-polymerization chemical transformation. These functionality can bind a metal precursor through a process called metalation, based upon an electrostatic interaction (ion-exchange, Figure 1.11, a-b) or the formation of a covalent bond (ligand-exchange or addition, Figure 1.11, c).

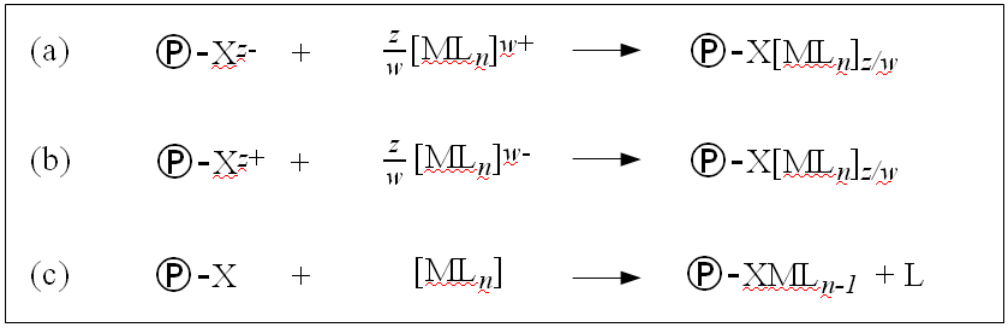

Figure 1.11: The possible interactions between functional group X of polymer matrix and the ionic and not-ionic metal precursor [ML_n].

Additionally the exchange of a metal complex active in homogenous catalysis may produce a *hybrid* heterogeneous catalyst [145].

It is important that the whole polymeric matrix is swollen for a reproducible metalation. Consequently the solvent must be a good solvent for the metal precursor and able to sufficiently swell the resin. Generally a low metal amount is loaded for catalytic applications and quantitative incorporation of the metal precursor can be easily achieved also under condition of high dilution. A gel-type resin completely swollen is fully accessible and the metal distribution is fairly homogeneous. Differently the distribution

of metal in a macroreticular material is much more inhomogeneous. The metal precursors are preferentially bound in the most accessible regions in diffusive regime, i.e. close to macro- and mesopores [146]. The best results are obtained when the swelling degrees of the resin in the preparation of catalyst and during the catalytic test are comparable, which calls for the use of the same solvent or of similar ones when this is not possible.

After the metalation, the reduction of the metal precursor generate zero-valent atoms which aggregate to form the nanostructured supported metal phase. Interestingly the conditions of this process can chemically modify the support. A simple example is the use of $NaBH_4$ as reducing agent. When a sulfonated resin in it acidic form is used as the support, its sulfonic groups are transformed into the sodium form salt by the acid-base reaction with $NaBH_4$ and this changes the swelling propriety of polymer in non-aqueous polar medium [83][120]. Furthermore the dimensions of metal aggregates depend on the method and the reduction rate, as the metallic species can migrate within the swollen matrix during this stage.

Other strategies for the preparation of metal-polymer nanocomposite can be applied. The former consists in the synthesis of the polymeric support in presence of the metal precursor, generating the metal nanoclusters in a following stage. The latter consists in the controllable insertion of pre-formed nanostructured metal aggregates in the polymeric matrix.

Recently an approach for the dimensional control of nanostructured metal systems based on the steric stabilization of nanoclusters due to the matrix has been proposed (Figure 1.12) with the term of “Template Controlled Synthesis, TCS” [147]. The results showed a good correspondence between the pore dimensions of swollen resin and those of metal aggregates, indicating that the process is mainly governed by steric factors.

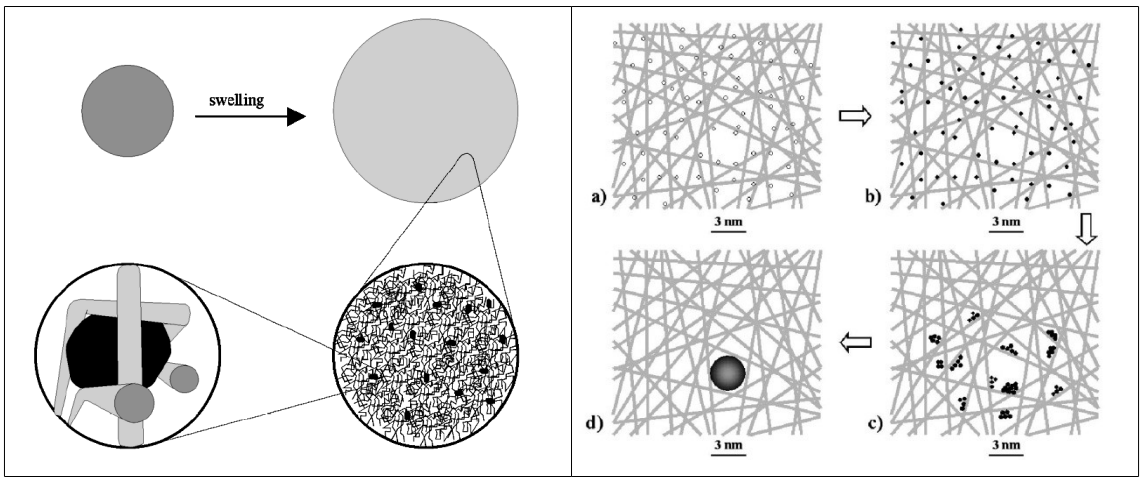

Figure 1.12: TCS approach in the synthesis of nanocomposite metal-polymer.

The support morphology can affect the reaction kinetics only if the overall process is governed by diffusive regime, i.e. the small pore size limits the inner mass transfer and the inner diffusion is the kinetically slow step. On the other hand if the chemical reaction occurs in the kinetic regime, the kinetically slow step is the reaction on metal surface and the structural features of organic matrix don't affect the process.

CHAPTER 2:

Effects of metal precursors and the reduction protocols in the preparation of catalyst for the direct synthesis of H_2O_2

The catalysts for the direct synthesis of hydrogen peroxide (DS) are most commonly prepared by incipient wetness impregnation of inorganic supports or carbon with aqueous solutions of noble metal precursors, quite often containing halides as $PdCl_2$ or $Na_2[PdCl_4]$ [6]. These materials are usually calcined and eventually reduced with a suitable treatment. The use of resins as the support allows a completely different approach: a wet synthesis under mild condition. The ion exchanger nature of resin allows to chemically bond a metal precursor to suitable functional groups of polymer matrix. In this case, the use of sulfonated poly(styrene-divinylbenzene) (SPS) resin [118] can be interesting as the material is able to exchange cationic species, like cationic metal complexes. Additionally, it is commercially available and relatively cheap.

This approach, not possible with the most part of inorganic supports, permits to readily control both the degree of loading of metal precursor and its distribution inside the material. Furthermore, the organic chains of the polymer matrix allows the physical entrapment of metal nanoparticles inside the material, limiting problems due to mobility of nanoparticles, as sintering.

It is interesting to observe that the effect of different metal precursors and reduction protocols on the catalytic performances have not been investigated so far.

In this study, the dependence of catalytic performances on the synthesis conditions will be examined, in order to understand how the choices of metal precursors and reduction protocols affect the behavior of catalyst in direct synthesis of H_2O_2.

In this work the commercially available K2621 resin has been selected as the

catalyst support. This CFP is a poly-PS/DVB matrix, partially sulfonated (1.92 mmol/g of exchange capacity) and in the acid form. The material shows fairly good proprieties of swelling in water and in methanol (1.6 ml/g and 0.8 ml/g, respectively [32]) and its morphology permits the rapid diffusion of reagents and products. Additionally, this support was already used in previous investigations on this reaction [31][32].

There are only a few commercially available cationic precursors of palladium, such as $[Pd(NH_3)_4]SO_4$ and $Pd(NO_3)_2$. They are both water soluble and stable in dilute solution. Additionally, it is possible to use $Pd(OAc)_2$ as the metal precursor, because the sulfonic groups are able to protonate the acetate ligands and to bind the formed cationic species.

A library of catalysts was prepared by metalation of K2621 with each one of available metal precursors, after swelling in water ($[Pd(NH_3)_4]SO_4$ and $Pd(NO_3)_2$.) or tetrahydrofuran ($Pd(OAc)_2$).

Hydrogen is the most used reducing agent for the preparation of metal catalysts supported on inorganic solids or carbon. The use of hydrogen, under semi-continuous or batch-wise conditions, at atmospheric or high pressure, and mild or high temperature , is widely reported in the open [1] and patent [6] literature. Since K2621 is accessible mainly in the swollen state, the reduction must be carried under wet conditions, with a good swelling agent as the solvent. Additionally, the choice of the solvent is restricted from two circumstances: the absence of red-ox activity towards the metallic precursor and an acceptable solubility of hydrogen. In the present Thesis, the solvent used for the reductions with hydrogen is THF, which does not reduce or oxidize the metal precursors and it is a good solvent for the hydrogen at room condition.

The metal-polymer nanocomposites obtain from the ion-exchange step (metalation) were characterized by TEM and elemental analysis (Table 1).

Table 1: Experimental data of the librery

Samples	Metal Precursor	Pd found (wt. %)	d (nm)*
1PdK2621N	$Pd(NO_3)_2$	1.03	7.4
1PdK2621H	$[Pd(NH_3)_4]SO_4$	1.01	6.7
1PdK2621A	$Pd(OAc)_2$	1.03	16.2

* Diameter estimated by lognormal fit on size distribution data

The size distributions of the nanoparticles in the fresh catalysts were assessed by TEM, with at least 250 particles counted for each sample. For all the samples, most

individual aggregates show a spherical morphology and are well dispersed on the polymeric support. They generally show a LogNormal size distribution, with a moderate statistical dispersions (Figure 1). The palladium aggregates of 1PdK2621N and 1PdK2621H samples (Figure 2 and 3, respectively) were featured by similar broad distributions centered a 7.4 and 6.7 nm, respectively.

On the contrary, the Pd nanoclusters of 1PdK2621A have an average diameter of 16.2 nm and a broader size distribution (Figure 4). In the first place it can be observed that 1PdK2621N and 1PdK2621H were prepared from water-soluble precursors taken up from aqueous and that 1PdK2621A was prepared from a precursor taken up from a THF solution. K2621 is macroreticular and only partially sulfonated and the way how it is obtained from the parent polystyrene-divinylbenzene resin, which implies that sulfonic groups are present in only in layers just beneath the pore walls (sulfonation occurs from the surface to the interior). The phenyl rings of the inner part of the polymer mass (the farthest from the pore surface) are not sulfonated. As the consequence K2621 is comprised of hydrophilic "external" (i.e. lying just beneath the pore surface) sulfonated layers, more or less thick, depending on the sulfonation degree, and hydrophobic internal (i.e. lying distant from the pore surface) unsolfonated mass. Although the accessibility of the permanent pore surface of macroreticular SPS resins is practically independent of swelling, the accessibility of the sulfonic groups is not. In fact most of them are bound to the polymer framework, hence are located within the polymer mass, and only a relatively small fraction is just on the pore surface and directly exposed [148]. Accordingly, to make sulfonic groups accessible some swelling is necessary even in macroreticular resins. Due to their relatively high cross-linking degree swelling in macroreticular resins is much less extensive than in the case of gel-type resins, but the presence of permanent pores allows for the absorption of liquids even when they are bad swelling agents. For K2621 this was assessed semi-quantitatively by means of its specific absorbed volume (SAV) in liquids of very different polarity (Table 2).

Table 2: The values of absorbed solvent are reported in ml/g

Form:	Toluene	THF	MeOH	Water
K2621/H^+	0.5	0.5	0.8	1.9
K2621/Na^+	0.2	0.4	0.7	2.0

Water is by far the liquid that is absorbed most. This is because it can effectively swell the sulfonated polymer layer just beneath the pore surface, making it relatively relatively highly accessible. However, as K2621 only is only partially sulfonated water cannot be absorbed in the inner part of the polymer mass, which is hydrophobic. Methanol can also be appreciably absorbed, but it is less polar than water so that its ability to swell the sulfonated polymer layer beneath the pore surface is lower . As the result a smaller amount of methanol is absorbed and the swollen polymer layer is thinner and less accessible than in the case of water. Finally, for THF and toluene the value of SAV corresponds more or less to the total volume of the permanent pores (0.6 ml/g) [149]. and the absorption process corresponds more or less to the simple filling of the pores. THF and toluene could swell the unsulfonated, hydrophobic inner part of the polymer framework, but to do so their molecules should cross the sulfonated, hydrophilic over-layer. This is not the case due to their hydrophobic, rather than hydrophilic, character. The transformation of K2621 into its sodium form, upon neutralization of the sulfonic groups with NaOH, does not substantially affect the behavior of the resin. Only in the case of toluene, the SAV decreases, which could be explained with an increased hydrophilicity of the sulfonated part of the polymer, which includes the pore surface, and a decreased ability to be wet by the least polar solvent (toluene) investigated, which prevents the complete filling of the permanent pores.

According to this findings, when the palladium precursors are taken up from water, they can readily penetrate into the well expanded, sulfonated polymer layer beneath the pore surface. As they were reduced with H_2 dissolved in THF, this layer was much less expanded and the final size of the nanoparticles was effectively limited by the entanglement amongst the polymer chains [147]. Whereas in the case of 1PdK2621H the palladium centers were incorporated as the tetra-amino complex, no ligands were present around Pd^{II} centers in the case of 1PdK2621N. As the consequence, the nanoparticles of 1PdK2621H are somewhat smaller, possibly due to the influence of the good NH_3 ligand on the reduction, nucleation and growth steps. Eventually ammonia, at least in part, was retained in the catalyst (likely as ammonium sulfonate), as shown by the change of the N/S ratio in the XPS spectrum.

With palladium acetate the precursor was taken up from a THF solution. In this case, the sulfonated layer beneath the pore surface was not expanded and was only little accessible top the metal centers, so that they were directly placed onto the pore surface or very close to it. It is therefore likely that during the reduction step palladium centers

back-diffused from the polymer to THF filling the pores, so that the nanoparticles were generated mainly out of the polymer framework and the only steric limit to their growth, if any, was imposed by the diameter of the permanent pores. In this connection, ISEC analysis of the water swollen K2621 resin shows a bimodal pore distribution [32] with centers at 1 and 19 nm, respectively. The latter value is very close to the center of size distribution of nanoparticles for the 1PdK2621A. Although the ISEC data were obtained in water, which is not the medium employed in the reduction step, 19 nm is not compatible with pore diameters in the swollen part of the polymer framework (usually less than 10 nm) [130]. Therefore 19 nm is most likely the diameter of the permanent pores, which is not expected to change too much from one liquid to another, and this suggests that in this catalyst the nanoparticles are formed inside the permanent pores. In conclusion, all these data indicate that the precursor is important in controlling the size of the nanoparticles from at least two points of view. On the one side, the liquid medium for the ion-exchange step must be chosen according its nature and, in particular, its solubility and on this depends the ability, if any, of the metal centers to penetrate inside the polymer framework. When this occurs the polymer framework will exert a relatively high degree of control (most likely for steric reasons) on the size of the nanoparticles during the reduction step (PdK2621H and PdK2621N), otherwise (PdK26121A) the nanoparticles will be formed mostly in the liquid which fills the permanent pores and their size will be larger. On the other side, even in the case of effective size control from the polymer framework (PdK2621H and PdK2621N), the presence of good ligands (e.g. ammonia) helps in achieving smaller nanoparticles, although this effect seems to be less important than the influence of the polymer framework.

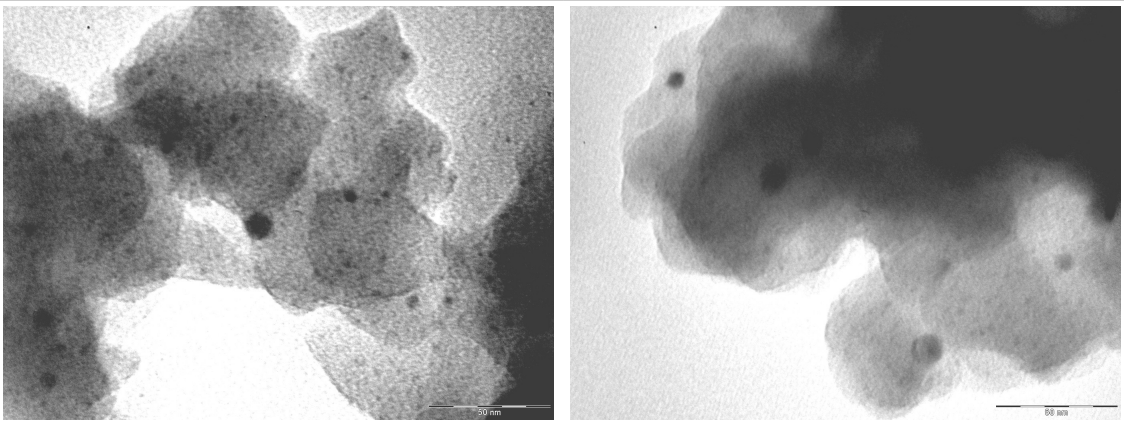

Figure 1: TEM images for fresh 1PdK2621N material. The scale bar is 50 nm.

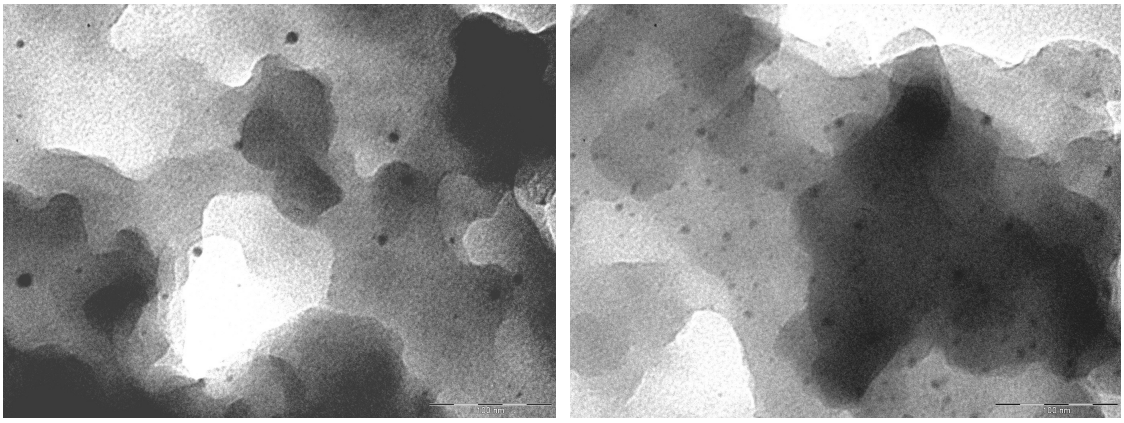

Figure 2: TEM images for fresh 1PdK2621H material. The scale bar is 100 nm.

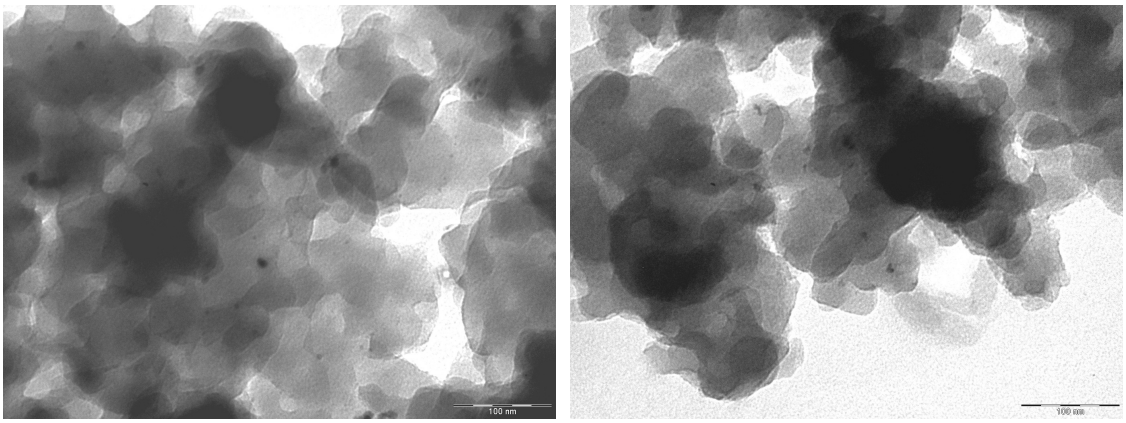

Figure 3: TEM images for fresh 1PdK2621A material. The scale bar is 100 nm.

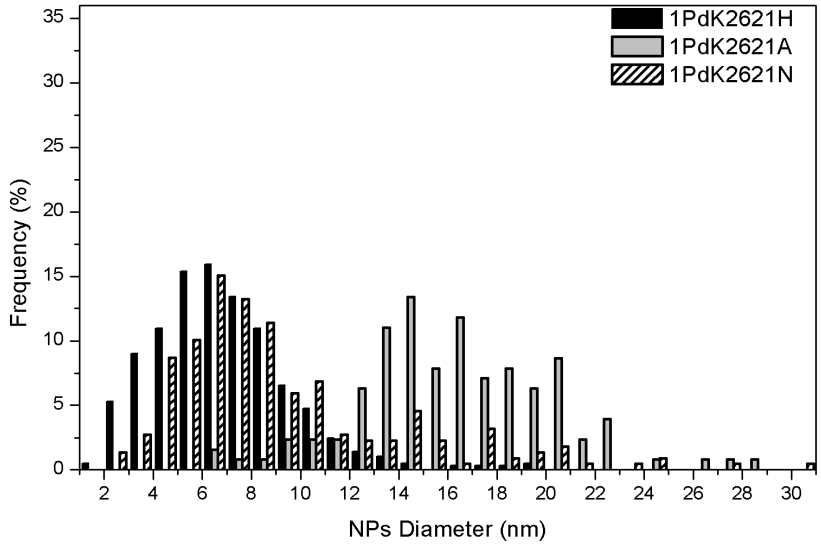

Figure 4: Particle size distributions of the catalysts as prepared, obtained from different metal precursors

The reduction conditions and the strength of reducing agents are a crucial key for the control of the morphological features of metal nanoparticles. The investigation of the relation between the synthesis parameters and the features of the Pd nanoparticles is important to improve the catalytic behavior of materials. For this purpose, a second library of catalysts has been prepared by metalation of K2621 with $[Pd(NH_3)_4]SO_4$ and using different reduction protocols. Samples of Pd^{II} anchored on K2621 are treated with methanol, formaldehyde and sodium borohydride as the reducing agents, to give dark gray materials coded as 1PdK2621M, 1PdK2621F and 1PdK2621B, respectively. The size distributions of the metal nanoparticles of the catalysts are shown in Figure 5. The protocols involving methanol and $NaBH_4$ have been already used in previous investigations, [32] and [150][151]. Additionally, another protocol based on the use of pressurized hydrogen as reductant at mild temperature (60°C) is used (coded as 1PdK2621HpT). The size distribution of the metal nanoclusters obtained with this approach is compared with that of 1PdK2621H sample in Figure 6.

All these metal-polymer nanocomposites were characterized with TEM and elemental analysis (Table 3).

Table 3: Experimental data of the librery

Samples	Reductant	Pd found (wt. %)	d (nm)*
1PdK2621M	MeOH	1.01	5.3
1PdK2621F	HCHO	1.00	8.3
1PdK2621B	$NaBH_4$	1.02	3.8
1PdK2621HpT	H_2	1.02	4.8

* Diameter estimated by lognormal fit on size distribution data

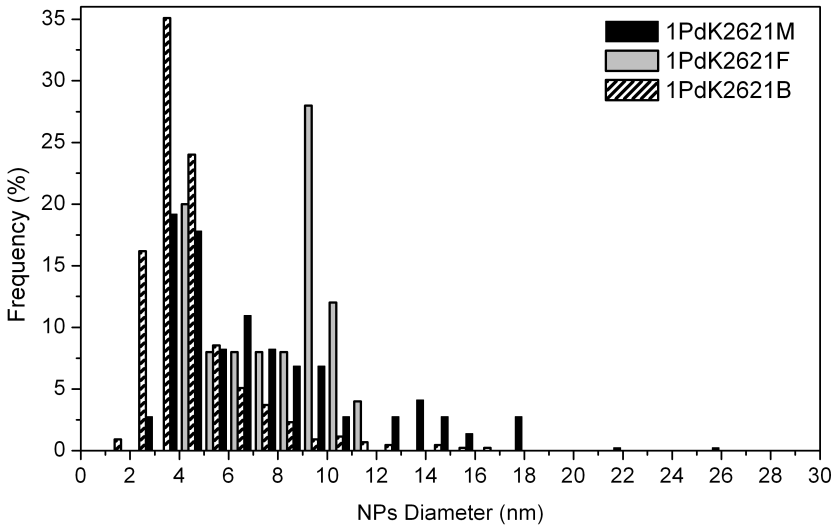

Figure 5: Particle size histograms of the catalysts as prepared, obtained with different reduction protocols.

Figure 5 shows the size distribution of Pd nanoparticles supported on the K2621 resin by treatment with formaldehyde (coded F), methanol (coded M) and sodium borohydride (coded B). Strong reducing agents are not needed for the reduction of noble metals such as Pd and Au: the red-ox potential of these metals is very high and even a moderate reductant is sufficient to generate zero-valent metal atoms. It is well-known that the red-ox properties of alcohols and aldehydes are enough for the reduction of gold and palladium under mild conditions [81]. In a previous work [32], a similar nanocomposite, Pd^0 supported on K2621, prepared by metalation with $Pd(OAc)_2$ and treated with methanol as the reducing agent, was tested with good results in H_2O_2 direct synthesis. The center and the width of the size dispersion seem to mainly depend on the kinetic of reduction. The sample prepared with the strongest reductant, the sodium borohydride, shows a narrow size distribution centered at 3.8 nm, whereas that one reduced with methanol produces a remarkably broader distribution centered at higher average diameter (5.3 nm). In both the materials, a few aggregates of nanoparticles can be also observed (Figure 7b). Additionally, the use of the methanol as the reducing agent seems to produce a remarkable number of non-spherical nanoclusters (Figure 8a). The formaldehyde is a reducing agent of intermediate strength and produces a size distribution centered at the highest average diameter (8.3 nm), but this statistical result is probably affected by an insufficient number of counted nanoparticles. With respect the previous samples (Figure 6a), in this sample the metal nanoparticles seem differently distributed within the polymer support and a large number of Pd nanoclusters

are deeply embedded inside the polymer matrix. In any case these samples prepared in polar environments (water or methanol) show much smaller nanoparticles as compared with PdK2621A, prepared in THF, showing again that "hydrophilic" conditions for the ion-exchange step are the most favorable to achieve relatively little nanoparticles.

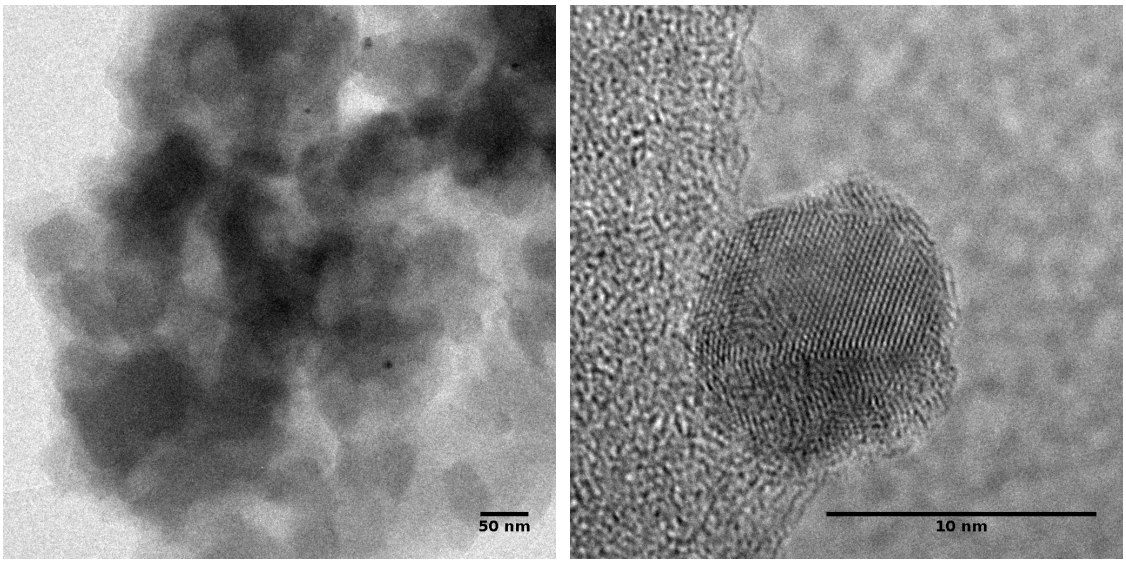

Figure 6: TEM images for fresh 1PdK2621F material.

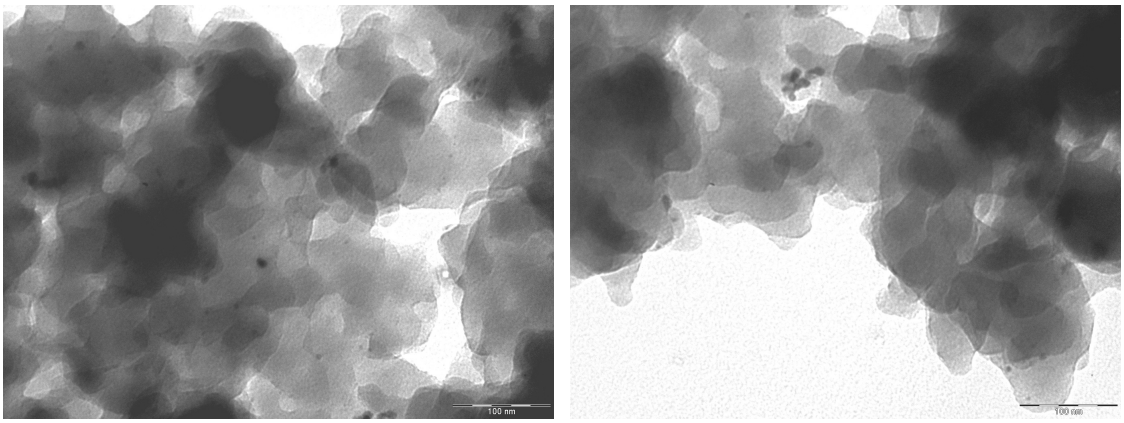

Figure 7: TEM images for fresh 1PdK2621B material. The scale bar is 100 nm.

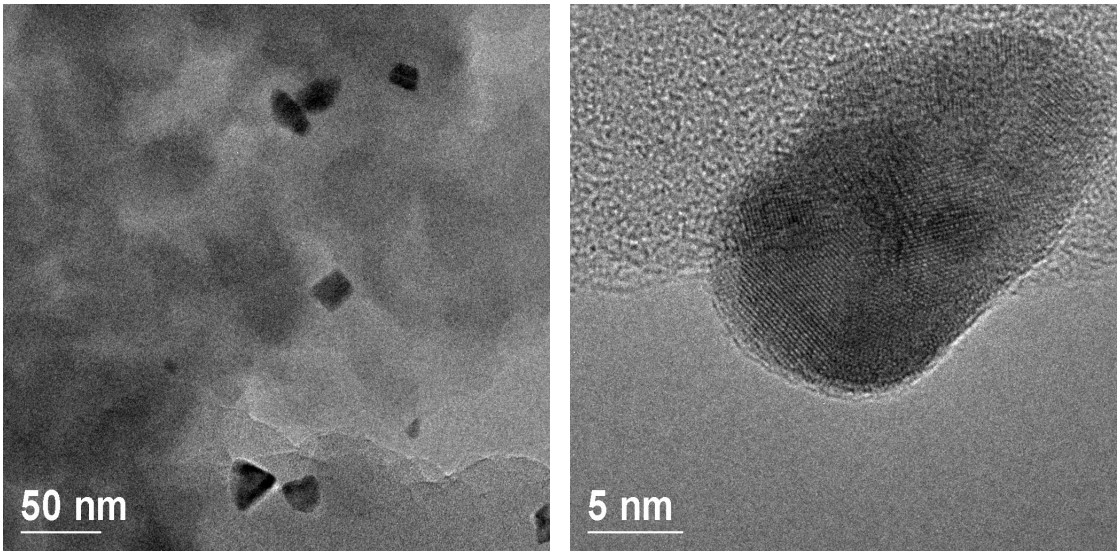

Figure 8: TEM images for fresh 1PdK2621M material.

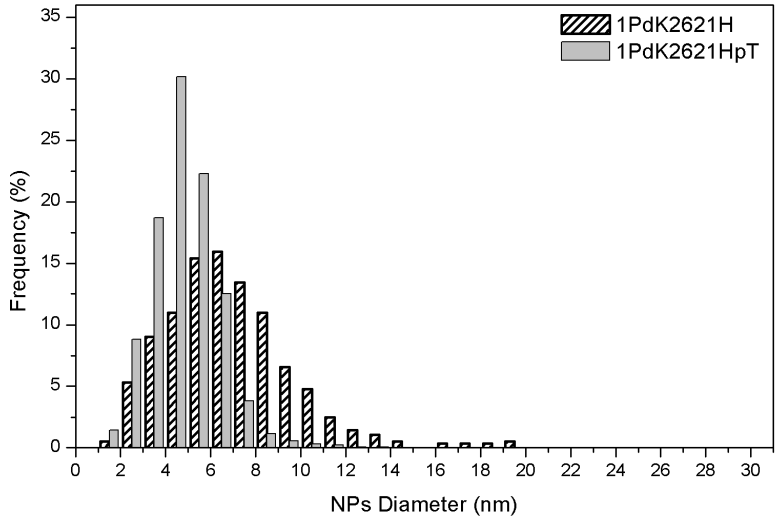

Figure 9: Particle size distributions of 1PdK2621HpT vs. 1PdK2621H samples

Figure 9 shows the size distributions of nanoparticles obtained from the samples reduced with hydrogen, one of which prepared in autoclave (coded HpT) at 5 bar and 60 °C. Both the size distributions have a LogNormal shape, but 1PdK2621HpT has a both a narrower dispersion and nanoparticle size, with the highest population at 4.8 instead of 6.7 nm. These results are consistent with the hypothesis that a higher reduction rate of metal precursor generates nanoparticles with smaller diameter [61]. Therefore the total number of counted Pd aggregates is remarkable higher for the 1PdK2621HpT sample, indicating that this reduction protocol generates a higher number of nanoparticles in the outer portion of polymer particle.

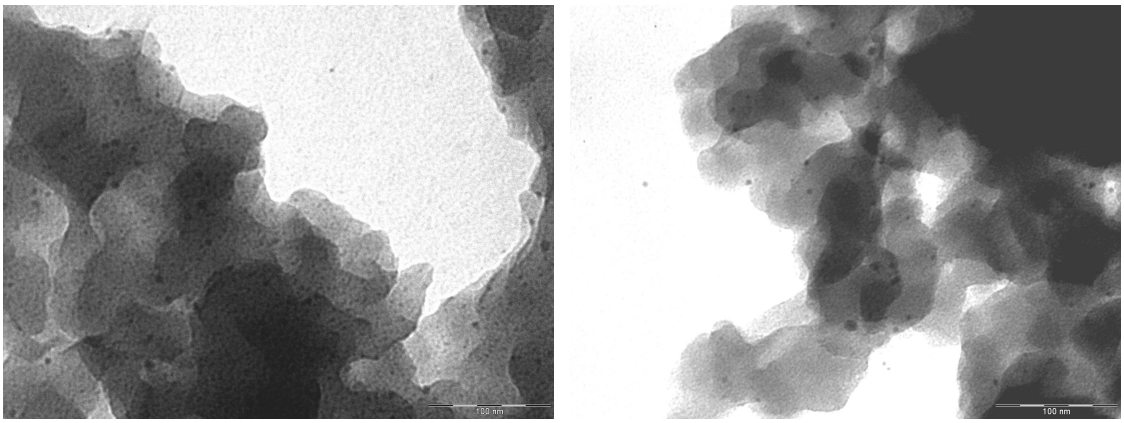

Figure 10: TEM images for the 1PdK2621HpT material, as prepared. The scale bar is 100 nm.

Catalytic performances

The catalytic effect in DS due to the type of metal precursor used in the preparation of materials is illustrated in Figure 11 and 12, as concentrations of products (H_2O_2 and water) and conversion/selectivity as the function of time, respectively. A commercial available catalyst, 1wt.% Pd on carbon, is used as reference.

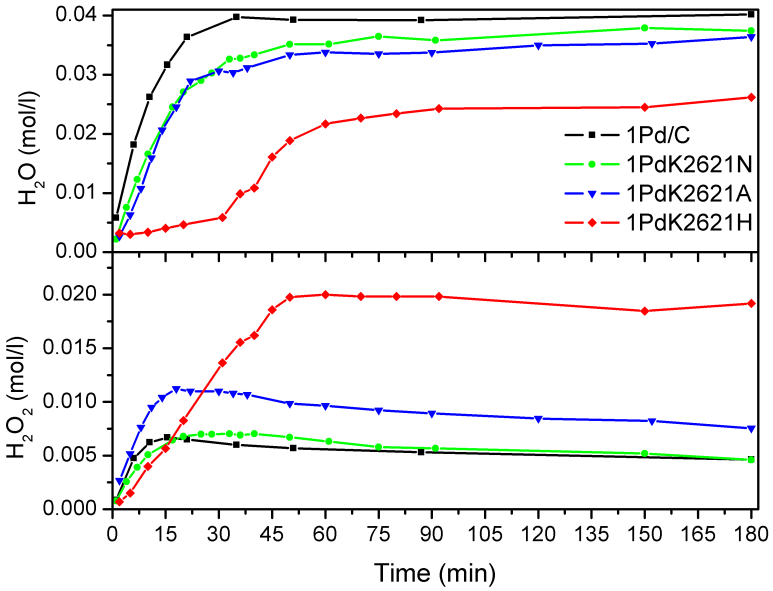

Figure 11: Molar concentrations of water and H_2O_2 during the experiments.

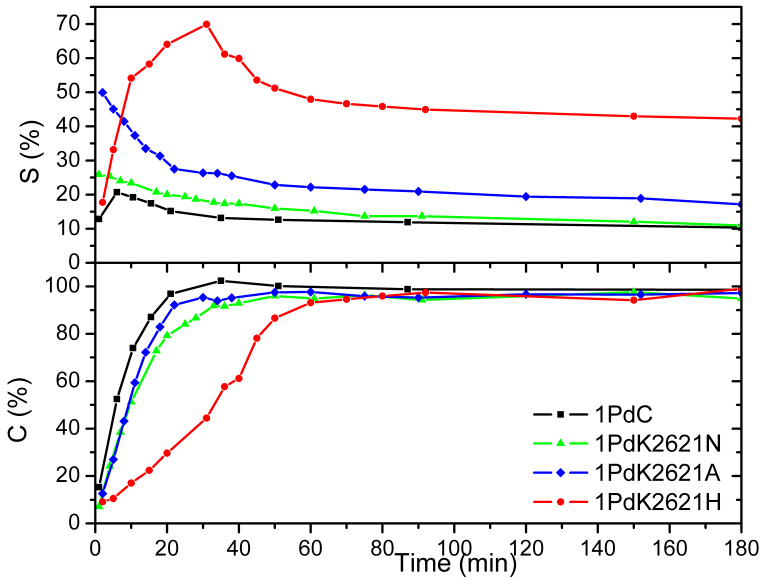

Figure 12: Conversion (%) and selectivity (%) of catalysts.

During the catalytic test, hydrogen (the limiting reagent) is consumed in DS (Figure 13, eq. 1), in direct synthesis of water (Figure 13, eq. 2) and in hydrogenation of hydrogen peroxide (Figure 13, eq. 3), as in the figure 13. In addition, it is also considered the dismutation of hydrogen peroxide (Figure 13, eq. 4), which does not consume hydrogen, but hydrogen peroxide to form water. On basis of these stoichiometric ratios, it is possible to follow the total process by the production of H_2O_2 and water. The concentrations of the two products are determined by independent titrations, but in particular the water is estimated by Karl Fisher titration, which is not trivial. As a matter of fact, the cumulative yield was found to be sometimes above 100 % which suggests that its values could be systematically overestimated.

$H_2 + O_2 \rightarrow H_2O_2$ $\quad r_1 = -d[H_2]_1/dt = d[H_2O_2]_1/dt$ (eq. 1)

$H_2 + ½\ O_2 \rightarrow H_2O$ $\quad r_2 = -d[H_2]_2/dt = d[H_2O]_2/dt$ (eq. 2)

$H_2O_2 + H_2 \rightarrow 2\ H_2O$ $\quad r_3 = -d[H_2]_3/dt = -d[H_2O_2]_3/dt = ½ \cdot d[H_2O]_3/dt$ (eq. 3)

$H_2O_2 \rightarrow H_2O + ½\ O_2$ $\quad r_4 = -d[H_2O_2]_4/dt = d[H_2O]_4/dt$ (eq. 4)

$-d[H_2]_{tot}/dt = r_1+r_2+r_3$ $\quad d[H_2O_2]_{tot}/dt = r_1-r_3-r_4$ $\quad d[H_2O]_{tot}/dt = r_2+2 \cdot r_3+r_4$

Figure 13: the single reactions which form the process and their rates.

In Figure 11 and 12, the product concentration and the H_2 conversion curves show that the catalytic runs can be divided into two well distinguished stages for all the catalysts. The increase of the concentration of products is relatively fast in the first stage and is much slower, if any is observed, in the second (Figure 11). In second stage, the amount of hydrogen peroxide in the second stage decreases either slowly or not at all and the amount of water slowly increases. In this case, the conversion is approximately constant with time.

The decrease of concentration of hydrogen peroxide in the second stage is practically due to the only reaction which takes place when the hydrogen is over, the dismutation of H_2O_2 (Figure 13, eq. 4). Accordingly, the analysis of the kinetic plot from the point of maximum H_2O_2 concentration onward allows to estimate the kinetic constant of the dismutation. The logarithm of the concentration of hydrogen peroxide in the second stage decreases linearly with time (Figure 2), showing that the reaction is first order in H_2O_2.

$$-d[H_2O_2]/dt = k'_{app}\cdot[H_2O_2] \qquad \text{(eq. 5)}$$

The apparent pseudo-first order kinetic constants (k'_{app}) can be easily extracted from the plots using the integral kinetic law:

$$\ln\{[H_2O_2]\} = \ln\{[H_2O_2]_0\} - k'_{app}\cdot t \qquad \text{(eq. 6)}$$

However, in the apparent constants depend on the concentration of the catalyst. For a homogeneous reaction the differential kinetic law can be expressed as:

$$-d[H_2O_2]/dt = k''\cdot[H_2O_2]\cdot[cat] \qquad \text{(eq. 7)}$$

Our system is not homogeneous, but the reaction was carried out with the catalyst suspended in the liquid phase and efficiently dispersed throughout its whole volume. Under these condition we can assume that the macroscopic catalysts concentration can be calculated as the ratio between the number of moles of metal and the volume of the liquid phase and that equation 7 holds also in our system, with $[H_2O_2]$ and [cat] corresponding to their macroscopic values in the liquid, provided that the diffusion and the adsorption of H_2O_2 are not determining. Under this point of view it can be appreciated that no gas are involved as reagents in the dismutation and that H_2O_2 is formed in the catalyst, hence kinetic control conditions are the most likely. The apparent first-order constant (k'_{app}) and the second-order one are shown in the table 3. These constants indicate that the dismutation of H_2O_2 is slow and contributes very little to its consumption, especially for the 1PdK2621H sample. Whereas for the other catalysts it is practically always the same, in this case it is one order of magnitude lower

Table 3: Kinetic constants of H_2O_2 dismutation estimated from catalytic data.

	1PdK2621N	1PdK2621A	1PdK2621H
k'_{app} (h^{-1})	0.150	0.115	0.032
k'' ($dm^3\cdot mmol^{-1}\cdot h^{-1}$)	4.41	3.38	0.95

The analysis of the initial overall rates of reactions is obtained from the slopes of the plots of the cumulative yield of the products, which is directly related to the consumption of hydrogen, in the first stage of the reaction. This allows to compare the

effect due to the preparation (i.e. the metal precursors) on the activity of the catalysts. It was carried out in the first 10-30 min, depending on the catalyst. In this range all the concentrations changed linearly with time and the sum of the concentrations of hydrogen peroxide and water changed at a rate corresponding effectively to the sum of the individual rates of accumulation of the two products (Fig. 14).

All the catalytic tests were carried out with the same amount of palladium and the initial activity of the catalysts was assessed as the cumulative amount of products per mole of palladium and unit time (Table 4).

Table 4: Initial performances of the palladium catalysts supported on K2621.

Cat.	Employed Pd amounts	Initial cumul. rate[b]	Initial cumul. productivity[c] vs Pd	Initial H_2O_2 productivity[d]	Initial Selectivity [e]
1PdK2621N	1.43	135.0	3964	944	24
1PdK2621A	1.43	135.9	3992	1618	40
1PdK2621H	1.42	38.7	1145	747	65

a: $mol \cdot 10^5$; b: $mmol(H_2O_2+H_2O) \cdot dm^{-3} \cdot h^{-1}$; c: $mol_{(H2O2+H2O)} \cdot mol^{-1}_{(Pd)} \cdot h^{-1}$; d: $mol_{(H2O2)} \cdot mol^{-1}_{(Pd)} \cdot h^{-1}$; e: %.

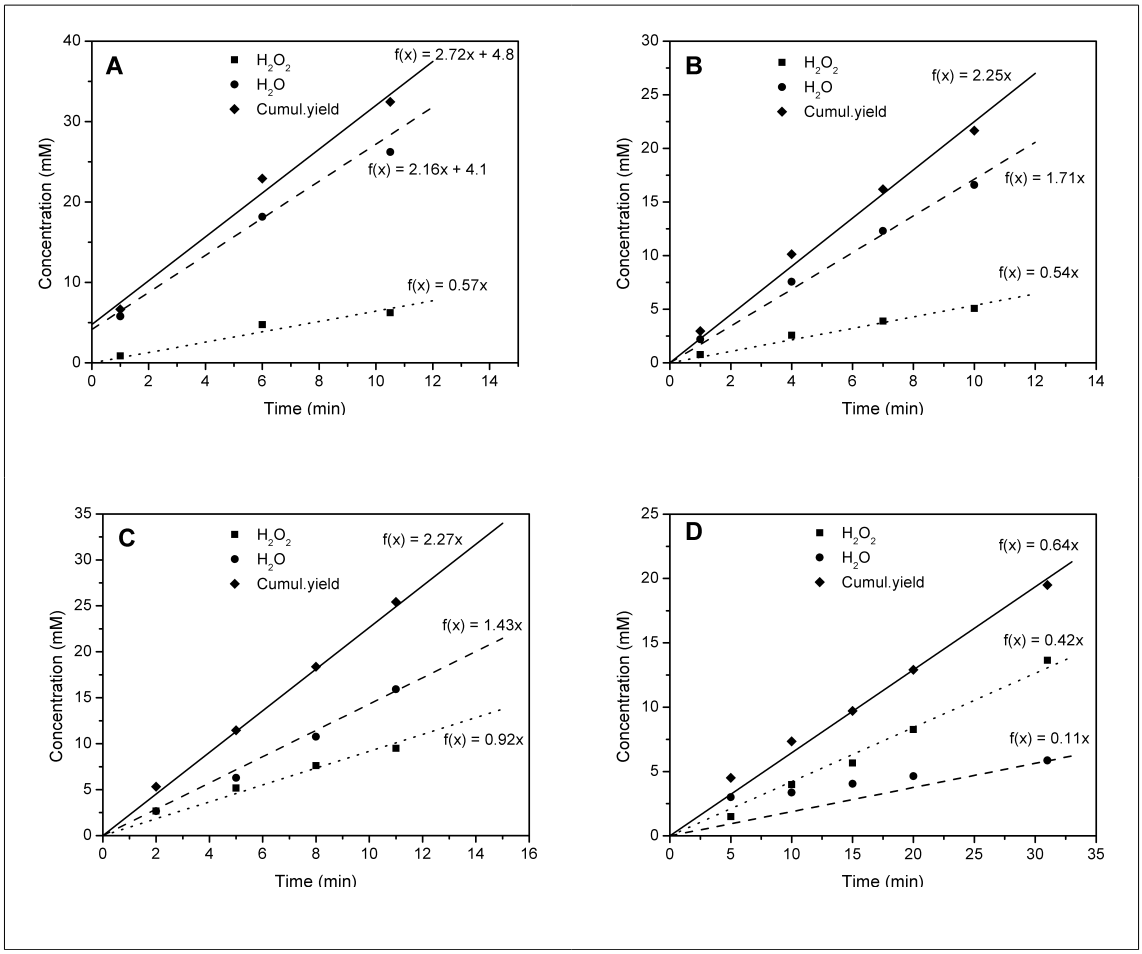

Figure 14: Initial performances of catalysts 1PdC (A), 1PdK2621N (B), 1PdK2621A (C) and 1PdK2621H (D), estimated by fitting of cumulative (H_2O_2 + H_2O, diamonds) and single product concentrations (H_2O, circles; H_2O_2 squares)

The analysis of the initial reaction rates allows also to estimate the selectivity towards hydrogen peroxide in the first minutes of reaction (Table 4, last column), as the ratio between the slopes of the H_2O_2 concentration and of the cumulative concentration lines of Figure 14.

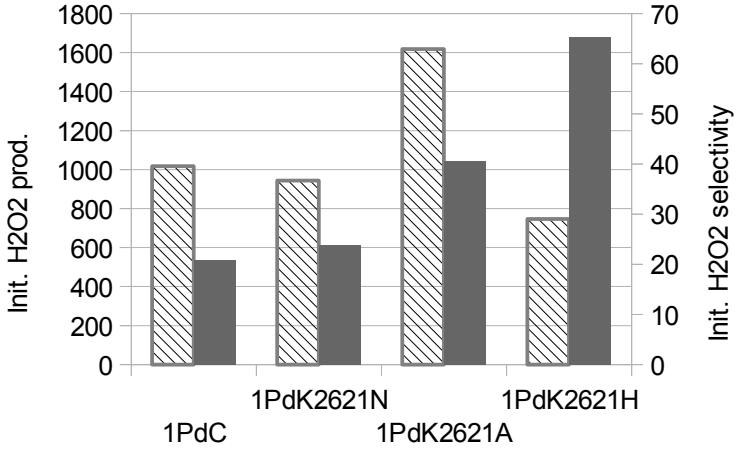

Figure 15: Initial performance of the library

The initial selectivity of the 1PdK2621N, 1PdK2621A and 1PdK2621H samples are 24, 40 and 65 %, respectively, and then they steadily decreases with time (Figure 12). The selectivity increases if in the order $Pd(NO_3)_2$ < $Pd(OAc)_2$ < $[Pd(NH_3)_4]SO_4$ are used as metal precursor. From the TEM analysis and relative size distributions of nanoparticles discussed in the previous paragraph, it appears that:

1) the nanoparticles in 1PdK2621A F seem to be situated on the surface of the macropores or very close to it, so that there is substantially little size control due to the polymeric framework. This kind of distribution of the metal and its broad size distribution could account for the high initial productivity in both the products and of the moderate rate of dismutation over this catalyst, leading to a poor selectivity in hydrogen peroxide.

2) the nanoparticles in 1PdK2621N and 1PdK2621H are embedded in the polymer framework of the resin, which could implies a better size control. In this case the difference in the catalytic performance could arise from the nature of the metal

precursor. The formation of noble metal nanoparticles is a complex process, as reported by Finke *et al.* [75], in which it can be difficult to rationalise the role of the other species present during the reduction of the precursor, e.g. the ligands of metal precursor. In this case it seems the use of palladium nitrate as precursor produces nanoparticles a much more defective surface, hence richer in catalytic sites, than those obtained by tetraaminopalladium complex, making the catalyst more active, but less selective towards H_2O_2. In fact, the initial cumulative productivity of 1PdK2621N is as high as that of 1PdK2621A and 3.5-fold higher than that of 1PdK2621H, but the initial H_2O_2 one is into a smaller range of values.

Interestingly, the initial trend of H_2O_2 selectivity is usually decreasing with time, but in case of 1PdK2621H sample, it increases up to 70% at 35 minutes (and 50% of H_2 conversion) and then rapidly decreases up to 50% when the hydrogen is over. This singular behaviour has been the object of further investigation by TEM analysis on the used catalyst (Figure 16). The size distribution of the used catalyst is broader with an average size which has moved to 10 nm (from 6.7 nm), indicating that the nanoparticles undergo appreciable structural changes also within the polymer framework during the DS process. This could be due in the first place to sintering, as already reported by Abate *et al.* [152].

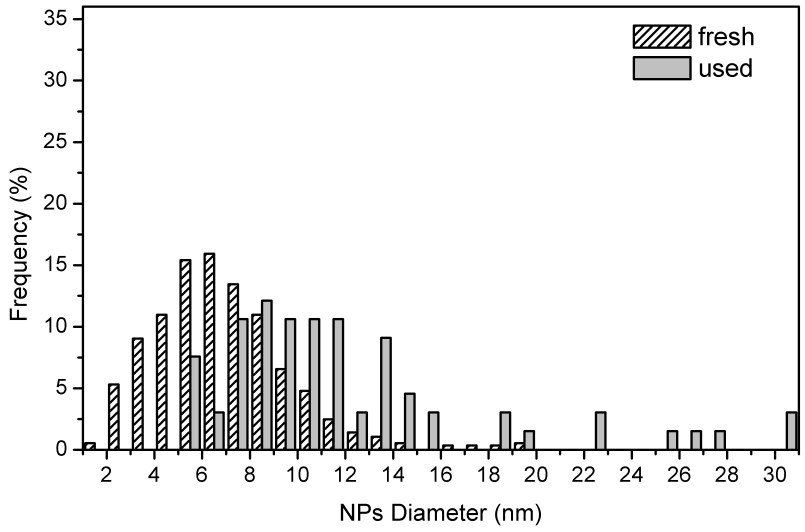

Figure 16: Size distribution of fresh and used 1PdK2621H catalyst.

The remarkable results obtained with 1PdK2621H material has attracted the attention on an other important phase in the preparation of the metal-polymer nanocomposite: the reduction protocol. The strength of the reductant and the

experimental conditions can play a crucial role on the final features of the nanoparticles. To take an insight, a second library of materials was prepared by metalation of K2621 with $[Pd(NH_3)_4]SO_4$.

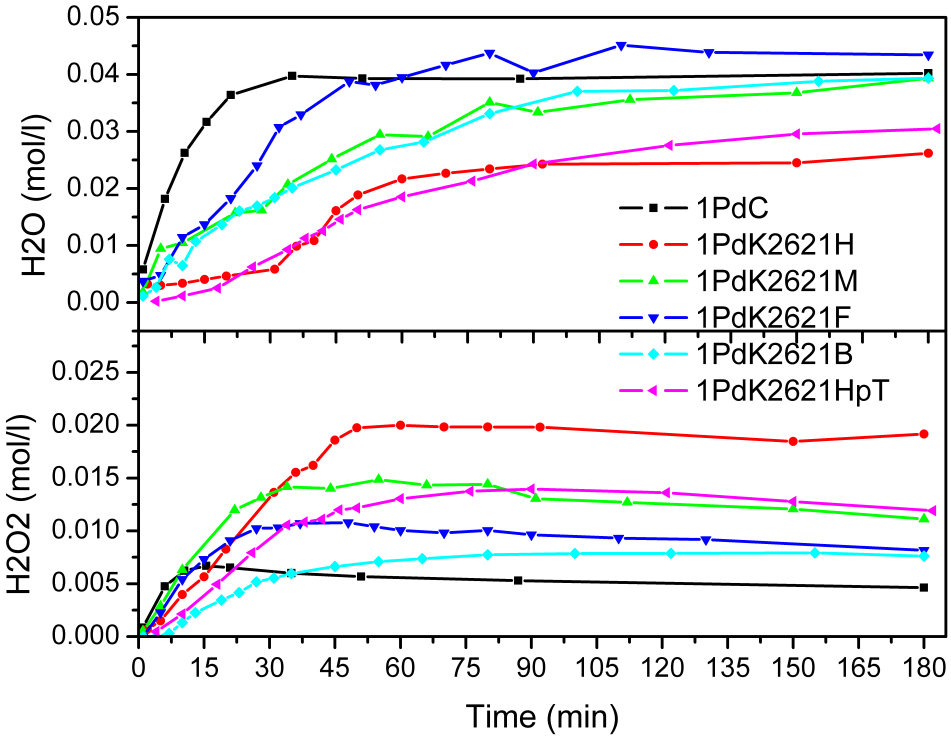

Figure 17: Molar concentrations of water and H_2O_2 during the experiments.

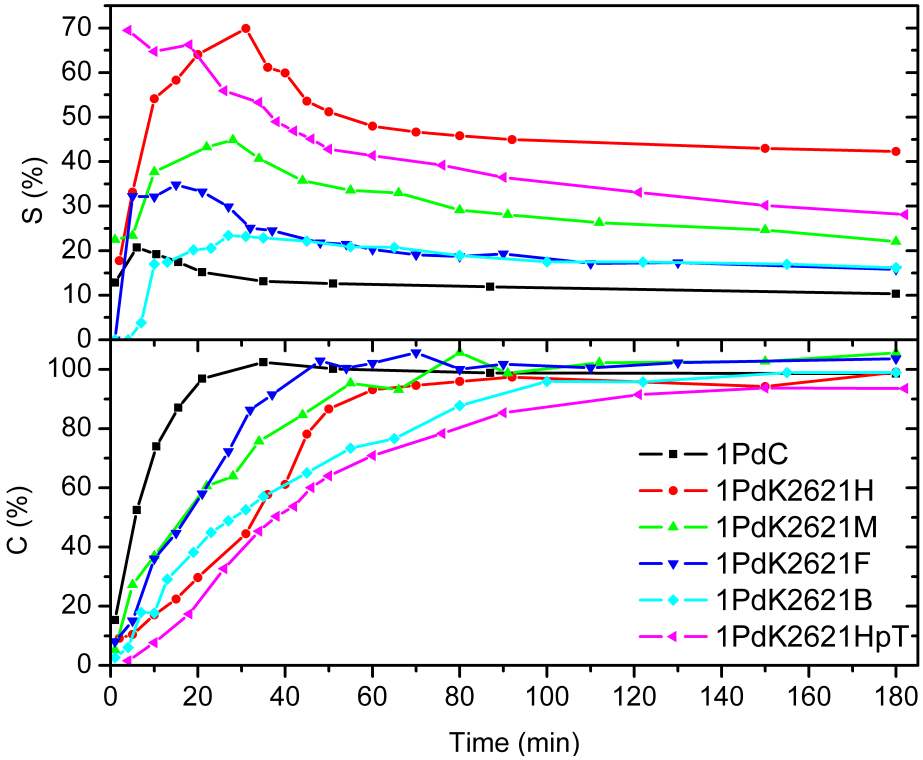

Figure 18: Conversion and selectivity (%) of catalysts in DS.

A number of water soluble reducing agents of different strength were employed, such as methanol, formaldehyde and sodium borohydride. Whereas sodium borohydride is a strong and reactive reducing agent and was used at room temperature, the other two required heating of their solutions to reflux temperature. In addition to these, another protocol was employed: a reduction carried out in autoclave at 60°C with 5 bar of hydrogen.

This library of catalysts was tested in DS of hydrogen peroxide in the same previous condition and the results are shown in Figure 17 and 18, including also the performance of two references, as 1PdK2621H and 1 wt.% Pd/C. These results are shown as change of concentration of water and H_2O_2 (Figure 17), from which it is possible to estimate the values of H_2 conversion and H_2O_2 selectivity (Figure 18). As already reported for the previous set of catalysts, two clearly distinguished stages feature the catalytic runs for all the catalysts. The increase of the concentration of products is relatively slower than the previous results, indicating generally this library of catalysts is less active, except for 1PdK2621F sample. In the first stage, the initial increase of the H_2O_2 concentration is quite similar for all the catalysts, whereas remarkable difference between the materials appears in the production of water (Figure 17).

The analysis of the initial overall rates of reactions, obtained from the slopes of the plots of the cumulative yield of the products, allows to compare the effect due to the use of different reduction protocols on the activity of the catalysts. In range of the first 10-20 minutes of reaction, all the concentrations changed quite linearly with time and the sum of the concentrations of hydrogen peroxide and water, which is directly related to the consumption of hydrogen, changed at a rate corresponding effectively to the sum of the individual rates of accumulation of the two products (Figure 19).

All the catalytic tests were carried out with the same amount of palladium and the initial activity of the catalysts was assessed as the cumulative amount of products per mole of palladium and unit time (Table 5).

Table 5: Initial performances of the palladium catalysts supported on K2621.

Cat.	Employed Pd amount[a]	Initial cumul. rate[b]	Initial cumul. productivity[c] vs Pd	Initial H_2O_2 productivity[d]	Initial Selectivity[e]
1PdK2621M	1.42	110.3	3262	1100	34
1PdK2621F	1.45	83.4	2416	904	37
1PdK2621B	1.44	60.1	1754	563	32
1PdK2621HpT	1.45	29.2	847	560	66

a: $mol \cdot 10^5$; b: $mmol(H_2O_2+H_2O) \cdot dm^{-3} \cdot h^{-1}$; c: $mol_{(H2O2+H2O)} \cdot mol^{-1}_{(Pd)} \cdot h^{-1}$; d: $mol_{(H2O2)} \cdot mol^{-1}_{(Pd)} \cdot h^{-1}$; e: %.

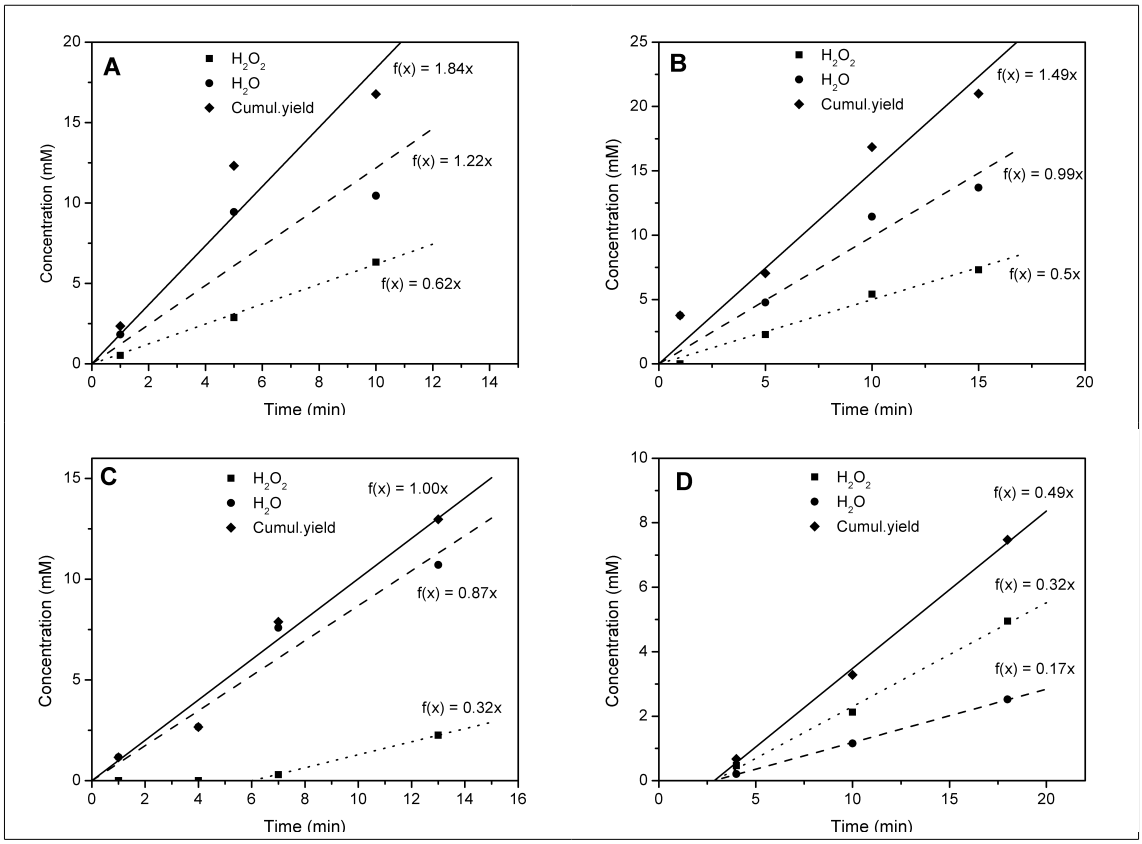

Figure 19: Performances of catalysts 1PdK2621M (A), 1PdK2621F (B), 1PdK2621B (C) and 1PdK2621HpT (D), estimated by fitting of initial cumulative (H_2O_2 + H_2O) and single product concentrations

1PdK2621M sample shows a relatively high cumulative rate of products, lower only to those of 1PdK2621N and 1PdK2621A, and also the highestH_2O_2 productivity (Table 5), involving a moderate initial selectivity. 1PdK2621F is initially less active and more selective than 1PdK2621M, mainly due to the lower cumulative productivity. The performances of these two catalysts change when over the 40% of the hydrogen is consumed: both decrease their selectivity, dramatically for 1PDK2621F, probably due to

the increase of the contribute of H_2O_2 hydrogenation (Figure 18). The size distribution of two catalysts are quite similar (Figure 5), but the sample of 1PdK2621M seems to have less defective nanoparticles located in a region of the polymer matrix close to the macropore surface. This could allow a relatively fast diffusion of hydrogen peroxide from the inner region of catalyst towards the bulk solution. On the other hand, the nanoparticles of 1PdK2621F, which seem to be deeply embedded in the matrix (Figure 6), could be able to consume H_2O_2 more rapidly than those of 1PdK2621M due to stronger diffusive constrains.

The activity of 1PdK2621B is even lower (Table 5), but with a similar initial selectivity. In the first six minutes, either the only active reaction is the combustion of hydrogen or hydrogen peroxide is immediately consumed as soon as it is formed (Figure 19-C). The build up of H_2O_2 starts later, but its productivity is less of 50% than that of 1PdK2621M. Although the average diameter of the metal nanoparticles is relatively small (3.8 nm, Figure 5), the total activity of this catalyst is poor. Also in this case effective diffusion restrictions could affect the catalytic performances.

The 1PdK2621HpT is as selective as 1PdK2621H, but is appreciably less active (in fact it is the least active catalysts in both the libraries) (Figure 20). It exhibits a clear induction time of about 5 minutes for all the reaction, also for the direct synthesis of water. Although the origin of this induction is unclear at the moment, this implies that some activation is required and this could account for its relatively low activity in comparison with the other catalysts.

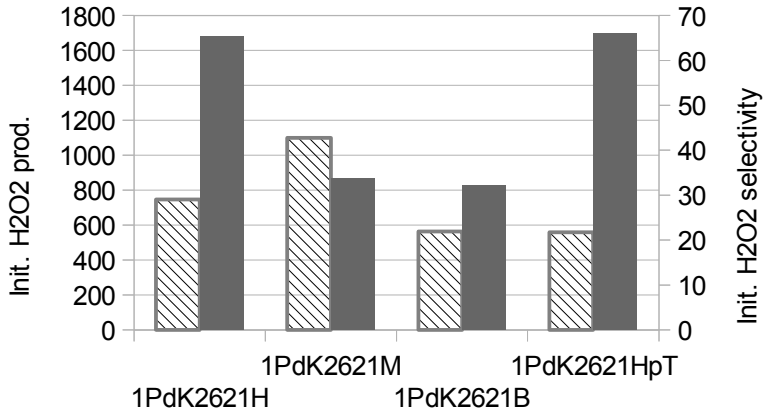

Figure 20: Initial performance of the second librery

The use of hydrogen as reductant at super-atmospheric pressure allows to obtain metal nanoparticles with a narrower size distribution but a lower total catalytic activity and, nevertheless, the same relative productivity in H_2O_2.

The second stage of the catalytic test, i.e. when the hydrogen is over and the dismutation of H_2O_2 is the only active reaction (Figure 18), should show a conversion approximately constant with time. This behaviour, exhibited from 1PdK2621M and 1PdK2621F materials, allows to estimate the apparent first-order constant (k'_{app}) (eq. 5 and 6) of dismutation (Table 6). The 1PdK2621B and 1PdK2621HpT samples do not completely consume the hydrogen in 180 minutes, therefore it is not possible to carry out this analysis.

Table 6: Kinetic constants of H_2O_2 dismutation estimated from catalytic data.

	1PdK2621M	1PdK2621F	1PdK2621B	1PdK2621HpT
k'_{app} (h^{-1})	0.104	0.120	n.d.	n.d.
k" ($dm^3 \cdot mmol^{-1} \cdot h^{-1}$)	3.1	3.4	n.d.	n.d.

These two catalysts show a low activity in dismutation, comparable with those of the previous library, except the 1PdK2621H material. Accordingly, the reduction protocol is a fundamental parameter for the preparation of an effective catalyst, which is able to exhibit a remarkable selectivity in direct synthesis of hydrogen peroxide, reducing the activity of the side reactions.

CHAPTER 3

The effect of the reduction with hydrogen on a library of bimetalic catalysts Pd-Au and Pd-Pt and their catalytic performances in direct synthesis

The design of the catalyst has been so far the main tool employed to resolve the selectivity vs. safety dilemma and a lot of studies on this topic have been continuously appearing in the literature. Most of them are devoted to palladium or bimetallic palladium/gold catalysts supported onto a number of different solids, such as SiO_2 [153], TiO_2 [42], ZrO_2 and CeO_2 [17][28], carbon [41] and ion-exchange resins (sulfonated polystyrene-divinylbenzene) [31][32][33]. Colloidal palladium [36][154] and gold-palladium systems were also reported as highly active in the DS [155].

The bimetallic supported catalysts showed particularly promising results. Pd/Au systems were accurately carefully investigated, showing the benefits of the gold promotion of palladium [6][42][155]. Although bimetallic platinum-palladium systems have been reported in the patent literature [156] more often than the gold-palladium ones, they received comparatively much smaller attention in the open literature [15][17]. Pd-Pt/SiO_2 catalysts (Pd/Pt = 95/5, mol/mol) showed excellent results, with a 2.5-fold increase in the production of H_2O_2 and only a slight decrease of the selectivity in comparison with unpromoted catalyst [15], but the addition of higher amounts of platinum resulted in a significant decrease of the selectivity.

It has been already shown in our laboratories that reduced palladium catalysts (1 %, w/w) supported by the macroreticular ion-exchange resin Lewatit K2621% are excellent catalysts for the DS in absence of acids and halides, performing better than Pd/SiO_2 catalysts [32]. We report herein a detailed investigation on the performance of Au/Pd and Pt/Pd catalysts supported on the same K2621 resin in the DS. All the reported catalysts contain 1 % (w/w) palladium, but the content of either gold or platinum differs from one to another (for gold 0.25 %, 0.5 % and 1 %, w/w; for platinum 0.1 %, 0.25 %,

0.5 % and 1 % w/w). Bromide or chloride ions in combination with an acid are effective promoters, which can enhance the selectivity [39], but their presence could hinder the real catalytic behaviour of the pristine catalyst, making difficult its optimization. For this the presence of halides was accurately avoided both in the preparation of the catalysts and in the catalytic tests. Under halide-free conditions the best results in terms of production rate and selectivity were obtained with Au-Pd/K2621 catalysts. The dismutation of H_2O_2 was also investigated to evaluate its contribution to the overall reaction rate in the direct synthesis.

Lewatit K2621 is a macroreticular, sulfonated polystyrene-divinylbenzene (S-PSDVB) resin. It possess permanent meso- and macropores both in the dry and in the swollen state and is a strongly acidic ion-exchanger, with an exchange capacity of 1.92 mmol/g. [32].

S-PSDVB resins have several features making them attractive supports for DS catalysts. The introduction of the metal precursors in the support can be easily accomplished with a simple ion-exchange between the counter-ions of the sulfonic groups (H^+ or Na^+, for instance) and cationic metal complexes. The reduction of the precursors to the metals takes place inside the polymer framework, which is able to control the dispersion, the size and, therefore, the catalytic properties of the metal nanoparticles. Under this respect, macroreticular resins like K2621 are less effective than gel-type ones, but the latter have no permanent porosity in the dry state and accessibility of the metal surface is strongly dependent on their swelling behaviour. By contrast, the permanent meso- and macropores of macroreticular make the diffusion of reagents and products less dependent on the polymer swelling and generally faster. In this connection, a good support must ensure that back-diffusion of hydrogen peroxide away from the metal surface is fast in comparison to its hydrogenation and dismutation.

Pt-Pd/K2621 materials

Bimetallic Pt-Pd systems have been reported as effective catalysts for the DS in both the open [15][17][157] and the patent [156] literature. The optimal Pt/(Pt+Pd) ratio was found to be close to 0.05 in several different systems [15][17][157] With this background we prepared a library of bimetallic Pd/Pt catalysts with a fixed palladium load (1 %, w/w) but different amounts of platinum (0, 0.1, 0.25, 0.5, 1 %, w/w), corresponding to ca. 0,

0.054, 0.135, 0.27 and 0.54 Pt/(Pt+Pd) ratios. The use of the cationic complexes $[Pd(NH_3)_4]^{2+}$ and $[Pt(NH_3)_4]^{2+}$ allowed the straightforward metalation of K2621 by ion exchange from aqueous solutions of their nitrate and sulfate, respectively. The ICP analysis of the filtrate after the ion-exchange reaction and the final washings of the metalated resin showed that K2621 took up the metal precursors quantitatively. The nanoclusters were eventually obtained upon reduction of the metal precursors with refluxing 37 % aqueous formaldehyde. This very simple method of preparation gave catalysts which were tested in the DS of hydrogen peroxide with no selectivity enhancer added.

The activity of the catalysts is illustrated as the cumulative yield of the products as the function of time (Figure 1). The cumulative yield is directly related to the consumption of hydrogen, as shown by the mass balance of the latter, which is the limiting reagent.

$H_2 + O_2 \rightarrow H_2O_2$ $\quad r_1 = -d[H_2]_1/dt = d[H_2O_2]_1/dt$ (eq. 1)

$H_2 + ½\ O_2 \rightarrow H_2O$ $\quad r_2 = -d[H_2]_2/dt = d[H_2O]_2/dt$ (eq. 2)

$H_2O_2 + H_2 \rightarrow 2\ H_2O$ $\quad r_3 = -d[H_2]_3/dt = -d[H_2O_2]_3/dt = ½ \cdot d[H_2O]_3/dt$ (eq. 3)

$H_2O_2 \rightarrow H_2O + ½\ O_2$ $\quad r_4 = -d[H_2O_2]_4/dt = d[H_2O]_4/dt$ (eq. 4)

$-d[H_2]_{tot}/dt = r_1+r_2+r_3$ $\quad d[H_2O_2]_{tot}/dt = r_1-r_3-r_4$ $\quad d[H_2O]_{tot}/dt = r_2+2 \cdot r_3+r_4$

In fact, H_2 is consumed in the direct synthesis, in the combustion of hydrogen and in the hydrogenation of hydrogen peroxide. In the latter two moles of water are formed per mole of reacted hydrogen, but at the same time one mole of hydrogen peroxide is consumed, so that the cumulative product moles correspond to the moles of reacted hydrogen. The dismutation of hydrogen peroxide does not bring about any change in the sum of the two products, as each mole of decomposed hydrogen peroxide produces one mole of water.

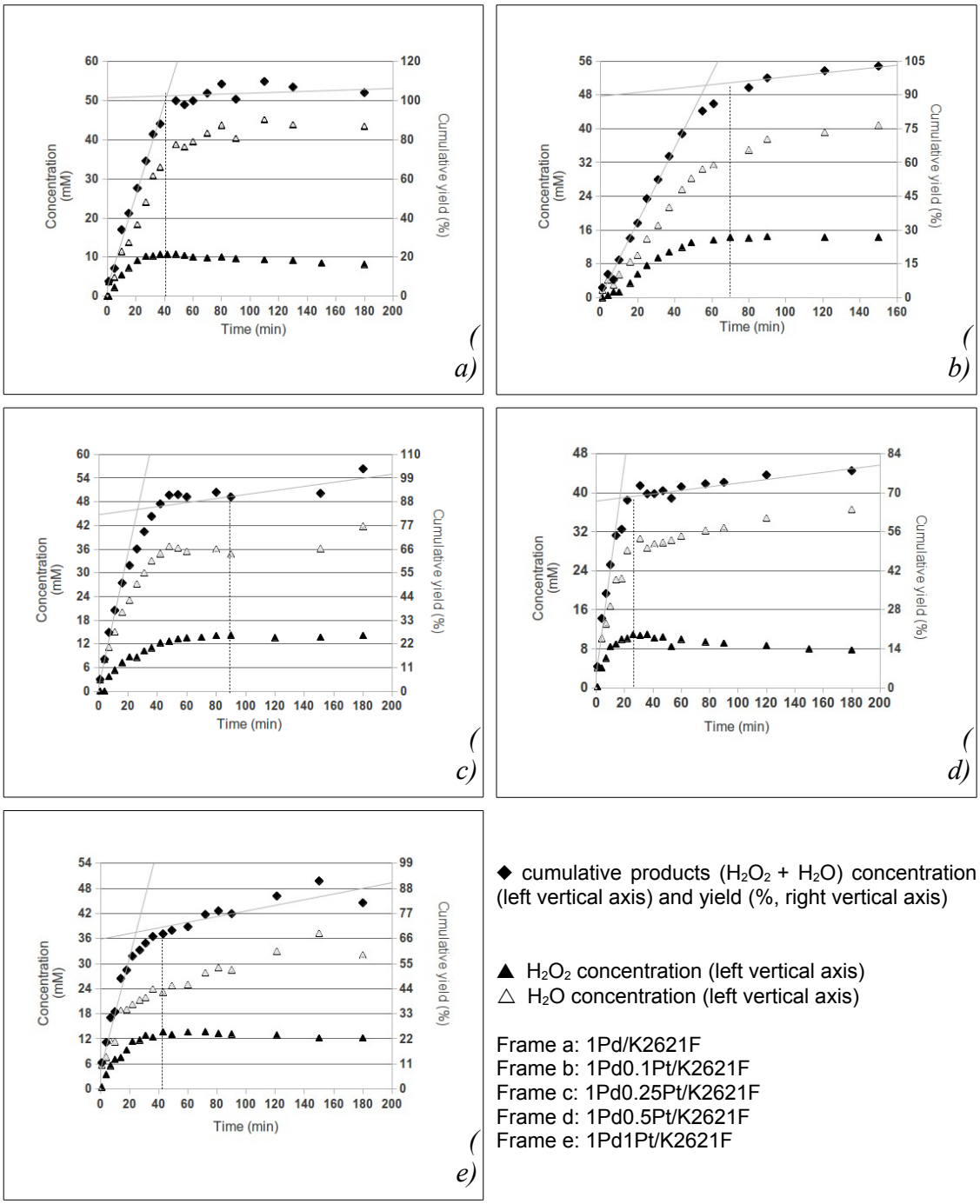

Figure 1. Complete kinetic plots of the catalytic runs over 1Pd/K2621F and the bimetallic 1PdXPt/K2621F catalysts (X= 0.1, 0.25, 0.5, 1).

The cumulative yield is the ratio between the sum of the water and hydrogen peroxide moles and the moles of hydrogen fed into the reactor, but it could be calculated only in an approximated way. In the first place our experimental set-up did not allow to take into account the amount of dissolved hydrogen, although this was kept as low as possible (the gas was added with the stirrer off). In the second place the moles of products were determined for each point from the results of two independent titrations,

one of which (the Karl Fisher determination of water) is not trivial. As a matter of fact, the cumulative yield was found to be sometimes above 100 % which suggests that its values could be systematically overestimated.

Figure 1 shows that the catalytic runs can be divided into two clearly distinguished stages for all the catalysts. The increase of the cumulative yield is relatively fast in the first stage and is much slower, if any is observed, in the second. In this case the slow increase is exclusively due to the increase of the amount of water. By contrast, the amount of hydrogen peroxide in the second stage decreases either slowly or not at all (1Pd0.1Pt/K2621F and 1Pd0.25Pt/K2621F). In both stages the cumulative yield changes approximately linearly with time.

For the monometallic palladium catalyst, Pd1/K2621F, the first stage ends when the concentration of hydrogen peroxide approaches its top value, i.e. when the rate of the formation of hydrogen peroxide (eq. 1) equals the sum of the rates of its hydrogenation and its dismutation. This occurs at practically full cumulative yield. In the second stage both the cumulative concentration and yield do not practically increase any longer. However, the concentrations of water and hydrogen peroxide slowly increase and decrease, respectively. This suggests that in the second stage the reactions involving hydrogen do not occur (H_2 is over) and that the only reaction taking place is the dismutation of H_2O_2 (eq. 4). Accordingly, the analysis of the kinetic plot from the point of maximum H_2O_2 concentration onward allows to estimate the kinetic constant of the dismutation. The logarithm of the concentration of hydrogen peroxide in the second stage decreases linearly with time (Figure 2), showing that the reaction is first order in H_2O_2.

$$-d[H_2O_2]/dt = k'_{app}\cdot[H_2O_2] \qquad \text{(eq. 5)}$$

The apparent pseudo-first order kinetic constants (k'_{app}) can be easily extracted from the plots using the integral kinetic law:

$$\ln\{[H_2O_2]\} = \ln\{[H_2O_2]_0\} - k'_{app}\cdot t \qquad \text{(eq. 6)}$$

However, in the apparent constants depend on the concentration of the catalyst. For a homogeneous reaction the differential kinetic law can be expressed as:

$$-d[H_2O_2]/dt = k''\cdot[H_2O_2]\cdot[cat] \qquad \text{(eq. 7)}$$

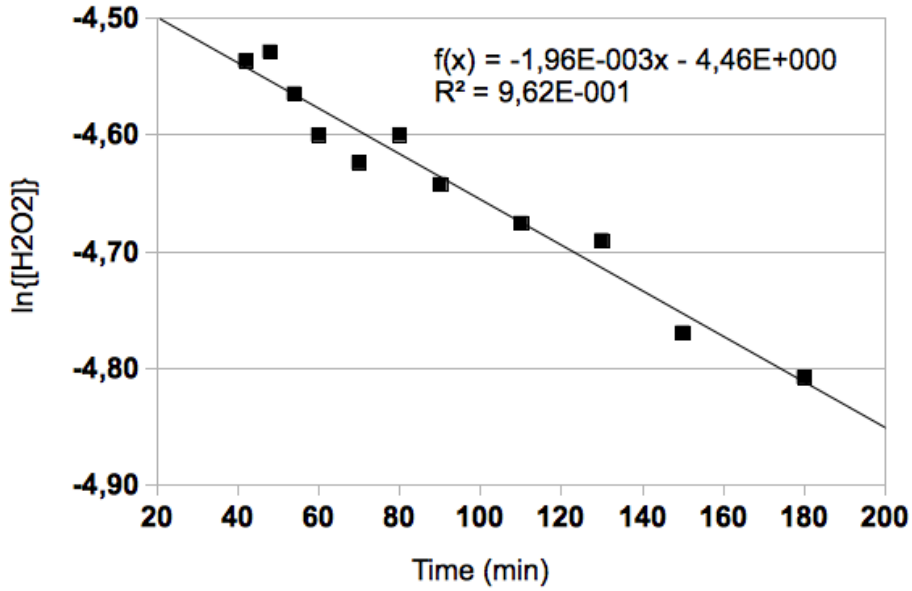

Figure 2. Logarithmic kinetic plot for the second stage over 1Pd/K2621F

Our system is not homogeneous, but the reaction was carried out with the catalyst suspended in the liquid phase and efficiently dispersed throughout its whole volume. Under these condition we can assume that the macroscopic catalysts concentration can be calculated as the ratio between the number of moles of metal and the volume of the liquid phase and that equation 7 holds also in our system, with $[H_2O_2]$ and [cat] corresponding to their macroscopic values in the liquid, provided that the diffusion and the adsorption of H_2O_2 are not determining. Under this point of view it can be appreciated that no gas are involved as reagents in the dismutation and that H_2O_2 is formed *in* the catalyst, hence kinetic control conditions are the most likely. The apparent first-order constant (k') is found to be 0.12 h^{-1} and the second-order one (k'') is 3.4·dm^3·$mmol^{-1}$·h^{-1}. These constants indicate that the dismutation of H_2O_2 is slow and contributes very little to its consumption.

For the bimetallic catalysts the concentration of H_2O_2 in the second stage decreases either slowly or not at all. In any case, the increase of water concentration is such that also the cumulative yield increases with time in the second stage. Moreover, as clearly

shown in Figure 1b-e, the top concentration of H_2O_2 is achieved before hydrogen is completely consumed. This implies that with the bimetallic Pd-Pt catalysts also all reactions, including the hydrogenation of H_2O_2 and the combustion of oxygen, can still occur and forbids the estimation of the kinetic constants of the dismutation reaction. Also the transition from the first to the second stage is observed before the complete consumption of hydrogen and occurs at conversions progressively decreasing as the platinum content increases.

The analysis of the initial overall rates of reactions, obtained from the slopes of the plots of the cumulative yield in the first stage of the reaction, allows to compare the effect of platinum addition on the activity of the catalysts. It was carried out in the first 8-16 min, depending on the catalyst. In this range all the concentrations changed linearly with time and the sum of the concentrations of hydrogen peroxide and water changed at a rate corresponding effectively to the sum of the individual rates of accumulation of the two products (Figure 3).

All the catalytic tests were carried out with the same amount of catalyst, hence with the same amount of palladium, but changing amounts of total metal (Pd+Pt). For each catalyst the cumulative amount of products was then normalized to the unit mass of either palladium (the active metal) or total metal (palladium+platinum) and the unit time to assess their initial productivity (Table 3).

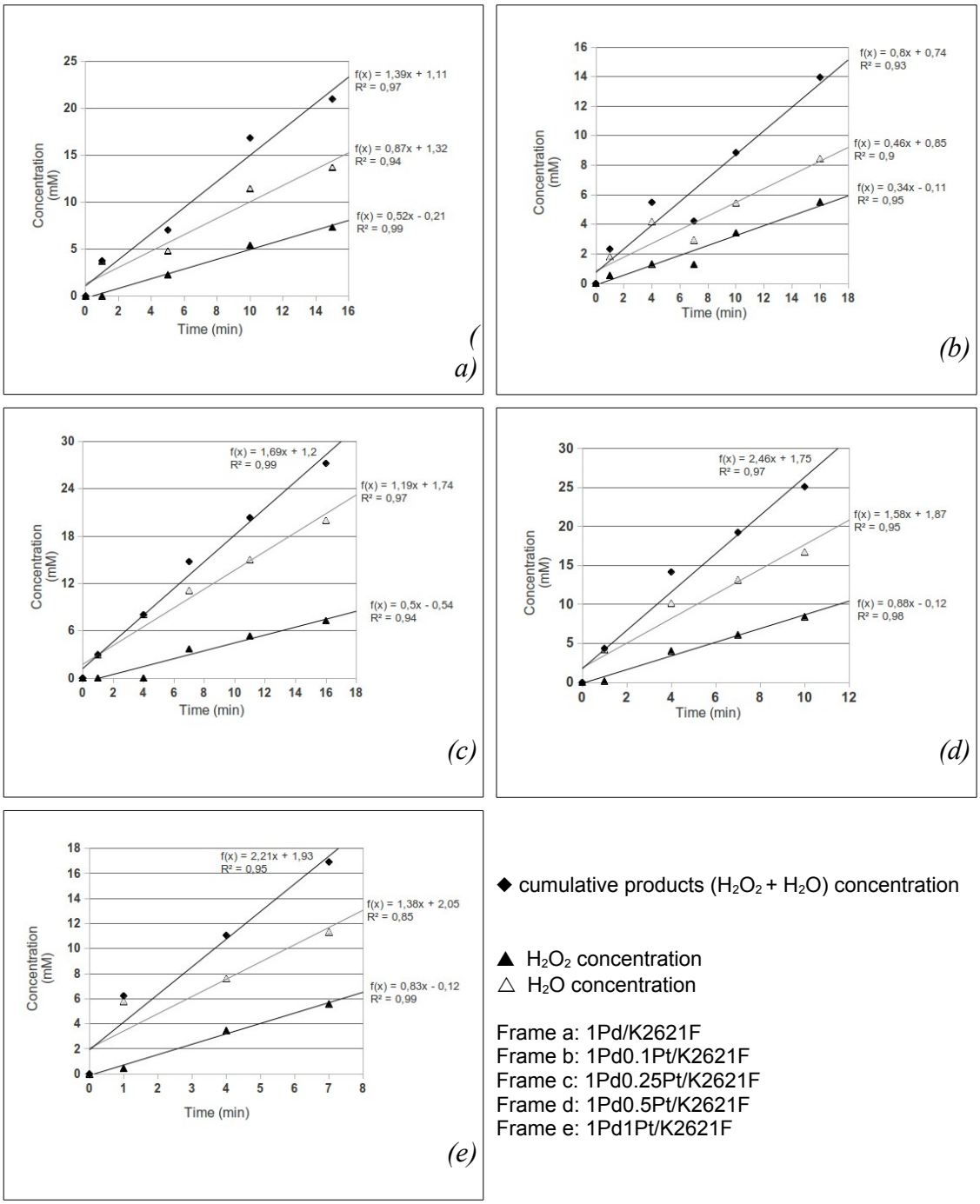

Figure 3. Kinetic plots for the first minutes (8-16) of the catalytic runs over 1Pd/K2621F and the bimetallic 1PdXPt/K2621F catalysts (X= 0.1, 0.25, 0.5, 1).

Table 3. Initial performances of the bimetallic palladium-platinum catalysts supported on K2621.

Cat.	Employed metal amount[a]		Initial cumul. rate[b]	Initial cumul. productivity[c]		Initial H_2O_2 productivity [d]	Initial Selectivity[e]
	Pd	Pd+Pt		vs Pd	vs Pd+Pt		
1Pd/ K2621F	1.45	1.45	83.4	2416	2416	904	37
1Pd0.1Pt/ K2621F	1.42	1.50	48.0	1421	1347	571	43
1Pd0.25Pt/ K2621F	1.42	1.61	101.5	3001	2641	845	30
1Pd0.5Pt/ K2621F	1.43	1.82	147.8	4340	3410	1218	36
1Pd1Pt/ K2621F	1.43	2.21	132.8	3899	2523	946	38

a: $mol \cdot 10^5$; b: $mmol(H_2O_2+H_2O) \cdot dm^{-3} \cdot h^{-1}$; c: $mol_{(H2O2+H2O)} \cdot mol^{-1}_{(Pd+Pt)} \cdot h^{-1}$;
d: $mol_{(H2O2)} \cdot mol^{-1}_{(Pd+Pt)} \cdot h^{-1}$; e: %.

With both methods similar trends in the change of productivity from one catalyst to another are obtained. Therefore, the H_2O_2 initial productivity was only referred to the total amount of metal (Pd+Pt).

The analysis of the initial reaction rates allows also to estimate the selectivity towards hydrogen peroxide in the first minutes of reaction (Table 4, first line), as the ratio between the slopes of the H_2O_2 concentration and of the cumulative concentration lines of Figure 3. Selectivity values for all the catalysts were also calculated (see Experimental) at fixed reaction times up to 90 minutes, to show how they changed with time (Table 4). The selectivity steadily decreases with time for all the catalysts but 1Pd0.25Pt/K2621F, for which it is more or less constant.

Table 4. Changes with time in the selectivity of 1Pd/K2621F and the bimetallic 1PdXPt/K2621F catalysts (X= 0.1, 0.25, 0.5, 1).

	Selectivity (H_2O_2, %)				
t (min)	*1Pd/K2621F*	*1Pd0.1Pt/K2621F*	*1Pd0.25Pt/K2621F*	*1Pd0.5Pt/K2621F*	*1Pd1Pt/K2621F*
Initial[a]	37 (16 min)	43 (16 min)	30 (16 min)	36 (12 min)	38 (8 min)
15	-	-	-	29	29
30	25	38	25	26	37
45	22	33	26	25	37
60	20	31	28	24	35
90	19	28	29	22	32

a: initial time range given in parenthesis after the selectivity value.

For the bimetallic catalysts the initial selectivity changes in the order 1Pd0.1Pt/K2621F> 1Pd0.25Pt/K2621F < 1Pd0.5Pt/K2621F < 1Pd1Pt/K2621F. This is the result of the changes in the apparent initial productivities of the bimetallic catalysts for the individual products (Figure 4). Both increase up to 0.5 % Pt (22 % atomic in the metal balance) and then drop for 1Pd1Pt/K2621F, but changes are larger for water.

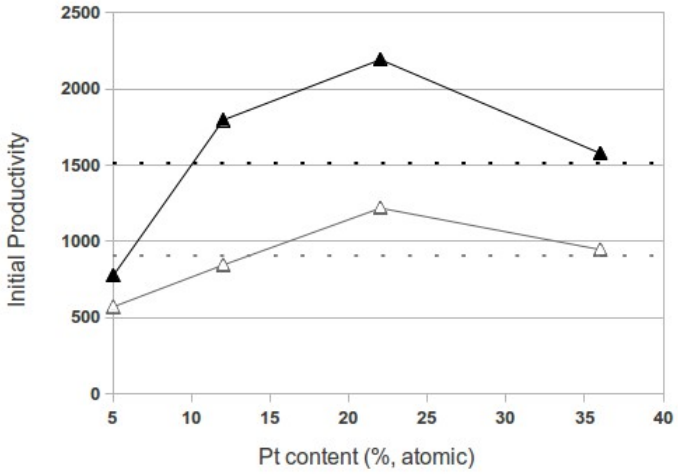

Figure 4. Initial overall productivity (hydrogen consumption rate, full triangles) and initial hydrogen peroxide productivity (void triangles) of 1Pd/K2621F and the bimetallic 1PdXPt/K2621F catalysts (X= 0.1, 0.25, 0.5, 1).

The volcano plot of the productivity of H_2O_2 is in line with the literature results [15], [17] showing that the addition of relatively high amount of platinum is eventually detrimental. In our case, the most productive catalyst is initially 1Pd0.5Pt/K2621F, and it has also the shortest time required to reach the top concentration of H_2O_2. However, as its selectivity decreases very quickly with time (Table 4) the top H_2O_2 concentration achieved is the lowest (10.8 mM). Differently form other cases reported in the literature [17] in this catalyst the enhanced productivity is not attributable simply to a relatively high selectivity.

To summarize, the effects of the addition of platinum to the polymer-supported palladium catalyst are the following:

1) a little amount of platinum (0.1 %, w/w) makes the catalyst less active, but more selective towards H_2O_2 than the monometallic one;

2) further addition of platinum initially increases the activity of the catalysts, but at relatively high platinum content the activity decreases again: the productivity of both

water and H_2O_2 change in the same way, but the former is affected most, so that the selectivity changes the other way round;

3) for the bimetallic catalysts the first stage of the reaction ends before total hydrogen consumption and at times and cumulative yields (i.e. hydrogen conversions) which decrease with the platinum amount.

As the direct synthesis and the combustion of oxygen are the main reactions of the first stage, the last finding indicates that the higher the platinum amount the earlier they tend to subside, in spite of the presence of higher and higher amounts of hydrogen. These reactions are the only ones involving oxygen and this suggests that its adsorption on the bimetallic catalysts is somehow inhibited by one of the products (H_2O or H_2O_2), which compete with it for the surface sites. This effect could be either of kinetic (slow desorption of the product from the metal surface) or thermodynamic nature (increased heat of adsorption with respect to monometallic palladium). On the other hand, enhanced inhibition by H_2O_2 with increasing platinum amount, which also implies increasing fractional coverage of the surface with H_2O_2, should favour the hydrogenation and the dismutation of H_2O_2 and this would explain why the selectivity decreases up to 0.5 % Pt. However a further increase in the fractional coverage of the surface with H_2O_2 in 1Pd1Pt/K2621F could eventually limit also the chemisorption of hydrogen. Accordingly, both its overall consumption and the hydrogenation of H_2O_2 get slower and this would explain why the apparent activity and the selectivity respectively decreases and increases from 1Pd0.5Pt/K2621F to 1Pd1Pt/K2621F.

Au-Pd/K2621 materials

Au-Pd catalysts have been the subject of intense research for years, not only for the reaction of direct synthesis of H_2O_2 [6][17][37][41], but also for the oxidation of alcohols, polyols, and CO and for the hydrogenation of aromatics, nitro-compounds and unsaturated organic compounds [1][6][88]. The straightforwardness of the method used for the preparation of the Pt-Pd catalysts described in the previous section prompted us to employ it also for the preparation of the Au-Pd ones, instead of the incipient wetness impregnation which so far has been reported to give the best results. As no cationic complex of gold is commercially available, for this purpose we synthesized $[Au(NH_2CH_2CH_2NH_2\text{-}\kappa^2\text{-}N,N')_2]Cl_3$ as reported in ref. [173]. Three catalysts, containing respectively 0.25 %, 0.5 % and 1 % (w/w) gold, were prepared and tested under the very same condition employed for the Pt-Pd catalysts.

Also for the Au-Pd catalysts the reaction can be divided into two stages, the first featured by a relatively high rate of overall products formation and of hydrogen consumption and the second with a much lower overall reaction rate. In every case the transition from the first to the second stage occurs before hydrogen is over, although for 1Pd0.5Au/K2621F and 1Pd1Au/K2621F the relevant conversion is only slightly lower than quantitative. Differently from the Pt-Pd catalysts, the conversion at which the first stage ends and the second begins seems to be a little bit lower at the lowest gold content. Being this the case, in the Au-Pd catalysts the product inhibition which seems to occur in Pt-Pd ones is negligible and, if any, it would affect the catalysts in the opposite way in connection with the change in the gold content.

The presence of some hydrogen at the end of the first stage makes possible hydrogenation reactions also in the second. In fact, the cumulative product yield clearly goes on increasing also in the second stage over 1Pd0.25Au/K2621F and 1Pd0.1Au/K2621F. For the former higher a larger amount of H_2 is available at the beginning of the second stage and the increase of the cumulative yield is faster. This is the only catalyst for which even the hydrogen peroxide concentration could be increasing, though to a small extent, also in the second stage. For these two catalysts, the dismutation is certainly not the only reaction still occurring in the final stages of the process and that some hydrogenation is still going on. Over 1Pd0.5Au/K2621F the increase of the cumulative yield during the second stage is much slower than over the

other two Au-Pd catalysts. In fact it is so slow that with 1Pd0.5Au/K2621F that the rate of reactions involving hydrogen seems negligible and the apparent kinetic constant of dismutation can be extracted from the kinetic plot (Figure 6) as in the case 1Pd/K2621F discussed above.

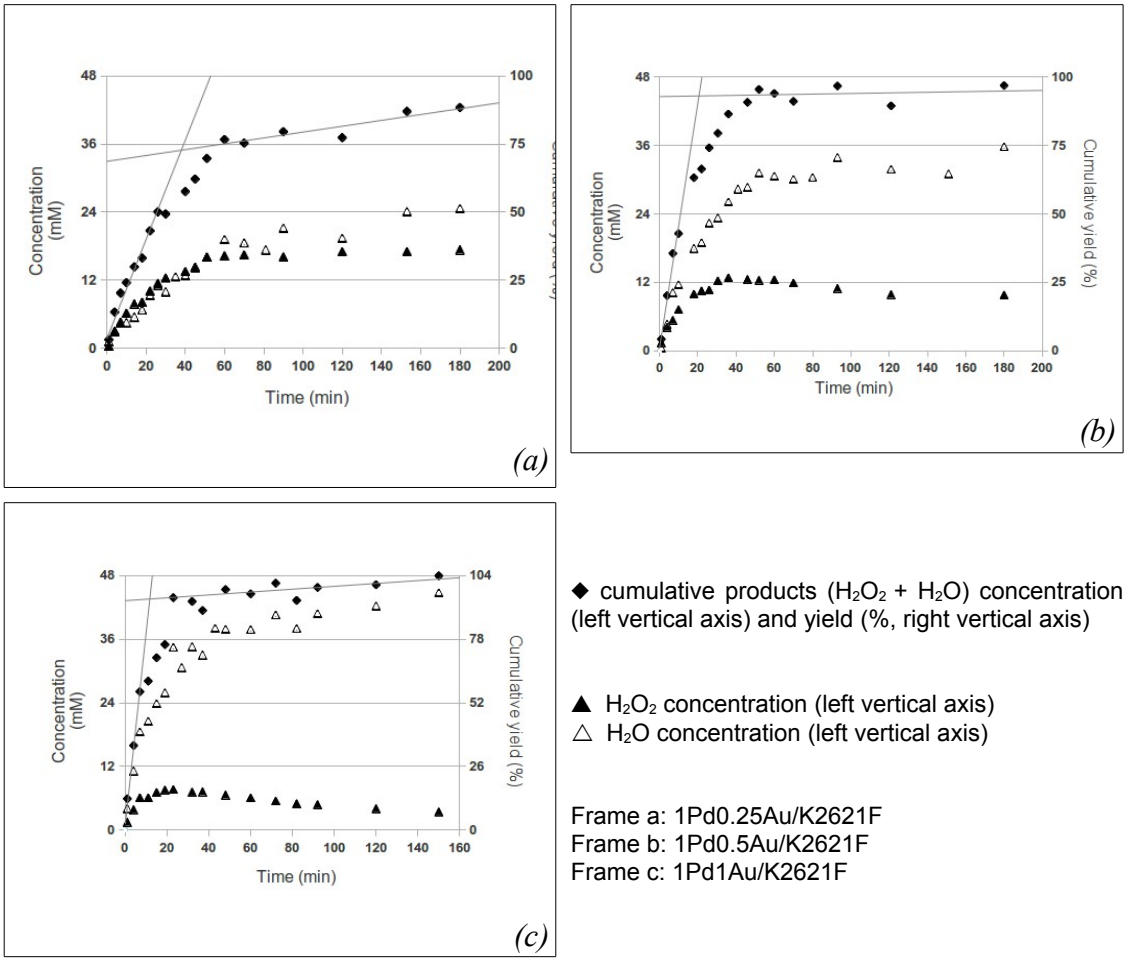

Figure 5. Complete kinetic plots of the catalytic runs over 1Pd/K2621F and the bimetallic 1PdXAu/K2621F catalysts (X= 0.25, 0.5, 1).

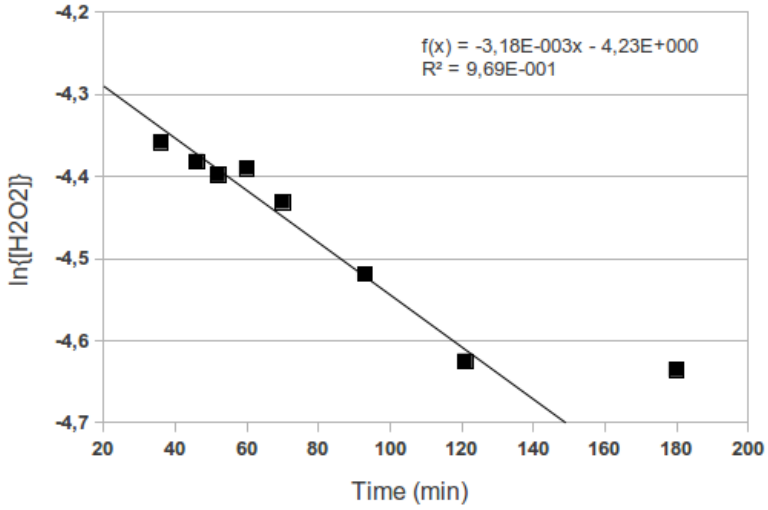

Figure 6. Logarithmic kinetic plot for the second stage over 1Pd0.5Au/K2621F (the point at 180 min was excluded from the interpolation)

For 1Pd0.5Au/K2621F the pseudo first-order kinetic constant, k', is 0.19 h^{-1} and the second-order kinetic constant, k", is 4.4·3.4·dm^3·$mmol^{-1}$·h^{-1}. The value of k" is practically the same found for 1Pd/K2621F, which shows that the dismutation of H_2O_2 is very little affected by the addition of gold in these catalysts.

For the Au-Pd catalysts the initial selectivity values were calculated too from the slopes of the kinetic plots in the first minutes (7-18, depending on the catalyst) of reaction (Figure 7 and Table 5). All the productivity values were calculated by normalizing the rates to the unit molar amount of total (Pd+Au) metal. Selectivity values for all the catalysts were also calculated (see Experimental) at fixed reaction times up to 90 minutes, to show how they changed with time (Table 6). The selectivity steadily decreases with time for all the Au-Pd catalysts.

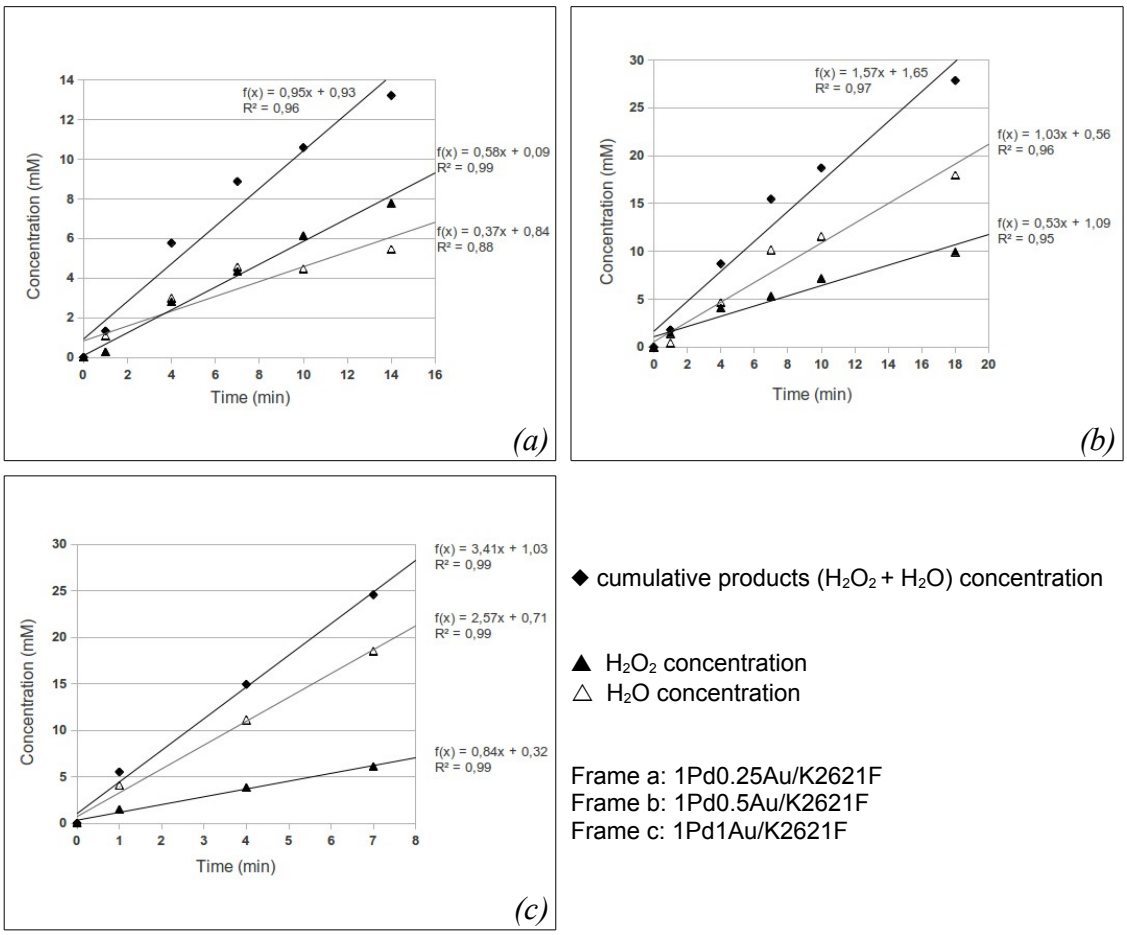

Figure 7. Kinetic plots for the first minutes (7-18) of the catalytic runs over 1Pd/K2621F and the bimetallic 1PdXAu/K2621F catalysts (X= 0.25, 0.5, 1).

Table 5. Initial performances of the bimetallic gold-palladium catalysts supported on K2621.

Cat.	Employed metal (Pd+Au) amount[a]	Initial cumul. rate[b]	Initial cumulative productivity[c] (vs Pd+Au)	Initial H_2O_2 productivity[d]	Initial Selectivity[e]
1Pd/ K2621F	1.45	83.4	2416	904	37
1Pd0.25Pt/ K2621F	1.61	57	1487	908	61
1Pd0.5Pt/ K2621F	1.82	94.2	2174	734	34
1Pd1Pt/ K2621F	2.21	204.6	3888	958	25

a: $mol \cdot 10^5$; b: $mmol(H_2O_2+H_2O) \cdot dm^{-3} \cdot h^{-1}$; c: $mol_{(H2O2+H2O)} \cdot mol^{-1}_{(Pd+Pt)} \cdot h^{-1}$; d: $mol_{(H2O2)} \cdot mol^{-1}_{(Pd+Pt)} \cdot h^{-1}$; e: %.

Table 6. Chenges with time in the selectivity of 1Pd/K2621F and the bimetallic 1PdXAu/K2621F catalysts (X= 0.25, 0.5, 1).

	Selectivity (H_2O_2, %)			
t (min)	*1Pd/K2621F*	*1Pd0.25Au/K2621F*	*1Pd0.5Au/K2621F*	*1Pd1Au/K2621F*
Initial[a]	37 (16 min)	61 (14 min)	34 (18 min)	25 (7 min)
15	-	-	-	23
31 (±1)	25	56	35	17
46 (±2)	22	50	30	15
60	20	46	29	14
91 (±2)	19	43	24	11

a: initial time range given in parenthesis after the selectivity value.

In the investigated composition range the initial activity of the Au-Pd catalysts increases as the gold content increases (Figure 8). A similar trend was observed with platinum, but in the 0.1-0.5 % (w/w) composition range, so that we cannot rule out that at some gold content higher than 1 % (w/w) activity would drop to lower value and a volcano-shaped plot would be obtained. At relatively low metal amounts (up to 0.5 %, w/w) the Au-Pd catalysts are less active than the Pt-Pd ones and even of monometallic palladium. For the Au-Pd catalysts the increase of the initial activity with the gold content is almost linear and the increase in the initial productivity of water as well. On the other hand, the productivity of hydrogen peroxide is more or less independent of the gold content, hence the lower the initial activity the higher the initial selectivity towards H_2O_2.

As the productivities of water and hydrogen peroxide depend on combinations of the rates of different reactions, these trends do not allow to say whether the increase of the initial build-up of water is due to either an increase of the rate of the combustion of hydrogen (r_2) or to an increase of the rates of both formation (r_1) and consumption (r_3+r_4) of hydrogen peroxide. In any case changes of r_1, r_3 and r_4 are such that the apparent initial rate of H_2O_2 accumulation is practically the same for all the investigated catalysts. However, it can be considered that 1Pd0.25Au/K2621F is much more selective than 1Pd/K2621F because it is equally productive in hydrogen peroxide and much more less productive in water. This strongly suggests that the main effect of the addition of gold in relatively little amount (in this case 0.25 % w/w, i.e. 11.9 % atomic with respect to the total metals) is the inhibition of the combustion of hydrogen. Accordingly, the increase in the productivity of water (and decreased selectivity towards hydrogen peroxide) with increasing gold amount in the catalysts can be most likely attributed to progressively enhanced rates of hydrogen combustion.

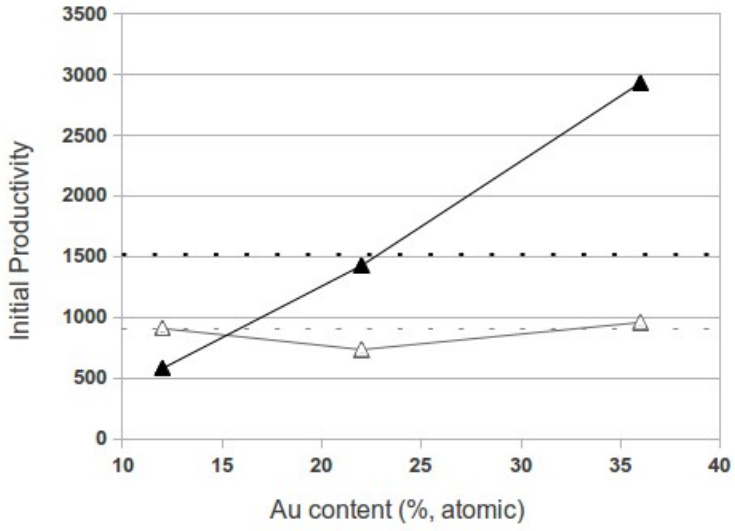

Figure 8. Initial overall productivity (hydrogen consumption rate, full triangles) and initial hydrogen peroxide productivity (void triangles) of 1Pd/K2621F and the bimetallic 1PdXAu/K2621F catalysts (X= 0.25, 0.5, 1).

The selectivity decreases with time for all the Au-Pd, but the order is always the same (1Pd0.1Au/K2621F > 1Pd0.5Au/K2621F > 1Pd1Au/K2621F; Table 6) so that the the top concentration of hydrogen peroxide attained with each catalyst follows the same order (17.0 mM, 12.8 mM and 7.5 mM, respectively).

The monometallic and the bimetallic Au-Pd catalysts have been also characterized with TEM and HRTEM to assess the morphology of their metal nanoparticles (Figures 9-12).

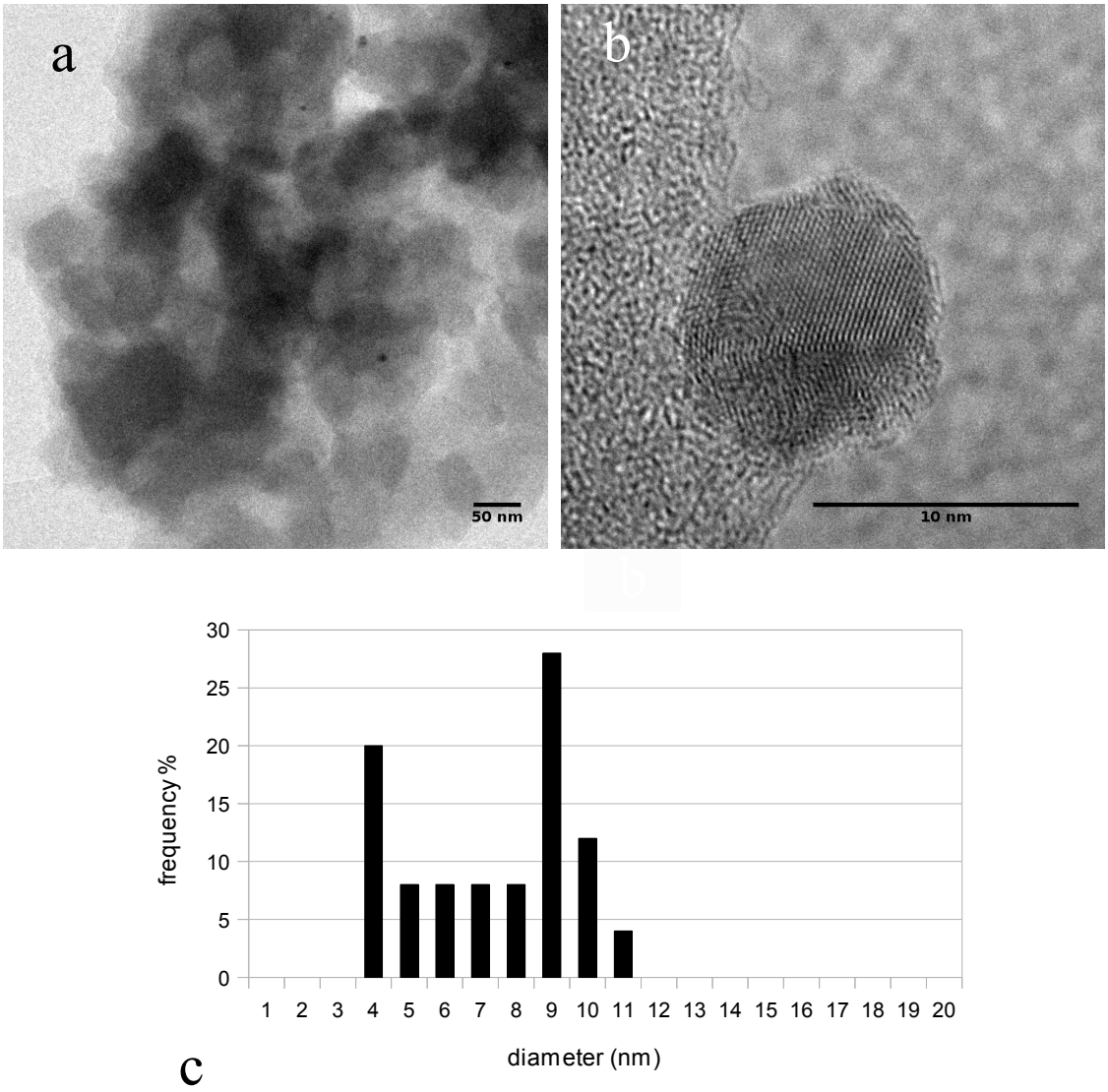

Figure 9. TEM (30K, a), HRTEM(800K, b) micrograph and size distribution (24 counted nanoparticles, c) of 1Pd/K2621F

For the 1Pd/K2621F sample only very few nanoparticles could be detected in comparison with other palladium catalysts supported on the same resin, but reduced with a methanol/water 1:1 solution [32] ot other agents [33]. This suggests that most of them are embedded in the polymer framework and only the few close to the surface of the powdered material can be observed. The low resolution images (Figure 8, a) show that these nanoparticles have diameters ranging from 4 to 11.

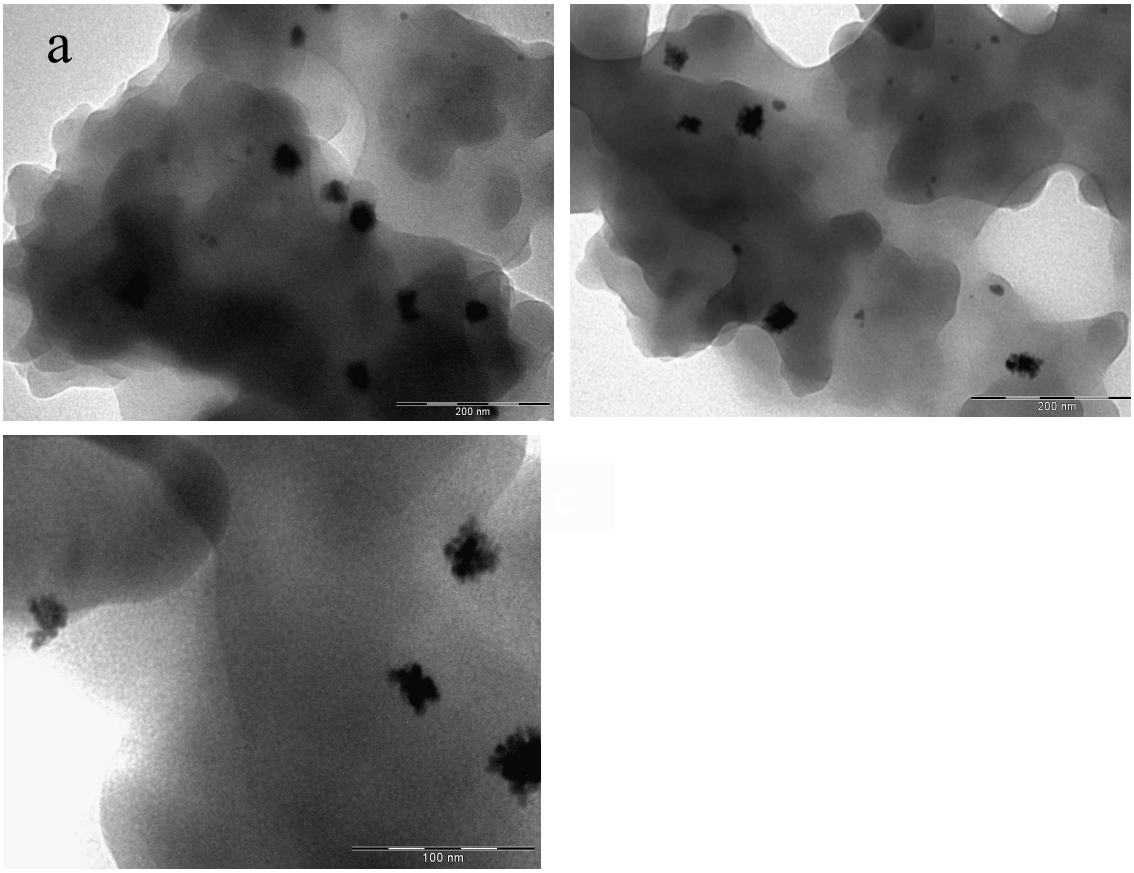

Figure 10. TEM micrograph (a and b scale bar 200 nm) of 1Pd0.25Au/K2621F.

The HREM characterization (Figure 9, b) show a multitwinned nanoparticles also featured by the presence of defects. In comparison with a 1 % (w/w) palladium catalysts supported on K2621, but prepared by a different protocol [32], the nanoparticles of 1Pd/K2621F are appreciably smaller. 1Pd/K2621Fi s also less selective than the previously reported catalyst and although the experimental set-ups are different and many variables could be taken into account, the difference in the selectivities could be connected to the different nanoparticle size too.

In all the bimetallic catalysts the nanoparticles are apparently aggregates of smaller nanoclusters, with diameters in the 5-7 nm range. In the HRTEM microphotographs of some nanoparticles we found evidence of the possible coalescence of the nanoclusters into a single crystal domain. This was not confirmed by a general analysis of the TEM data and nanoparticles are more likely formed by the simple superposition of the small nanoclusters.

The size distribution of the three bimetallic catalysts is illustrated in Figure 13.

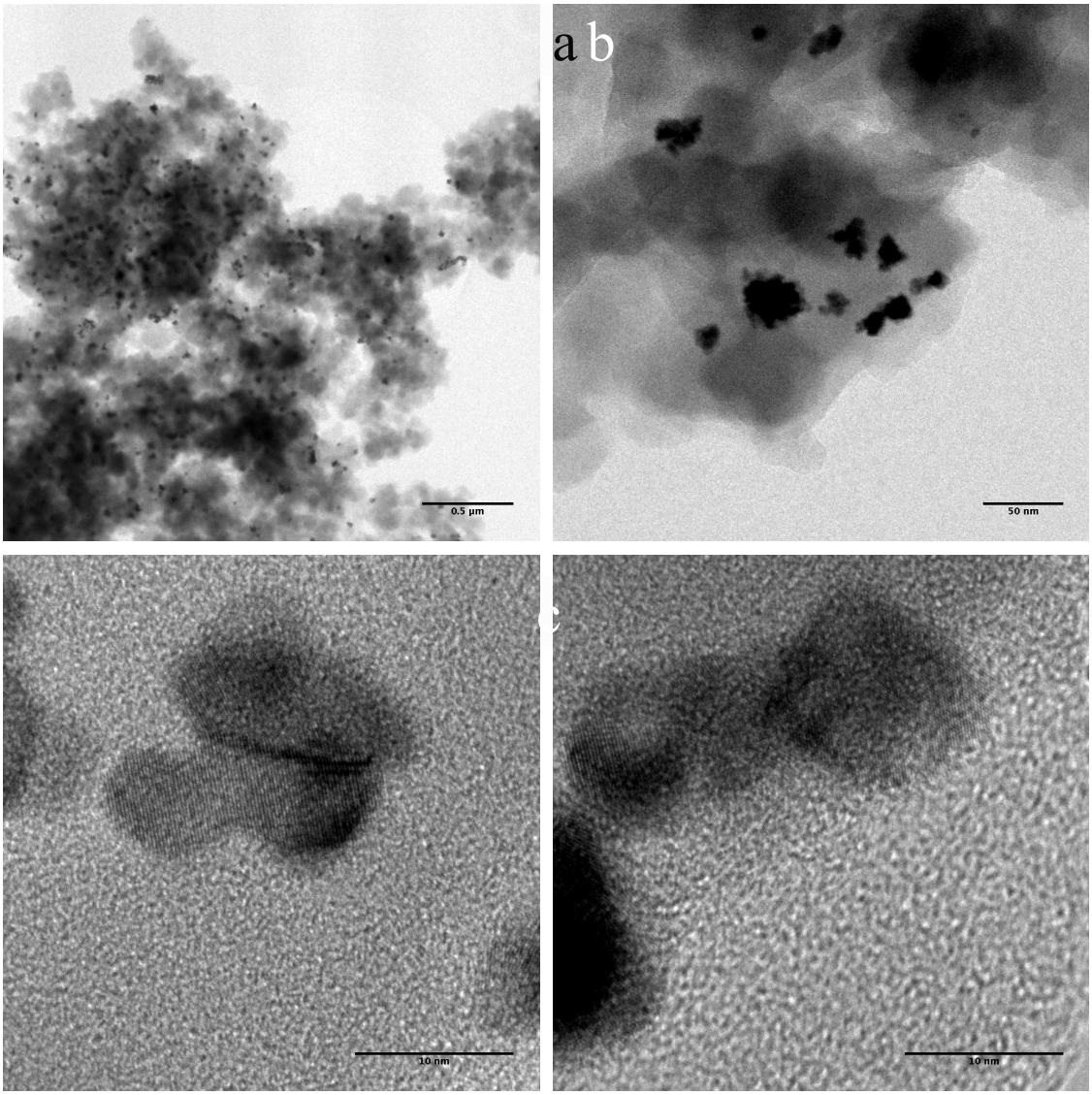

Figure 11. TEM (6K, a; 50K, b) and HRTEM (500K, c and d) of 1Pd0.5Au/K2621F.

The most active catalyst, 1Pd1Au/K2621F (the only one more active than 1Pd/K2621F) has the smallest nanoparticles and practically none of them is larger than 12 nm. The size distribution, centred around 6-7 nm, is also relatively narrow. The other two catalysts have much broader size distributions, with nanoparticles as large as 32-33 nm, but somewhat different.

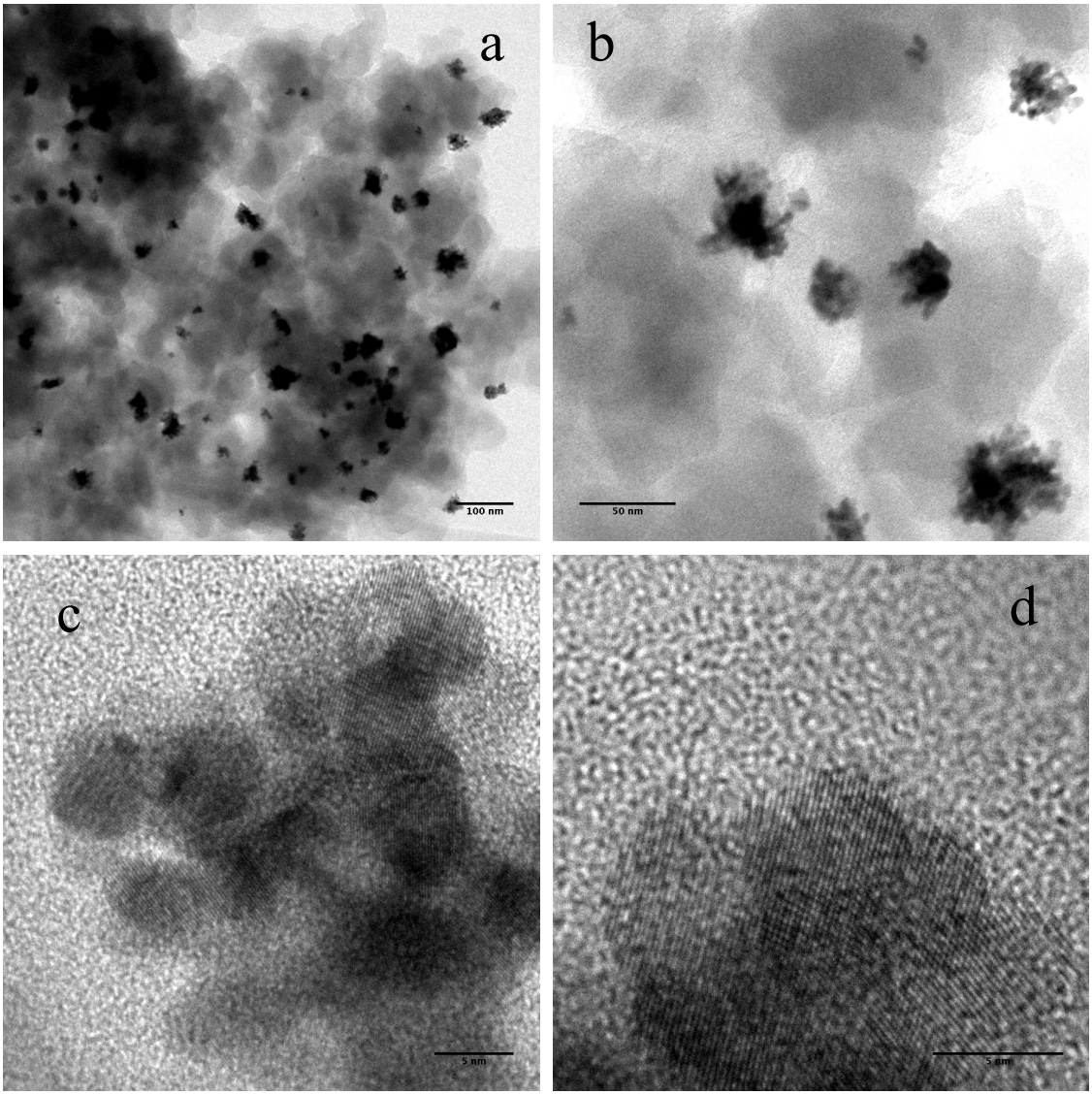

Figure 12. TEM (20K, a; 60K, b), and HRTEM (500K, c; 800K, d) of 1Pd1Au/K2621F.

Two populations, one around 7-8 nm and the other around 12-13 nm, could be present in 1Pd0.5Au/K2621F. For 1Pd0.25Au/K2621F if two populations are present, the one with the smaller nanoparticles (centred around 6-8 nm), is much more abundant than the other, if any. There is not any simple correlation between the productivity of hydrogen peroxide or the selectivity towards it. This not very surprising, because other nanoparticle features such as their structure (nanoalloy or core-shell) [41] or variable composition with size could play a role [44]. It can only be observed that 1Pd1Au/K2621F, which is featured by the absence of large nanoparticles is at the same time the most active and the least selective catalyst. This suggests that the presence of

large aggregates of nanoparticles is beneficial for the selectivity towards hydrogen peroxide.

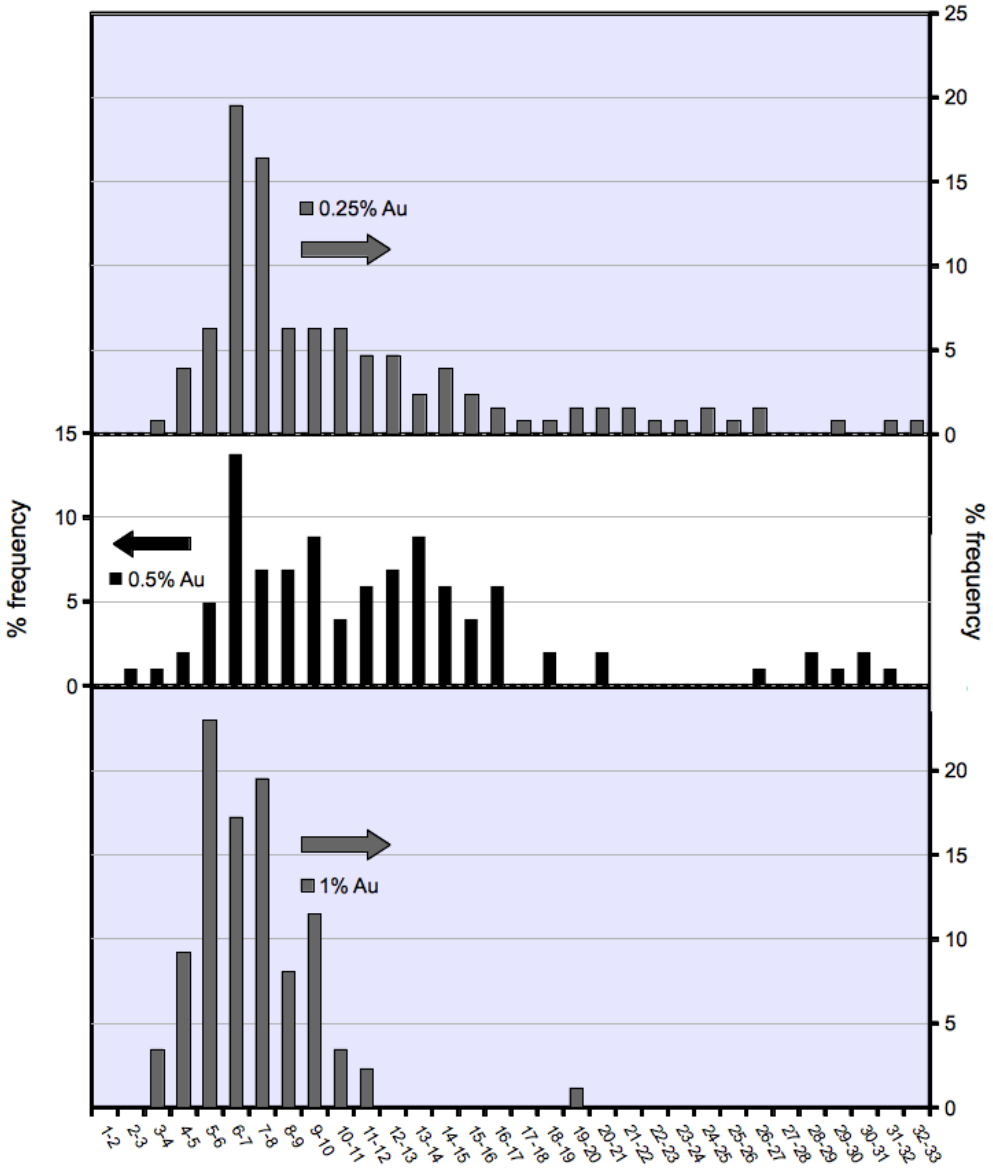

Figure 13. Nanoparticle size distribution for 1Pd0.25Au/K2621F (top,128 nanoparticles counted), 1Pd0.5Au/K2621F (middle, 128 nanoparticles counted) and 1Pd01Au/K2621F (bottom, 87 nanoparticles counted).

The effect of the reduction with hydrogen on a library of bimetalic catalysts Pd-Au and Pd-Pt

Lewatit K2621, the macroreticular sulfonated polystyrene-divinylbenzene resin (S-PSDVB), is been used, as in the previous sections, due to several interesting features of the attractive supports for DS catalysts. As already reported, the introduction of the metal precursors in the support can be easily accomplished with a simple ion-exchange between the counter-ions of the sulfonic groups (H^+ or Na^+, for instance) and cationic metal complexes. The reduction of the precursors to the metals takes place inside the polymer framework, which is able to control the dispersion, the size and, therefore, the catalytic properties of the metal nanoparticles.

For comparing the effect of different protocol of reduction, two library of bimetallic Pd/Pt and Pd/Au catalysts were prepared with a fixed palladium load (1 %, w/w) but different amounts of platinum or gold (0, 0.25, 0.5, 1 %, w/w). The use of the cationic complexes $[Pd(NH_3)_4]^{2+}$, $[Pt(NH_3)_4]^{2+}$ and $[Au(en)_2]^{3+}$ allowed the straightforward metalation of K2621 by ion exchange from aqueous solutions of their nitrate, sulfate and chloride, respectively. The nanoclusters were eventually obtained upon reduction of the metal precursors with hydrogen in autoclave (5 bar) at 60°C (denominated as HpT).

The activity of the catalysts is illustrated as the concentrations of the products, hydrogen peroxide and water (Figure 14 and 15), H_2 conversion and H_2O_2 selectivity (Figure 16 and 17), and the cumulative yield of the products as the function of time (Figure 18 and 19). All the catalytic tests were carried out with the same amount of palladium, but changing amounts of total metal (Pd+Pt) and (Pd+Au) and the initial activity of the catalysts was assessed as the cumulative amount of products per mole of either palladium or total metal (Pd+Pt) and (Pd+Au) and unit time (Table 7 and 8).

For the monometallic palladium catalyst, 1PdK2621HpT, exhibits initially a clear induction time of 5 minutes for all the reaction, surprisingly also for the direct synthesis of water. The analysis of the initial overall rates of reactions, obtained from the slopes of the plots of the cumulative yield in the first stage of the reaction, allows to compare the effect of platinum and gold addition on the activity of the catalysts. It was carried out in the first 10-20 min, depending on the catalyst.

In this range all the concentrations changed linearly with time and the sum of the concentrations of hydrogen peroxide and water changed at a rate corresponding effectively to the sum of the individual rates of accumulation of the two products (Figure 18 and 19).

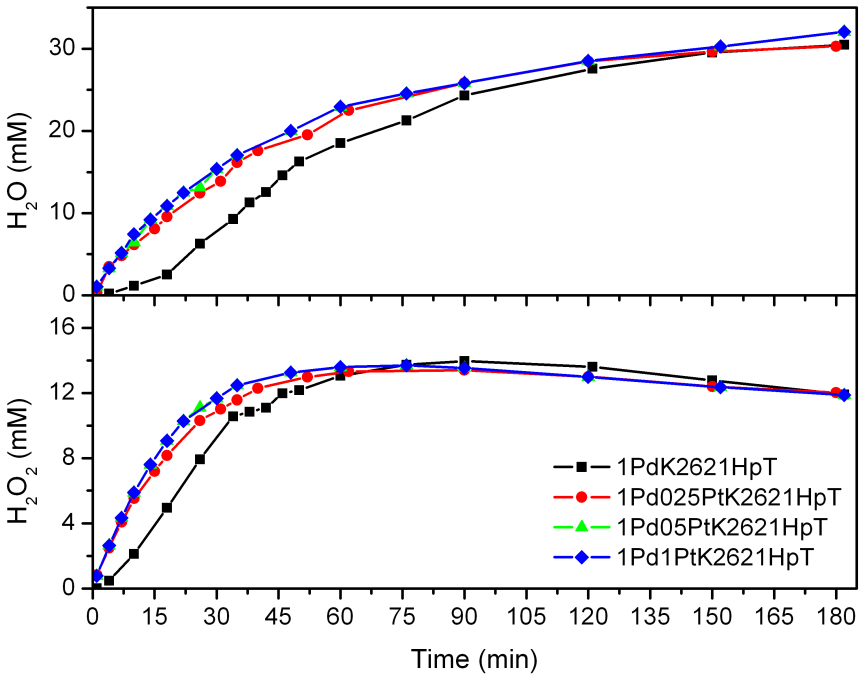

Figure 14: The concentration of water and hydrogen peroxide vs time produced by the library of Pt-Pd materials

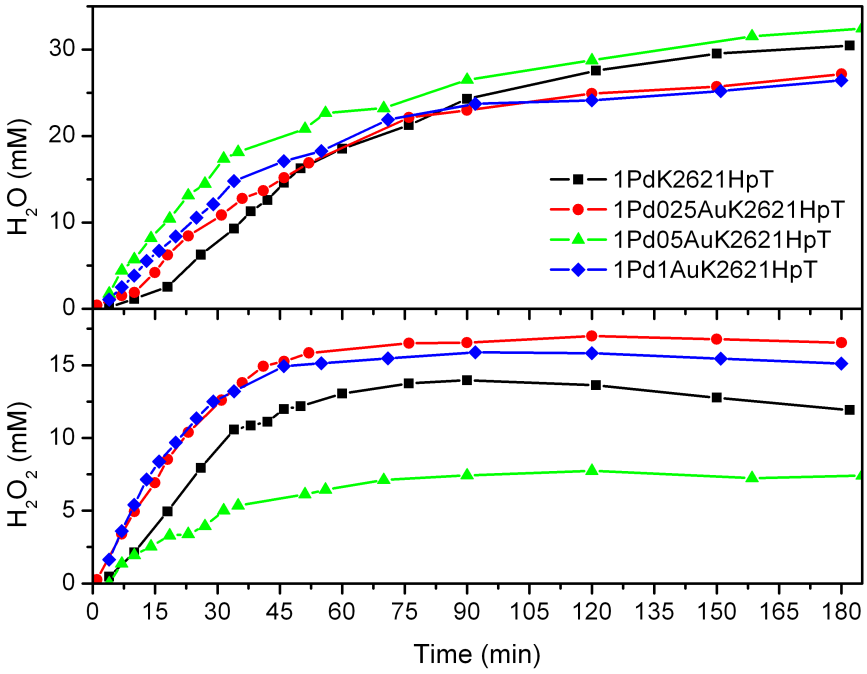

Figure 15: The concentration of water and hydrogen peroxide vs time produced by the library of Au-Pd materials

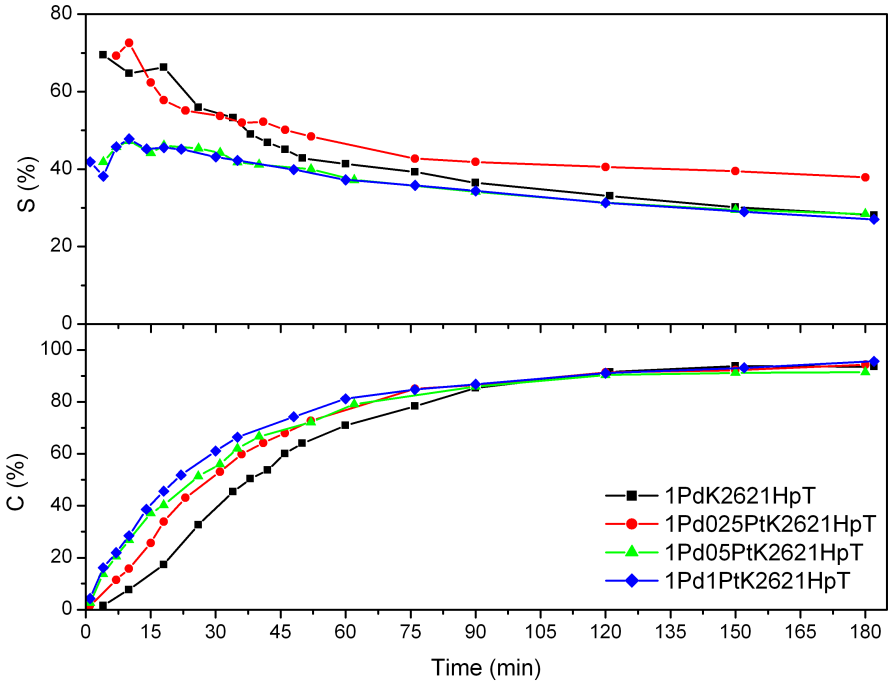

Figure 16: The H_2 conversion and H_2O_2 selectivity vs time exhibited by the library of Pt-Pd materials

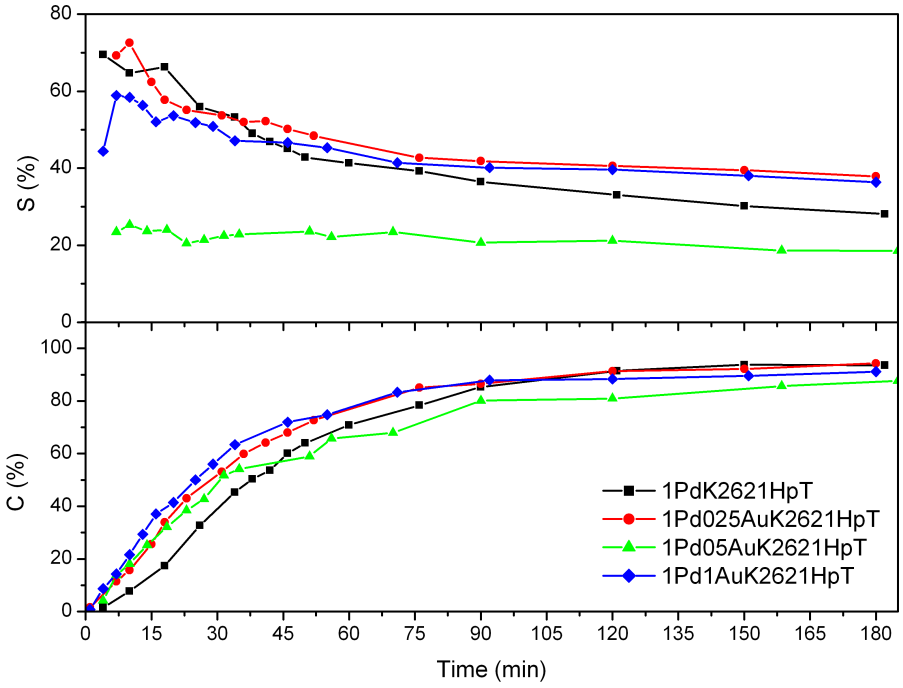

Figure 17: The H_2 conversion and H_2O_2 selectivity vs time exhibited by the library of Au-Pd materials

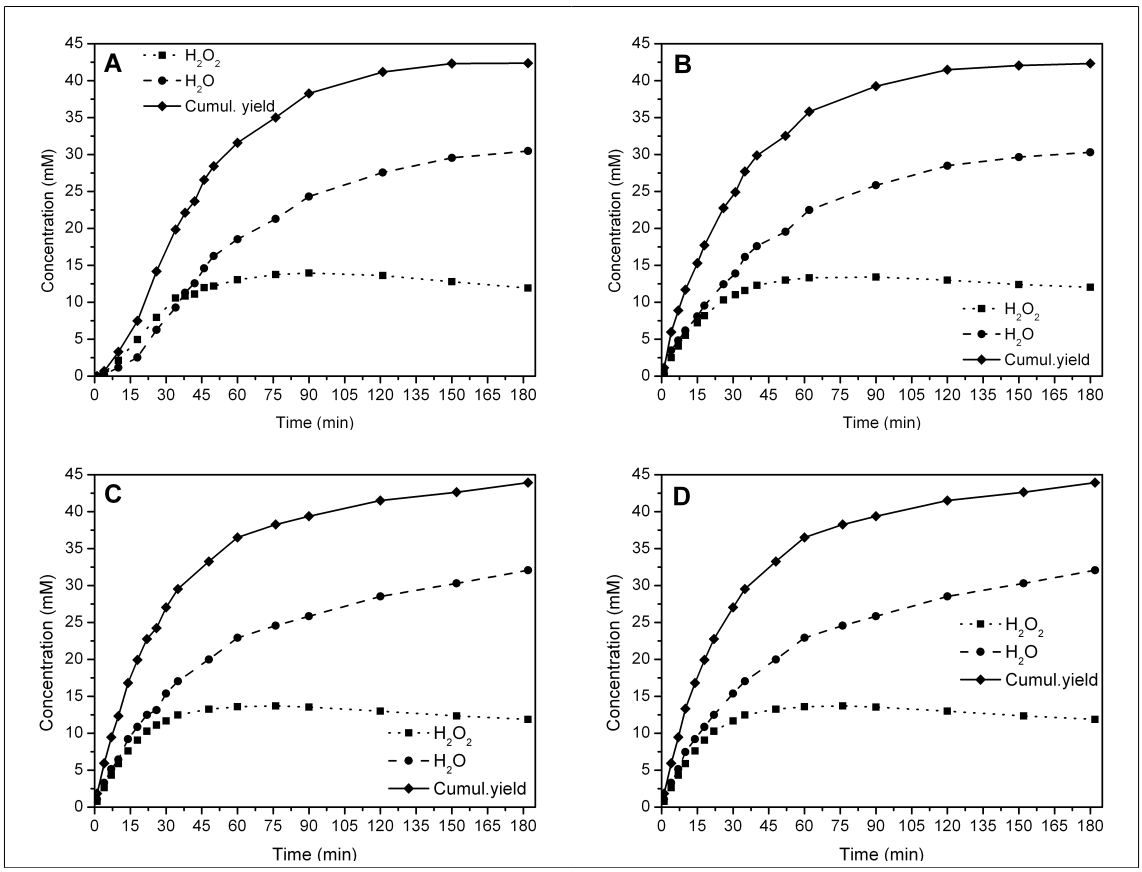

Figure 18: The concentration of products and the cumulative yield vs time of 1PdK2621HpT (A), 1Pd025PtK2621HpT (B), 1Pd05PtK2621HpT (C), 1Pd1PtK2621HpT (D).

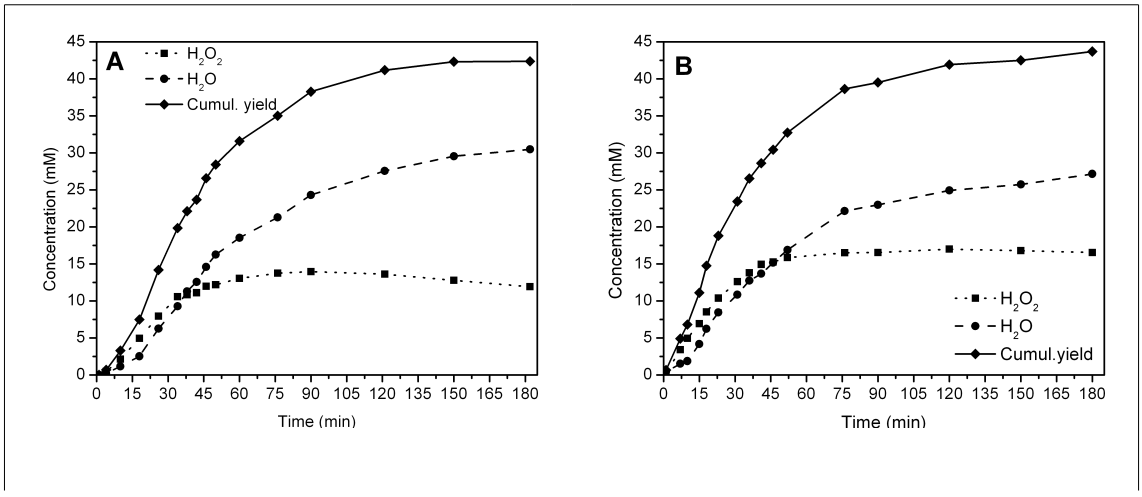

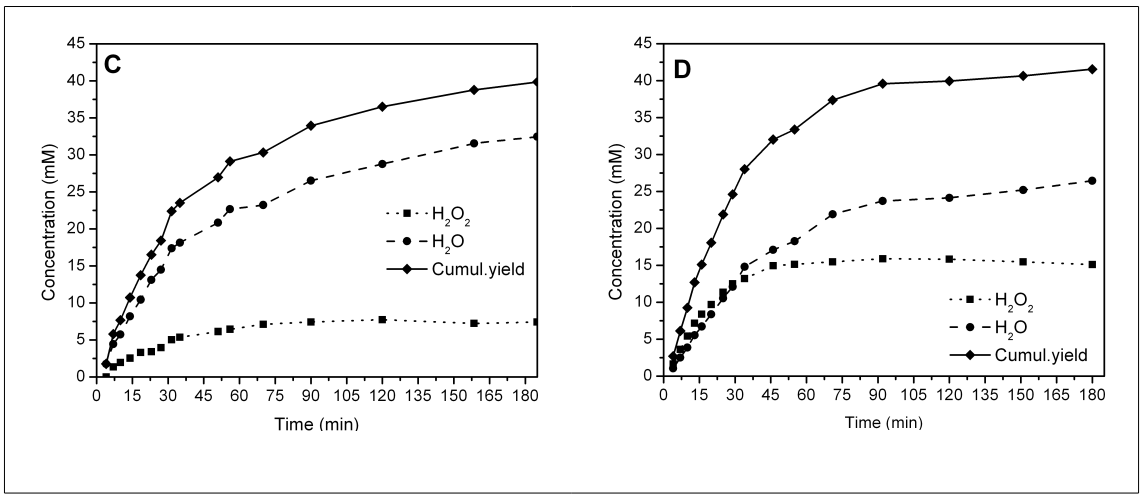

Figure 19: The concentration of products and the cumulative yield vs time of 1PdK2621HpT (A), 1Pd025AuK2621HpT (B), 1Pd05AuK2621HpT (C), 1Pd1AuK2621HpT (D).

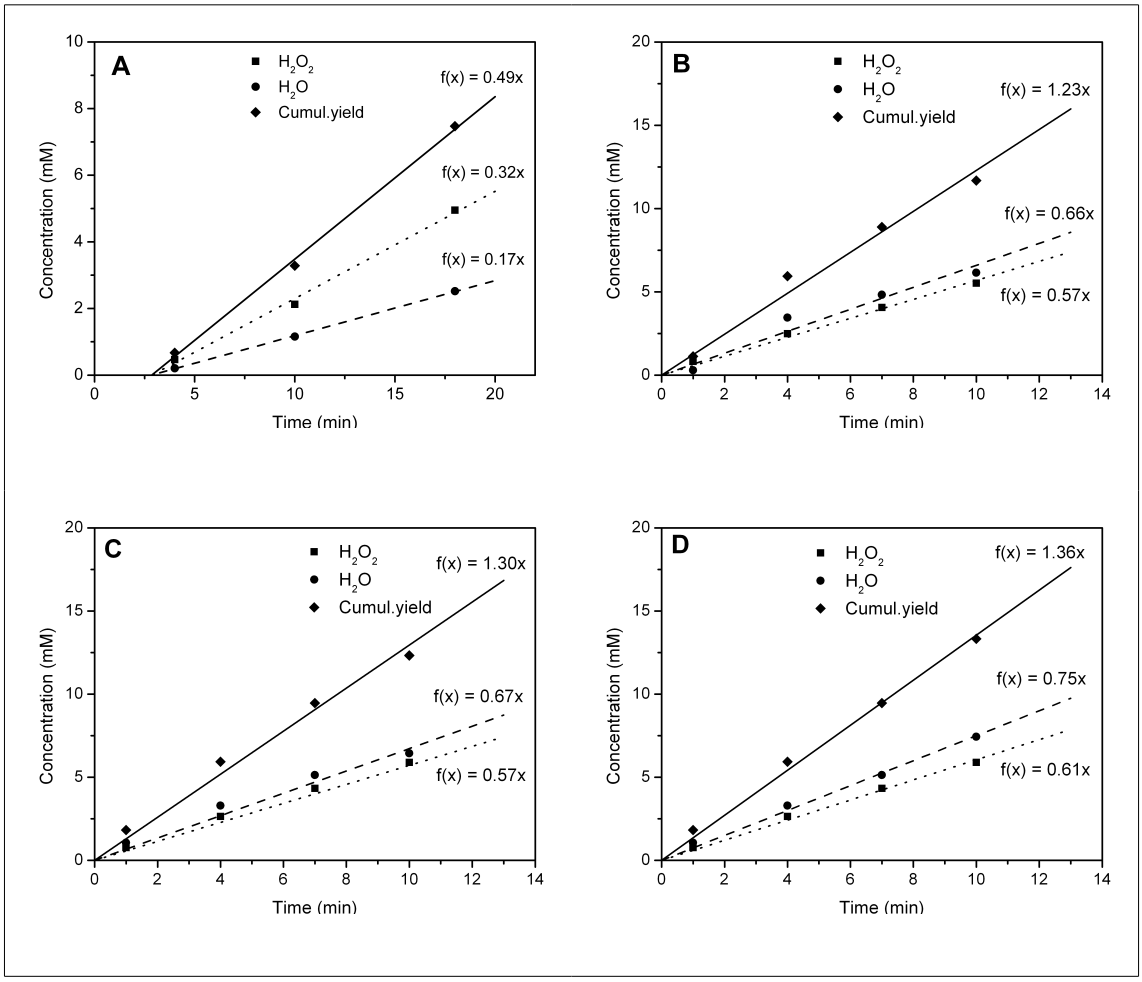

Figure 20: The evaluation of the rates of production of hydrogen peroxide (■), water (●) and the cumulative yield (♦) of 1PdK2621HpT (A), 1Pd025PtK2621HpT (B), 1Pd05PtK2621HpT (C), 1Pd1PtK2621HpT (D).

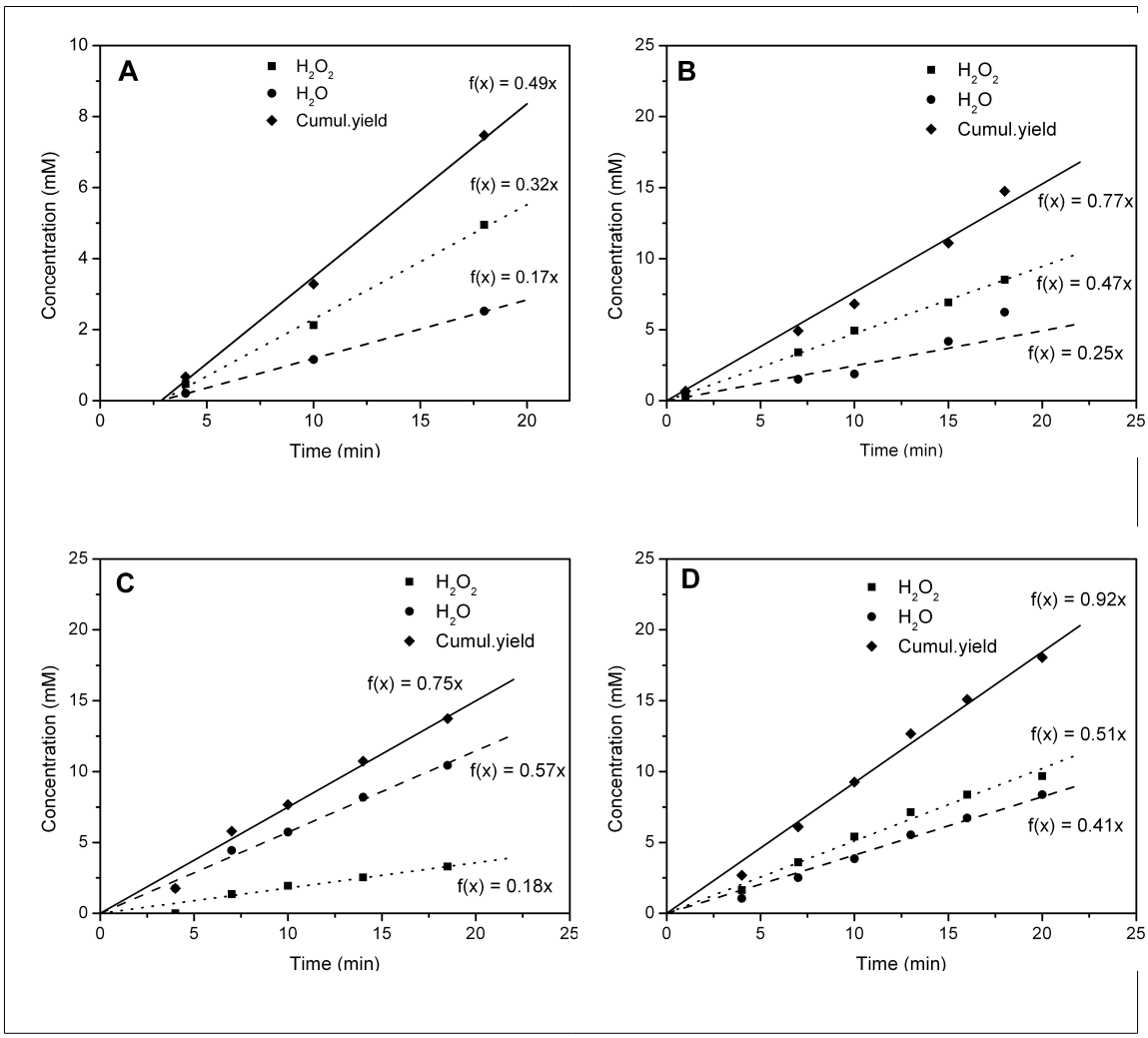

Figure 21: The evaluation of the rates of production of hydrogen peroxide (■), water (●) and the cumulative yield () of 1PdK2621HpT (A), 1Pd025AuK2621HpT (B), 1Pd05AuK2621HpT (C), 1Pd1AuK2621HpT (D).

Table 7: Initial performances of the bimetallic palladium-platinum catalysts supported on K2621.

Cat.	Employed metal amount[a]		Initial cumul. rate[b]	Initialcumul. productivity[c]		Initial H_2O_2 productivity[d]	Initial Selectivity[e]
	Pd	Pd+Pt		vs Pd	vs Pd+Pt		
1Pd K2621HpT	1.45	–	29.3	847	–	560	66
1Pd025Pt K2621HpT	1.44	1.64	73.8	2151	1891	875	46
1Pd0.5Pt K2621HpT	1.44	1.84	77.7	2267	1774	783	44
1Pd1Pt K2621HpT	1.42	2.2	81.3	2406	1553	694	45

a: $mol \cdot 10^5$; b: $mmol(H_2O_2+H_2O) \cdot dm^{-3} \cdot h^{-1}$; c: $mol_{(H2O2+H2O)} \cdot mol^{-1}_{(Pd+Pt)} \cdot h^{-1}$; d: $mol_{(H2O2)} \cdot mol^{-1}_{(Pd+Pt)} \cdot h^{-1}$; e: %.

Table 8: Initial performances of the bimetallic palladium-gold catalysts supported on K2621.

Cat.	Employed metal amount[a]		Initial cumul. rate[b]	Initial cumul. productivity[c]		Initial H_2O_2 productivity[d]	Initial Selectivity[e]
	Pd	Pd+Au		vs Pd	vs Pd+Au		
1Pd/ K2621HpT	1.45	–	29.3	847	–	560	66
1Pd0.25Au/ K2621HpT	1.43	1.63	45.9	1349	1184	614	62
1Pd0.5Au/ K2621HpT	1.42	1.81	45.1	1334	1047	249	24
1Pd1Au/ K2621HpT	1.42	2.19	55.4	1637	1062	588	55

a: $mol \cdot 10^5$; b: $mmol(H_2O_2+H_2O) \cdot dm^{-3} \cdot h^{-1}$; c: $mol_{(H2O2+H2O)} \cdot mol^{-1}_{(Pd+Au)} \cdot h^{-1}$; d: $mol_{(H2O2)} \cdot mol^{-1}_{(Pd+)} \cdot h^{-1}$; e: %.

The estimate of selectivity from the ratio of the rates show similar values for all the Pd/Pt catalysts, partially in agreement with the instant evaluation of selectivity, depicted in Figure 16. This last method overestimates the result of the 1Pd025PtK2621HpT sample, which produces a performance comparable with the other Pd-Pt materials.

The end of the first stage occurs at same time (about 60 min) for all the Pt-Pd catalysts and in the second stage the decrease of the selectivity for the bimetallic catalysts with time is never as high as in the case of the monometallic palladium catalyst (Figure 16).

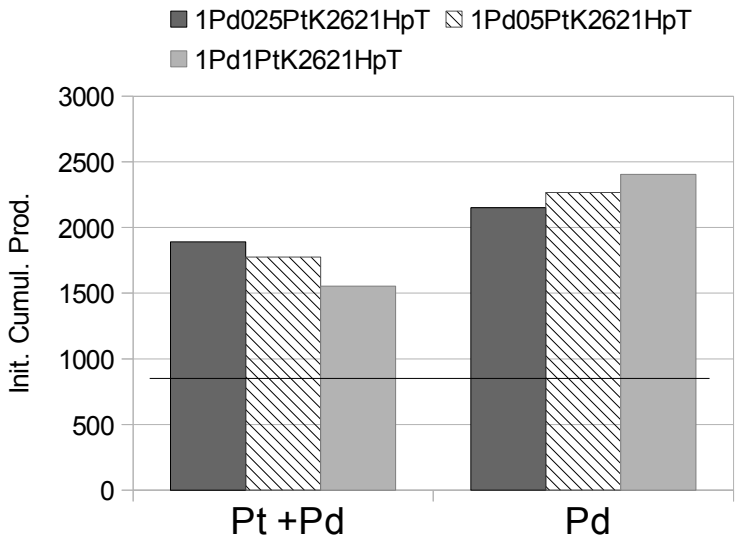

Figure 22: Initial cumulative productivity considering the contribute of only the Pd and the sum of Pd and Pt; the black line is the result of monometallic material, 1PdK2621HpT.

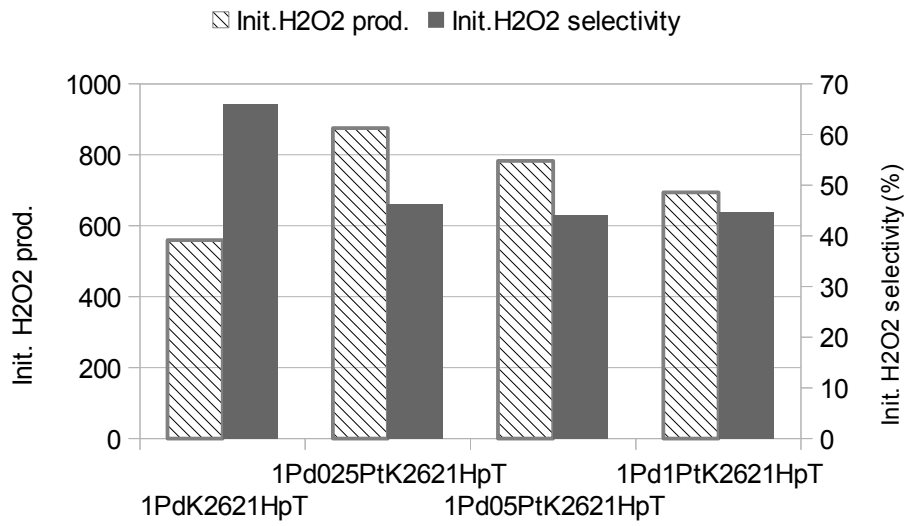

Figure 23: Initial performances of the library of catalysts

To summarize, the effects of the addition of platinum to the polymer-supported Pd-Pt catalyst seems to show that in the 0.25-1% w/w range of platinum amount, the catalyst seems to be more active, but less selective towards H_2O_2 than the monometallic one (Figure 23). All these results are very different compared with the library Pd/Pt treated with formaldehyde and, at the moment, these are not evidences to understand because the metal composition of the catalyst did not change the catalytic performance. These materials are already object of further investigations on the nature of nanostructured metal phase.

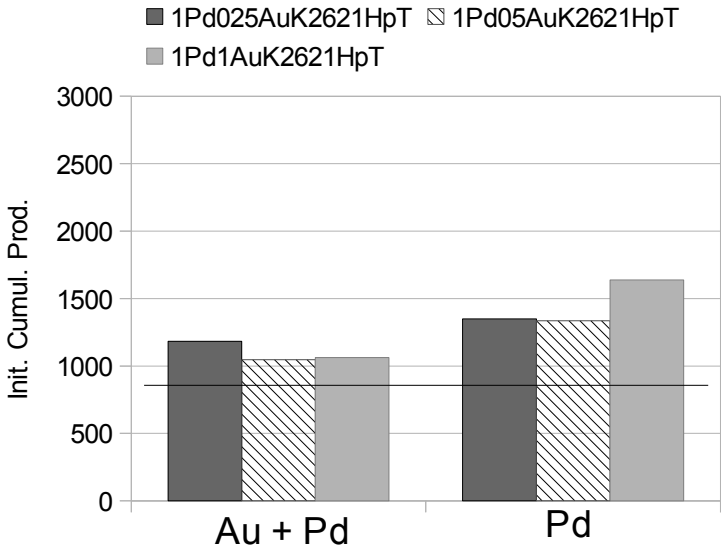

Figure 24: Initial cumulative productivity considering the contribute of only the Pd and the sum of Pd and Au; the black line is the result of monometallic material, 1PdK2621HpT.

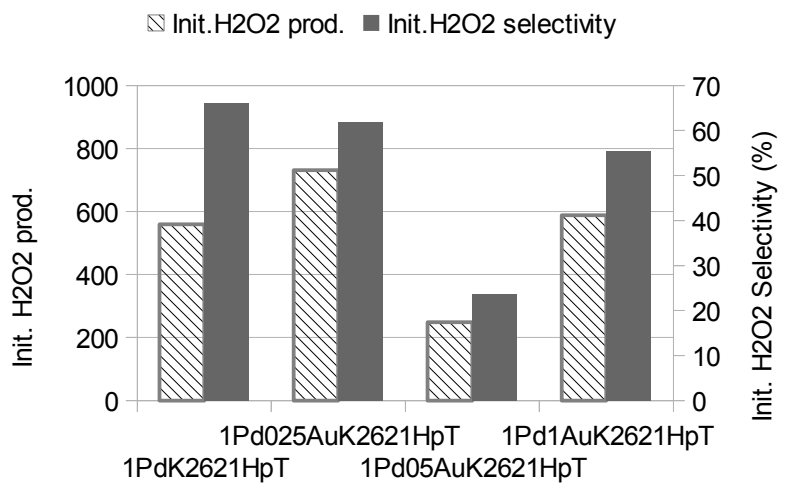

Figure 25: Initial performances of the library of catalysts

The library of Pd/Au nanocomposites show an apparent behaviour similarly to the Pd/Pt library, except for the 1Pd05AuK2621HpT sample. In this case the initial cumulative rates seem to be lower whereas the initial H_2O_2 rates are only slightly modified, increasing the selectivities of the catalysts. The use of this protocol of reduction (hydrogen under 60°C and 5 bar) carry out to the catalysts with an unique catalytic behaviour. Further investigations are already in progress.

CHAPTER 5

Synthesis and characterization of a mesoporous polydivinylbenzene and its catalytic role as the support for Pd nanoparticles in direct synthesis of H_2O_2

Crosslinked polymers are very versatile materials for applications under solid-liquid conditions, like heterogeneous catalysis, solid phase synthesis and separation processes. When the compatibility between the polymer matrix and the reactants is good, the solvation of the polymer chains (swelling) is potentially the most effective way to ensure the access of the reactants from the fluid phase to functional groups attached to the polymer. However, this is not always the case and polymeric supports possessing porosity stable even in dry state were developed to allow their application under conditions of poor or no swelling. For this purpose monomers are generally diluted with a suitable porogenic solvent before the polymerization [118]. The polymers turn out to have a heterogeneous morphology, in which pores are spaces between polymer particles clustered together, most often in multi-level hierarchical way, as the consequence of syneresis and phase separation, which occur during the polymerization under these conditions (see in Introduction, par. 3) [118].

To prevent the collapse of these pores during drying the polymer matrix must be rigid enough and this is obtained with an appropriate level of cross-linking. Essentially, the higher is the cross-linking, the higher level of dispersity of the solid phase can be achieved. The specific surface area as measured from nitrogen adsorption data using BET equation is a widely accepted parameter to assess the degree of dispersity. In styrene-co-divinylbenzene polymers the increase of the divinylbenzene (the cross-linker) content makes possible to achieve apparent specific surface areas as high as about 700 – 800 m^2/g. Even apparent surface areas as high as 2000 m^2/g can be obtained upon post-polymerization cross-linking. This can be accomplished, as proposed by Tsyurupa and Davankov [158][159], with the chloromethylation of the phenyl rings of

styrene-co-divinylbenzene polymers. This is followed by the Friedel-Craft reaction of the chloromethyl groups again with the phenyl rings, which eventually leads to the formation of cross-linking methylene bridges. An alternative way is the exploitation of the residual vinyl groups in Friedel-Craft alkylation of the phenyl rings [160][161], which can lead to the formation of further cross-links. Practically all these high-surface area polymers contain rather narrow pores, an appreciable proportion of which has characteristic dimensions smaller than 2 nm ("micropores" according IUPAC classification [162]).

Recently a Chinese research group described a novel approach to the synthesis of porous polymers based on a "solvothermal" synthetic method. A mixture of tetrahydrofuran and water was used as the porogenic solvent in the homo-polymerization of divinylbenzene, which was carried out at relatively high polymerization temperature (100°C) in an autoclave [163]. The polymers (poly-divinylbenzene, p-DVB) were obtained as monoliths. These rather unusual polymerization conditions lead to materials with very high specific surface area and unusually large pore size as compared with the surface area. The morphological properties of these novel polymers were so far evaluated only from nitrogen adsorption/desorption data obtained on dried samples. However, drying inevitably deforms the original polymer morphology created in contact with the porogenic liquid. New information on the morphology of these porous polymer in their swollen state can be obtained by inverse steric exclusion chromatography (ISEC) [164] and compared with the data on the dry materials obtained with conventional porosimetric techniques.

Synthesis and characterization

Poly-divinylbenzene resins synthesized with conventional procedures have very highly cross-linking degrees, no porosity in the dry state and a negligible swelling ability in all solvents [118]. The use of the solvothermal approach introduced by Feng-Shou and co-workers allows to prepare polymeric materials with new properties, in particular with an uncommon high porosity also in the dry state.

The preparation of the polymeric material pDVB1 was a replica of the material described in ref. [163]. The other samples were prepared to investigate the influence of some synthesis conditions on the morphology of the final material. The amount of divinylbenzene was double in the synthesis of pDVB2 and the autogenic pressure was

raised to 5 bar with nitrogen for the pDVB1b5 sample. The pDVB1 was also functionalized with sulfonic groups, in order to obtain the acidic ion-exchange resin pDVB1S. The latter is featured by a concentration of acid groups of 4.4 mmol/g, as estimated from the acid-base back titration.

These materials were characterized by SEM microscopy (Figure 1), FT-IR and solid ^{13}C-NMR spectroscopy (Figure 2 and 3, respectively, by courtesy of Prof. Grassi, Università of Salerno), thermal analysis (TGA and DSC, Figure 4), and compared with those of ref. [163][165]. Finally, these materials were accurately investigated with nitrogen adsorption/desorption measurements and ISEC technique to study the porosity in the dried and swollen state, respectively (by courtesy of Prof. K. Jeřábek, Institute of Chemical Process Fundamentals, Academy of Science of the Czech Republic)

The SEM images of the dry samples (Figure 1) show a very rough surface with an extensive presence of macropores in all the samples, confirming the results of BET analysis (see below). The morphology of the sulfonated sample appears unchanged at micrometer scale. However, pDVB1b5 appears to be considerably more compact and its pores narrower in comparison to pDVB1 and pDVB2, which show a very similar morphology.

Figure 2 shows the IR spectra of pDVB1, pDVB2 and pDVB1S samples. According to the literature [ref], absorption bands at 3000 cm^{-1}, in the 1380-1630 cm^{-1} and 700-1000 cm^{-1} ranges are expected in the spectra of pDVB1 and pDVB1S. They arise from C-H stretching, C-C stretching and C-H bending of aromatic rings, respectively. All of them are observed and in the case of pDVB1S sample strong bands at 1050-1210 cm^{-1} (S-O stretching of sulfonic groups) are detected too.

Figure 3 shows the solid state Carbon-13 nuclear magnetic resonance spectra (^{13}C-NMR) using cross-polarization (CP) and magic angle spinning (MAS) of pDVB1, pDVB2 and pDVB1b5.

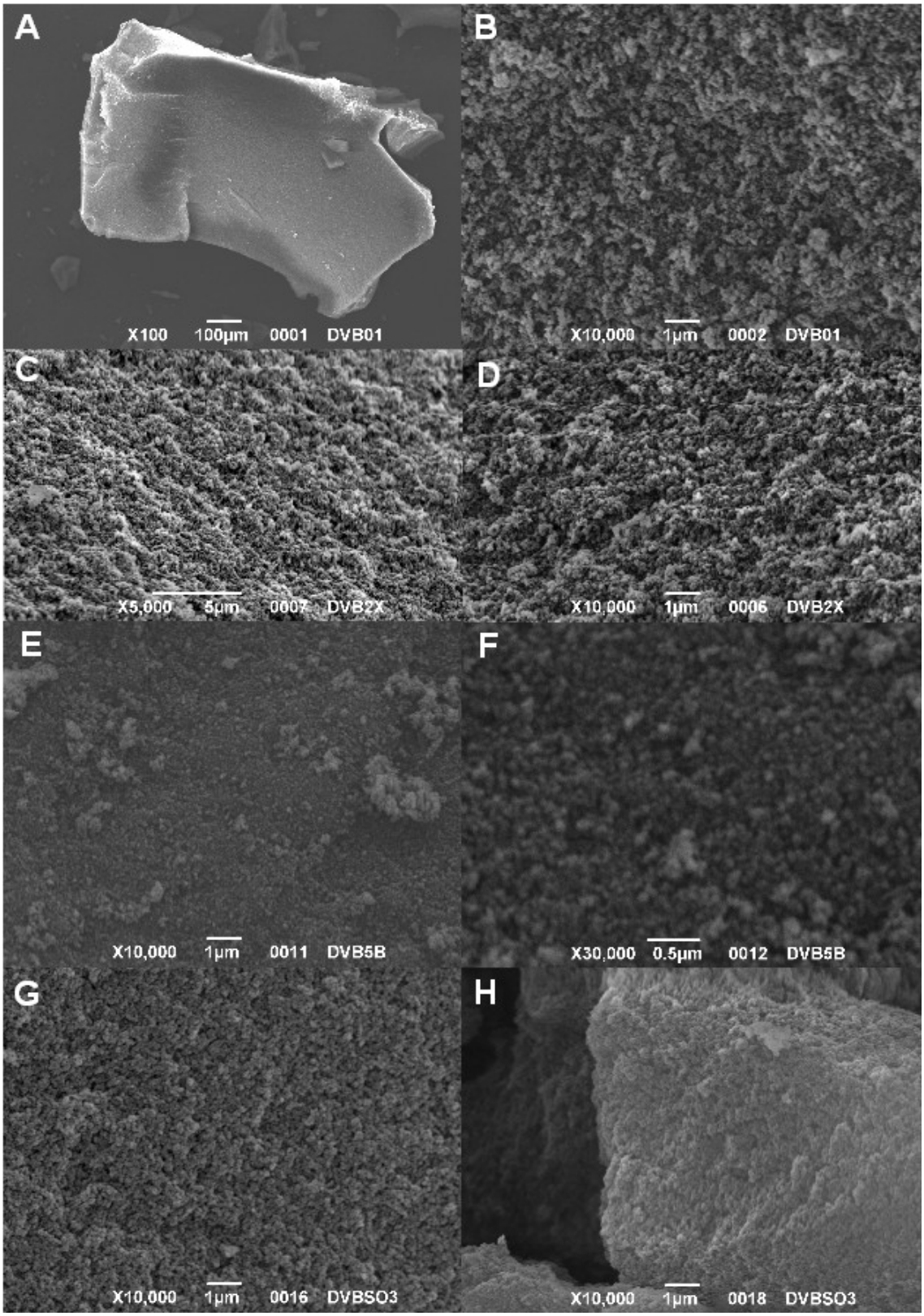

Figure 1: SEM images of pDVB1 (A, B), pDVB2 (C, D), pDVB1b5 (E, F) and pDVB1S (G, H) samples.

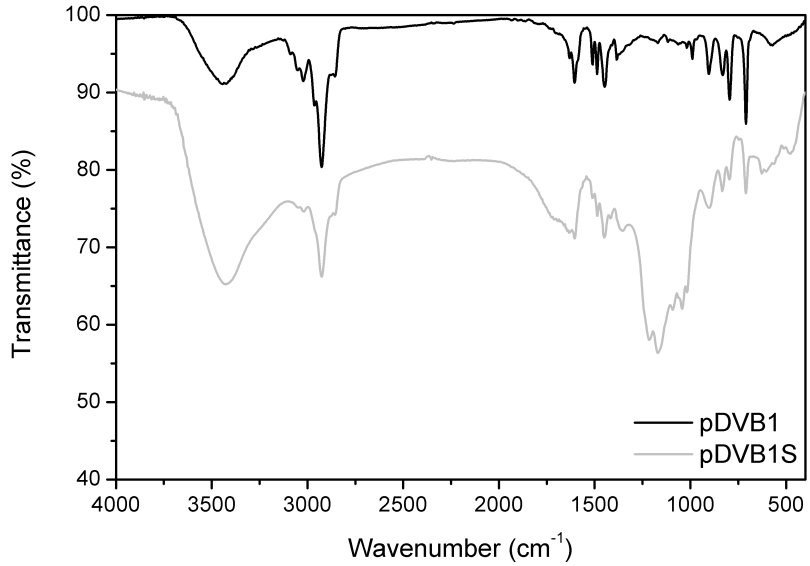

Figure 2: FTIR spectra relative to pDVB1 (black) and pDVB1S (grey) samples, respectively.

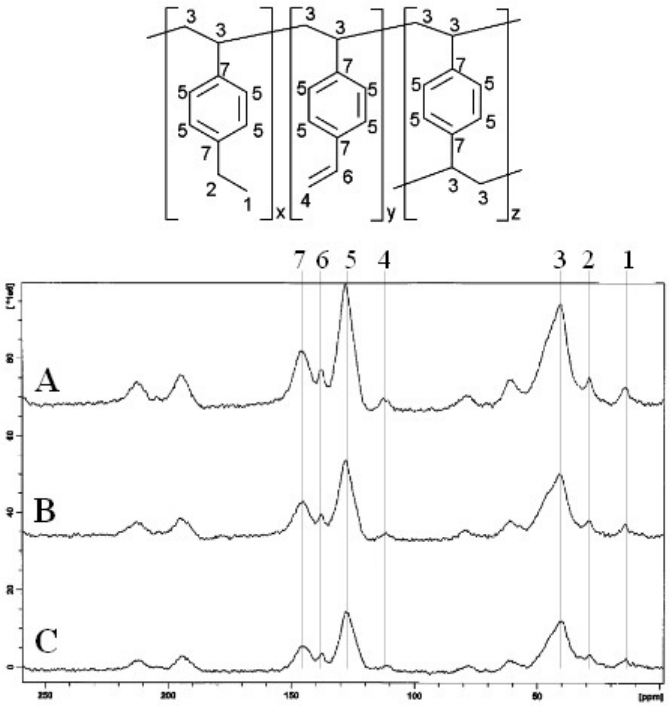

Figure 3: ^{13}C-NMR spectra of pDVB2 (A), pDVB1 (B) and pDVB1b5 (C).
(by courtesy of Prof. Grassi, Università of Salerno)

The strong signal at 41.2 ppm (signal 3 in Fig. 3) is attributed to the aliphatic carbon atoms of the polymer chains. The other two strong signals at around 127.4 and 144.9 ppm are attributed respectively to the unsubstituted and substituted carbon atoms of the aromatic rings (signals 5 and 7 in Fig. 3). The couple of low intensity signals at 111.4

and 137.5 ppm is associated to the carbon atoms of the residual vinyl groups (signals 4 and 6 in Fig. 3), resulting from the incomplete polymerization of divinylbenzene, and the couple of peaks at 14.2 and 29.3 ppm is associated to the aliphatic carbons of ethyl groups (signals 1 and 2 in Fig. 3). The latter signals are due to the presence of ethylvinylbenzene which is the second most abundant component of technical grade commercial divinylbenzene after divinylbenzene itself. The results of NMR analysis are different from those reported in ref. [165] and the signals due to the residual vinyl groups is more intense than reported in the literature. This likely indicates that the polymerization is not complete, but is sufficient to obtain a rigid polymer framework, which cannot collapse after drying. The presence of a remarkable number of unreacted vinyl groups is not necessarily a disadvantage. For instance they can be exploited for the post-functionalization of the materials, making poly-DVB potentially interesting as a scaffold for the preparation of a variety of functional polymers.

TG-DSC (Figure 4) curves show that pDVB1 has a remarkable thermal stability. The main weight loss was observed above 300°C. The slight weight loss of about 2.5 % between 240 and 270°C seems too high in temperature to be assigned to the removal of residues of solvents, but in the case of this strongly cross-linked polymer, it is possible that their release is retarded by the compactness of the polymer framework. The sulfonated resin (pDVB1S) exhibits weight losses in the temperature ranges 30-100, 100-375 and 300-650°C. In the first range, the weight loss is about 14 % and the temperature is compatible with the desorption of solvents (water and THF, corresponding to a). In the 100-375 °C a loss of about 35 % is observed. It correspond to the loss of ca 4.4 mmol/g of SO_3, due to the more or less complete desulfonation of the aromatic rings. In conventional sufonated co-polystyrene-divinylbenzene this ends at temperatures much lower than 375 °C. In this case also the release of SO_3 could be retarded by the compact polymer framework. In fact the weight loss rate is low until 350 °C and then it suddenly increases. This could be explained by the fact that the polymer framework starts to decompose, too, making the release of gases easier.

The dry-state morphological properties of all the materials determined from nitrogen adsorption/desorption data are shown in Table 1.

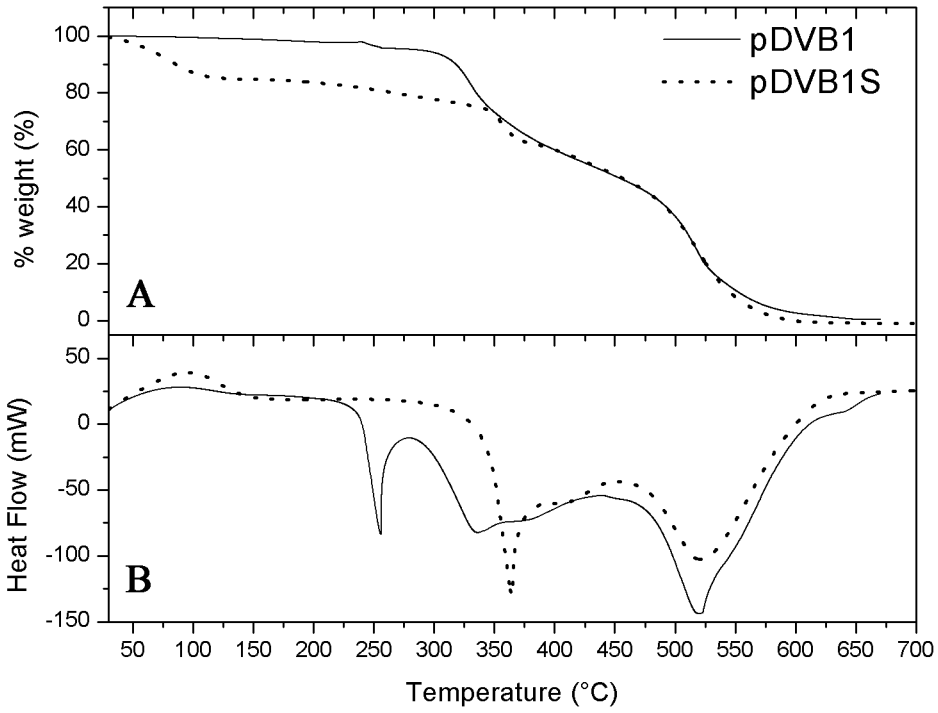

Figure 4: Thermogravimetric (A) and differential thermal analysis (B) relative to pDVB1 (solid line) and pDVB1S (dotted line) samples, respectively.

Table 1: Dry-state porosity of materials evaluated from N_2 adsorption/desorption measurements with the reference materials data reported in ref. [§163][§§ 165].

	Polymer	pDVB1	pDVB2	pDVB 1b5	pDVB1S	PDVB1 ref. [§]	PDVB1S ref. [§§]
1	Solvent-monomer molar ratio	20 : 1	10 : 1	20 : 1	20 : 1	16 : 1	16 : 1
2	BET surface area (m^2/g)	1096	899	912	697	702	377
3	External surface area from t-plot slope* (m^2/g)	1091	922	-	572	-	-
4	Micropore volume** (cm^3/g)	0.008	0.000	-	0.049	-	-
5	Cumulative surface area in pores < 4 nm** (m^2/g)	436	392	-	270	-	-
6	Total pore volume (cm^3/g)	2.07	1.89	-	1.22	1.35	0.61
7	Average pore size (nm)	7.5	8.4	7.5	7.0	22	21

*See Fig. 1; ** see text

(by courtesy of Prof. K. Jeřábek, Institute of Chemical Process Fundamentals, Academy of Science of the

Czech Republic)

All the materials prepared prepared under "solvothermal" conditions exhibit exceptionally high surface area as assessed by both BET measurement and t-plot analysis according to Harkins and Jura [166]. It is even larger than reported in [163][165]. However, the t-plot, in which the adsorbed amount of nitrogen is represented as the function of the adsorbed layer thickness, also shows a negligible presence of micropores (Fig. 5).

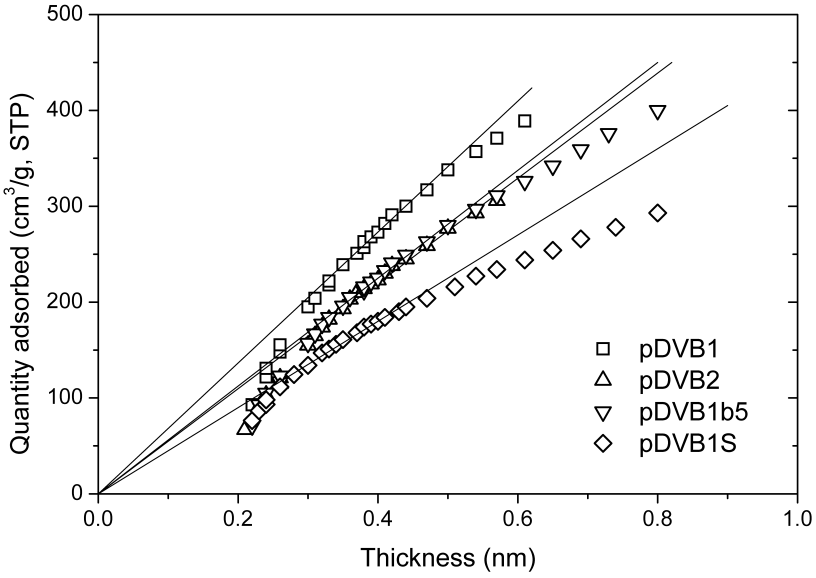

Figure 5: Amount of adsorbed nitrogen as a function of the statistical thickness of the adsorbed layer (t-plot; after Harkins and Jura [166]).

This is very different from what usually occurs in all the other porous polymer families reported so far, where high values of the specific surface area arise mainly from micropores. In these cases nitrogen is sorbed in micropores upon pore filling rather than multi-layer adsorption, so that BET surface area values can be used only as indicators of dispersity of the material. By contrast in the case of the p-DVB samples described herein the very high specific surface area was remarkably obtained in the absence of micropores.

Figure 6: Pore-size distribution of dried polymers evaluated from the desorption branch of N_2 sorption isotherm.

The pore size distributions of pDVB1 and pDVB2 (Fig. 6) exhibit distinct peak with maxima at 50 and 33 nm, respectively. The narrowest pores observed in the distribution curves are about 4 nm in diameter. On the one hand the cumulative specific surface areas of the pores larger than this (column 6, Table 1) are substantially lower than the total BET surface area. on the other hand, the t-plot analysis shows that no micropores are present. This implies that mesopores just larger than micropores ($d > 2$ nm), but smaller than 4 nm contribute very significantly to the extensive total specific surface area. This contribution amounts to 39% and 44 % for pDVB1 and pDVB2, respectively. A similar value is observed also for pDVB1S, showing that the sulfonation does not affect too much this range of pores although the morpholgy of the dry polymer undergoes appreciable changes under many respects (surface area, pore-size distribution, total pore volume, micropore volume, etc...).

Also the total volume of the pores in the dried polymers is very high for both pDVB1 and pDVB2 (2.07 and 1.89 cm^3/g, respectively) if compared with the values found in macroreticular or hypercrosslinked polymers, usually limited to only 0.3 - 0.5 cm^3/g [167]. However, the total pore volumes of pDVB1 and pDVB2 is much lower than the volume fraction of the porogenic solvents in the polymerization mixture and their ratio does not reflect the initial different dilution levels employed in the synthesis of pDVB1 and pDVB2. This can be very likely attributed to the collapse of the polymer morphology during drying. This seems to occur to a larger extent in pDVB1, obtained under relatively high dilution, and to a smaller extent for the probably more rugged polymer pDVB2.

Inverse Steric Exclusion Chromatography (ISEC) provides much more valuable information on the pore morphology as it was created in the presence of the solvent during the polymerization and before its collapse during drying. On the basis of this technique, which is applied to the polymers in their swollen state, the morphology of the material is represented as a set of discrete fractions of pores of simple geometry and a characteristic uniform size. In the present investigation the cylindrical pore model was applied to both “swollen-state” and “dry-state” characterization. The data on the "true" pore size in the polymers swollen in THF are collected in table 2 (why they are referred to as “true” will be clear later).

Table 2: ISEC characterization of PDVB, pDVB2, pDVB5b and pDVB1S presented using the cylindrical pore model.

Polymer	Solvent-monomer molar ratio	"True" pore diameter (nm)	"True" pore volume (cm^3/g)	"True" pore wall surface area* (m^2/g)
pDVB1	20 : 1	46	1.03	90
		82	6.47	316
		620	0.59	3
			8.09 (total)	409 (total)
pDVB2	10 : 1	21	1.13	213
		46	3.53	307
			4.63 (total)	520 (total)
pDVB1b5	20 : 1	46	0.49	65
		82	7.41	543
		620	0.70	6.6
			8.60 (total)	615 (total)
pDVB1S**	20 : 1	31	0.44	58
		41	4.36	428
		62	2.09	135
			6.89 (total)	621 (total)

*Computed as 4V/d; ** 0.2 M Na_2SO_4 aqueous solution as the mobile phase

(by courtesy of Prof. K. Jeřábek, Institute of Chemical Process Fundamentals, Academy of Science of the Czech Republic)

The total volume of the pores detected in the polymers swollen in THF was much higher than in the dry state and comparable with the volume of the porogenic solvents used for the polymer synthesis. In spite of this, the surface area of the "true" pores in the swollen state is not too different from the cumulative surface area of the dried materials in mesopores larger than 4 nm (column 6, Table 1) detected in the dry-state pore size distribution (Fig. 1). This suggests that these pores are likely only deformed, but not totally closed, upon drying. From the ISEC results the data the volume-weighed average diameter of the "true" pores can be calculated and it is 116 nm and 40 nm, 124 nm and 47 nm for pDVB1, pDVB2, pDVB1b5 and pDVB1S, respectively. These values are not far from those corresponding to the peaks observed in the size distribution of mesopores in the dry state and are so large that they cannot exist within within a swollen polymer gel. That's why they can be considered as "true" pores

and are referred to as such in this discussion.

On the other hand the comparison between the pore volumes at the dry and swollen state also suggests that the amount of porogenic solvents is too high to be completely accommodated only inside the "true" pore volume for pDVB1, pDVB2 and pDVB1b5. This indicates that the polymer matrix of these materials is able to swell in spite of their high divinylbenzene content. As the consequence, regions of swollen polymer gel are formed in these poly-divinylbenzene resins when they are in contact with THF. Swollen polymer gels are featured by the presence of pores with effective dimensions smaller than about 10 nm [168]. In these cases the swollen polymer morphology can be better modelled on the basis of the Ogston's model [169]. This model describes the pores within a swollen polymer gel as spaces among randomly oriented polymer chains, represented as rigid rods with high expectation ratios. In this case the polymer chain concentration (in units of length per unit volume of the gel) replaces that pore diameter as the characteristic parameter for the quantitative description of the "porosity" of the swollen gel. Also in this case relevant data can be obtained from ISEC experiments for all the samples (Table 3).

Table 3: Swollen-state porosity modelled as set of polymer gel fractions of various densities.

Polymer	Polymer chain concentration (nm/nm^3)	Polymer fraction volume (cm^3/g)
pDVB1	0.1	0
	0.2	0.06
	0.4	0.18
	0.8	0.20
	1.5	0.54
pDVB2	0.1	0.06
	0.2	0
	0.4	0
	0.8	0.30
	1.5	0.51
pDVB1b5	0.1	0.0
	0.2	0.0
	0.4	0.0

	0.8	0.0
	1.5	1.53
	0.1	0.0
	0.2	0.0
pDVB1S*	0.4	0.0
	0.8	0.0
	1.5	0.0

*0.2 M Na_2SO_4 in water as the mobile phase

(by courtesy of Prof. K. Jeřábek, Institute of Chemical Process Fundamentals, Academy of Science of the Czech Republic)

The porosity in the gel fraction of pDVB1 and pDVB2 in the swollen state was found to be very similar and little affected by the different monomer/porogen volume ratio. On the contrary, the pDVB1b5 sample seems to have a completely different gel fraction porosity in the swollen state. In gel-type resins the porosity of the swollen gel is generally temporary and vanishes upon drying the polymer, because of the collapse of the lightly cross-linked matrix. Also for pDVB1 and pDVB2 their gel fractions, which are detected in the swollen state (THF), are expected to collapse upon drying. However, as mentioned above, in these materials there must exist a significant amount of pores narrower than 4 nm, which are responsible for more almost half of the total surface area (row 3 and 4, Table 1). In view of the above these pores seem to be something like “wrinkles” on the pore walls or “chinks” intruding from the pore walls into the polymer mass, which are formed during the collapse of the swollen polymer gel structure. Therefore, the swollen gel fractions in these resins, differently from the case of the gel-type resins, do not seem to collapse completely upon drying, probably as the consequence of the high amount of DVB in the matrix, and the smallest mesopores ($d < 4$ nm) and the micropores indirectly observed in the dry state are the result of this situation.

In any case, the volume of the pores in the samples of p-DVB is far higher, both in dry and in the swollen state, to be compatible with the morphology of the most common porous polymer, where pores are spaces between aggregated polymer microparticles. Such a high porosity can be achieved only with a foam-like morphology, in which the polymeric matrix forms a continuous phase with thin walls surrounding bubble-like cavities. A similar geometry is known to occur in high internal phase emulsion polymers (poly-HIPE) (Figure 7), but in this case it is obtained under very

different conditions in comparison with the ones employed for p-DVB. In particular, the foam-like morphology is created from emulsion polymerization if the aqueous phase and the organic one, which contains the monomers, are emulsified in such a way that the latter is the continuous one and solidification produces a continuous polymer matrix [118]. Why the "hydrothermal" conditions used by Feng-Shou Xiao and co-workers [163] should induce an inverse situation is not known at the moment.

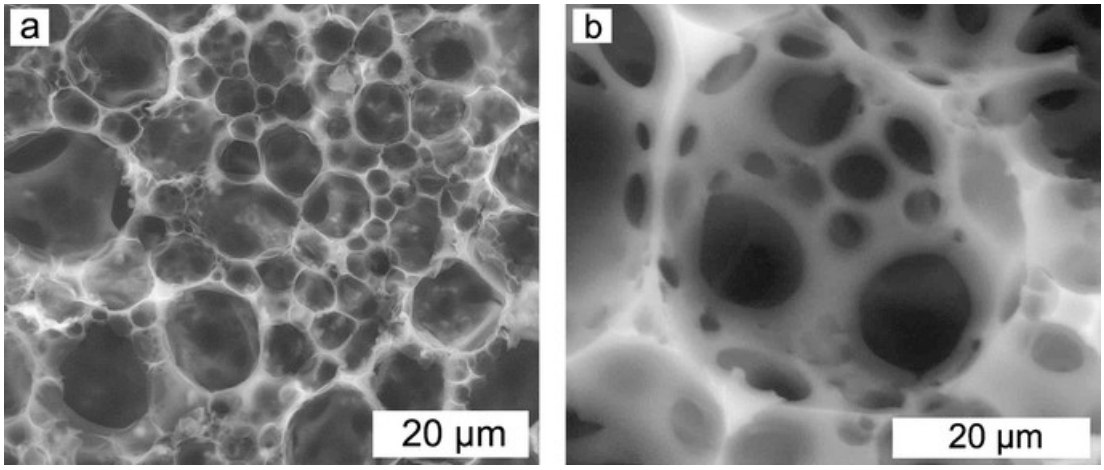

Figure 7: SEM images of poly-HIPE by ref. [170]

The sorption/swelling behaviour of these materials in liquids which are not applicable to ISEC, such as methanol, was also estimated by SAV (Specific Absorbed Volume) analysis, that is the gravimetric determination of solvent volume absorbed by the polymeric matrix (Table 4).

Table 4: SAV data expressed in ml/g of the pDVB based materials

SAV	Toluene	THF	Methanol	H_2O
pDVB1	8.4	8.7	8.2	0
pDVB2	5.8	4.8	4.0	0
pDVB1S	3.0	1.6	2.3	3.4

The polymers before sulfonation (pDVB1 and pDVB2) absorb appreciable amounts of any organic solvent, but not water. These amounts compare reasonably well with the "true" pore volume found with ISEC for both materials, i.e. with the volume of the porogenic agent employed in the polymerization. Therefore, also methanol seems able to restore the state of the polymer matrix as it was created during the synthesis. Water is

expectedly the liquid with the lowest compatibility with the highly hydrophobic frameworks of both pDVB1 and pDVB2. Not only water is not able to produce any swelling of the materials, but it is neither able to wet it and is totally excluded also from their permanent macro- and mesopores.

The introduction of the sulfonic groups into the poly-divinylbenzene matrix of pDVB1 makes the material much more hydrophilic. The concentration of the acid groups of pDVB1S is 4.4 mmol/g, as estimated with acid-base back titration. This value corresponds to the sulfonation of ca. 92 % of phenyl rings and compares well with the exchange capacity of fully sulfonated commercial macroreticular resin (for example 4.7 mmol/g of Amberlyst A15).

The sulfonated polymer pDVB1S shows a generally much lower sorption capacity. The SAV values of pDVB1S in different solvents are much closer to the BET pore volume (dry state) found for pDVB1 (2.09 $cm^3 \cdot g^{-1}$) than to the "true" pore volume estimated with ISEC. This suggests that in pDVB1S the framework cannot expand as much as before sulfonation, i.e. that sulfonation promotes an extensive collapse, though not complete, of the polymer framework. As the consequence only the pore existing at the dry state can be involved in sorption and no additional porosity can arise from swelling.

In aqueous environment the ISEC and the SAV data give conflicting indications. On the one hand, ISEC results suggest that in aqueous environment pDVB1S can expand practically to the same extent of pDVB1 in THF (the total volumes of the "true" pores are comparable and similar to the total volume of the porogenic agent employed in the polymerization). On the other hand, SAV in water is in agreement with the values found for all the other solvents and is compatible with only a partial swelling of the polymer matrix. The reason of this disagreement is not clear, but it could arise from the fact that for ISEC experiments 0.2 M Na_2SO_4 water solutions must be employed as the mobile phase. The presence of the electrolyte can remarkably influence the swelling behaviour of the polymers [171], so that the SAV value in pure water and the "true" pore volume in the sodium sulfate solution can be different.

This is consistent with the ISEC and BET analysis and indicates that the matrix partially collapses upon sulfonation. For instance, the "true" pore volume found with ISEC in water (actually a 0.2 M solution of sodium sulfate is used as the mobile phase in ISEC experiment, rather than water) was still comparable with the volume of the porogenic solvent used in the synthesis of pDVB1, but the pore diameters are clearly smaller and

the "true" pore surface area is roughly 50% higher than in the parent poly-divinylbenzene matrix. However, the presence of relatively high sulfonic functionality completely changes the swollen state of the material. The polymer fairly swells in both water and toluene whereas the absorbed volume value of methanol and THF is closer to the pore volume estimated by BET and this indicates that the material swells less. The remarkable swelling propriety of pDVB1S in water and also in toluene indicates the change of morphology after the sulfonation doesn't produce total loss of swelling with lipophilic solvents. This behaviour of polymeric matrix in the swollen state can be indicative about the level of hydrophylicity/lipophylicity in the inner surface of pores and this might had interesting consequences in the application of these materials as catalytic supports.

Synthesis and catalytic behaviour of 1 wt.% Pd supported on pDVB1S in the direct synthesis of H_2O_2

The preparation of the palladium-polymer nanocomposite was made according to [172]. After the ion-exchange between the cationic metal precursor and the sulfonic groups of pDVB1S, the material, already containing 1 wt.% palladium was treated aqueous formaldehyde to reduce the metal and generate its nanoparticles. The final material, 1Pd/pDVB1S, was tested in the DS reaction, with no addition of any promoter (selectivity enhancer). Its catalytic performance was compared with that of a commercial 1 wt.% Pd/C, as shown in Fig. 8 and Fig. 9.

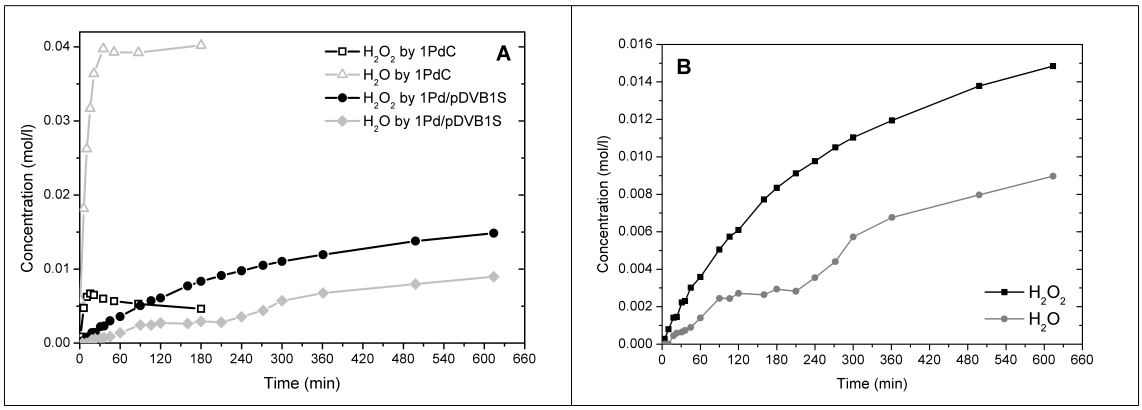

Figure 8: Formation of hydrogen peroxide and water with 1Pd/pDVB1S and 1 wt.% Pd/C as catalysts

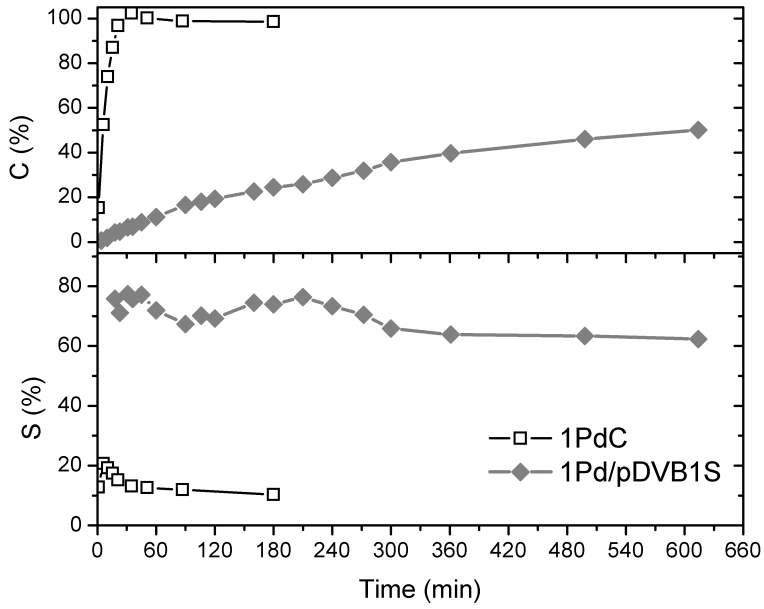

Figure 9: H_2 Conversion (%) and H_2O_2 selectivity (%) for 1Pd/pDVB1S and 1 wt.% Pd/C.

The two catalysts have completely different behaviors: 1 wt.% Pd/C, consumes

hydrogen (the limiting reagent) very quickly, which is totally converted in less of 30 minutes. however it produces mostly water, that is it is highly active, but poorly selective towards hydrogen peroxide. Selectivity tops at 20% after 20 minutes and later drops to slightly more than 10%.

1Pd/pDVB1S is indeed much less active: it takes 10 hours to achieve 50% hydrogen conversion. On the other hand, the selectivity in H_2O_2 is remarkably high and relatively stable during 10 hours of working time (from 80 to 70 %). The water concentration has a peculiar step-wise trend: it steadily increases for the first 90 minutes, but in the following two hours it remains more or less constant. Then it start to increase again. Differently from water, for H_2O_2 the concentration never stop to increases, although its build-up clearly slows down with time.

These data could be explained by product inhibition of the direct production of water. When the concentration of hydrogen peroxide is high enough, it starts to act as a poison blocking the sites responsible for the direct production of water. This implies a progressive increase of the concentration of hydrogen peroxide on the metal surface, which eventually favours its hydrogenation. As this reaction also produces water, the concentration of the side-product starts to increase again.

Why this occurs with pDVB1S as the support and not for carbon is not clear at the moment. It can be speculated that the meso- and microporous nature of the polymeric support favours the retention of hydrogen peroxide close to the metal surface, making site-blocking effective.

1Pd/pDVB1S was also characterized with TEM before and after the reaction (Figures 10 and 11).

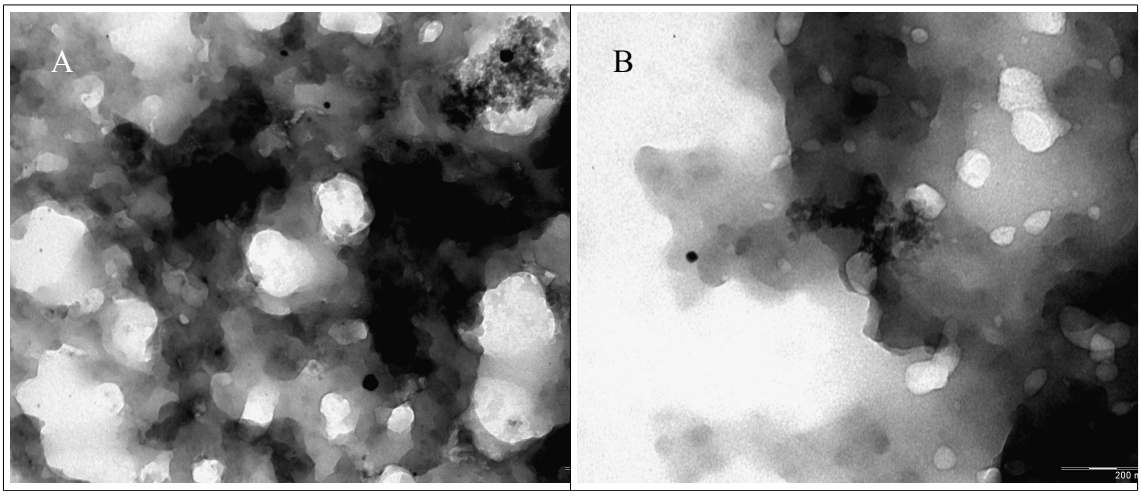

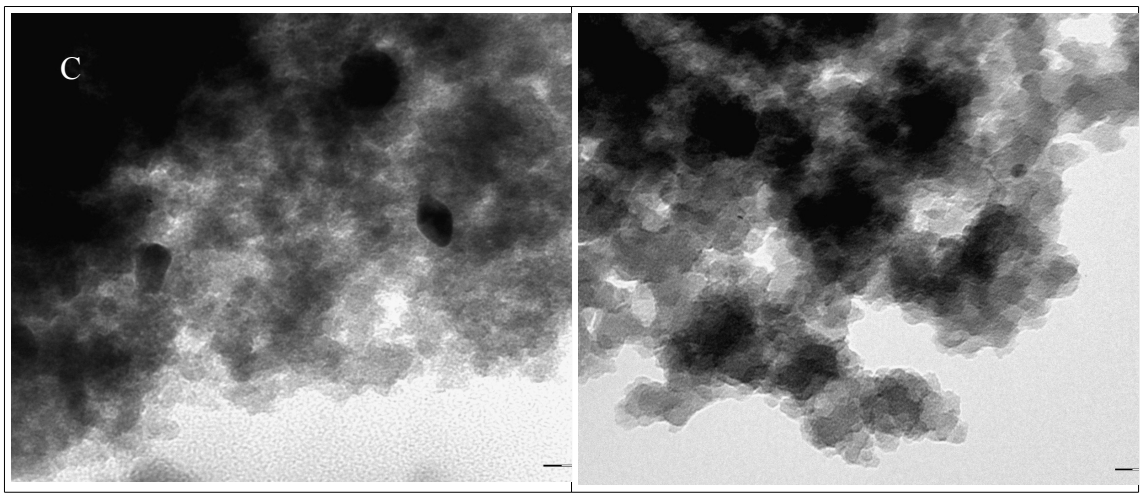

Figure 10: TEM images of fresh (A and B) and used (C e D) 1Pd/pDVB1S.
The scale bar is 200 nm and 50 nm for A-B and C-D images, respectively.

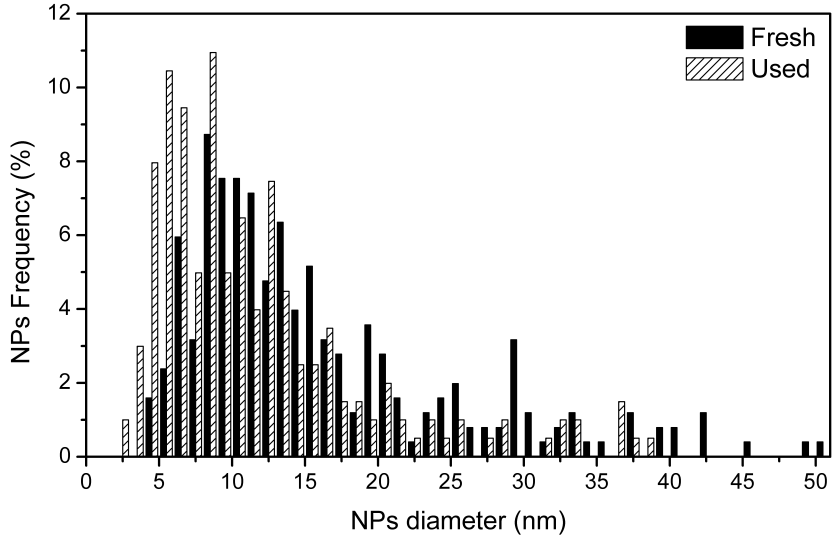

Figure 11: Size distribution of Pd nanoparticles for fresh and used 1Pd/pDVB1S sample.

As shown in Fig. 11, both the size distributions (more than 2o0 particles counted for each sample) have a broad Log-Normal shape, with centers at 12 and 9 nm for the fresh and the used catalyst, respectively. These results indicate that the support is not very effective in the size control of the Pd nanoparticles. However, they are much smaller than the narrowest pores detected in the water-swollen state of pDVB1S (31 nm), under which they were generated (aqueous formaldehyde as the reducing agent). The nanoparticles after the reaction are somawhat smaller than before. This could be due to some erosion of the metal (possibly associated to palladium leaching) or restructuring of the catalyst during the reaction.

The TEM images also shows other two features already discussed of the polymer matrix:

1) the presence of meso- and macropores as measured by ISEC analysis;
2) the experimental confirm that the matrix has a foam-like structure (Figure 10 A and B).

CHAPTER 5

CONCLUSION

The aim of the present research project is to develop new advanced materials for the direct synthesis of hydrogen peroxide.

As reported by previous works, the nanocomposites between noble metals and cross-linked polymers are effective catalysts for the direct synthesis. For investigate in detail some important parameters of synthesis, a set of monometallic catalysts obtained varying the metal precursor, the reductant and the reduction protocol was prepared and tested al fine di valutare the consequences on the catalytic performances. In particular, the use of tetraaminepalladium (II) sulfate as the metal precursor and the reductive treatment with hydrogen under mild condition seems to lead to a catalyst with noteworthy catalytic performances, specially a remarkable selectivity (70%).

Two sets of bimetallic Pt-Pd (Pd: 1.0; Pt: 0.1-1.0 %, w/w) and Au-Pd (Pd: 1.0; Au: 0.25-1.0 %, w/w) catalysts supported on the macroreticular ion-exchange resin Lewatit K2621 were prepared by simple ion-exchange in water of suitable precursors and reduction thereof with a refluxing aqueous solution of formaldehyde. It was found that the addition of a small amount of metal for both platinum (0.1 %) and gold (0.25 %) makes the catalysts less active and more selective than a 1 % palladium catalyst on K2621. However, the analysis of the initial rates of reaction shows that the effect of further addition is different for the two metals.

In the case of platinum the productivity in hydrogen peroxide increases and goes through a maximum at 0.5 % platinum. The activity, expressed as the rate of hydrogen consumption, fas a function of platinum content follows a similar volcano-shaped plot and changes are larger than in the case of H_2O_2 productivity. As the consequence the most active catalyst (1Pd05PtK2621F) is the most productive, but the least selective.

Moreover, the hydrogen consumption rate, fast in the first stage of the reaction, appreciably decreases at conversions which become lower and lower as the platinum content increases. The changes in the performance of these catalysts suggests that they undergo inhibition by one of the product, most likely hydrogen peroxide.

Also in the case of gold the activity increases with its amount in the catalysts, but in the investigated composition range no relative maximum was attained. The productivity of hydrogen peroxide is very little sensitive to the amount of gold and is not very different from one to another and from the monometallic palladium catalyst. Under this respect the Pt-Pd and the Au-Pd catalysts on K2621 are distinctly different. The characterization of the Au-Pd catalysts with TEM showed that the least selective catalyst is the most active, but the least selective. This suggests that the presence of large aggregates of nanoparticles is beneficial for the selectivity towards hydrogen peroxide, probably because aggregation occurs in the regions of highest surface energy so that the relative proportion of the most active sites is decreased.

An other set of bimetallic Pt-Pd (Pd: 1.0; Pt: 0.25-1.0 %, w/w) and Au-Pd (Pd: 1.0; Au: 0.25-1.0 %, w/w) catalysts, supported on K2621 and treated with hydrogen under 60°C and 5 bar, was tested in the direct synthesis of hydrogen peroxide. The results are very different compared with the previous set of bimetallic catalysts and, in particular, the catalytic performances seem to be quite independent from the composition of the nanostructured metal phase. Further investigations are in progress.

Finally, a deep investigation of a new class of porous cross-linked polymers and their use as support for a palladium catalyst is been object of attention. These materials are featured by high surface area both at the dry state and at swelling state. This non-commercial polymer has been investigated in details for the unique structure, which gives remarkable diffusion properties. This material exhibited simultaneously a modest activity and a remarkable (70 – 80%) and constant H_2O_2 selectivity: this unique features makes this catalyst a good candidate for a mechanistic study of the direct synthesis of hydrogen peroxide.

APPENDIX

Materials

Unless otherwise stated, all the reagents and the materials were used as recived from the supplier. A batch of Lewatit K2621 (sulfonated polystyrene-divinylbenzene macroreticular ion-exchange resin; exchange capacity = 1.92 mmol/g) was kindly provided by Lanxess. It was used after carefully washing with water and methanol.
Metal precursors for the preparation of monometallic catalysts were $[Pd(NH_3)_4]SO_4$, and $Pd(NO_3)_2$ (Alfa Aesar), $Pd(OAc)_2$ (Aldrich). $[Au(en)_2]Cl_3$ was synthesized according to ref. [173]; $[Pt(NH_3)_4](NO_3)_2$ was purchased from Alfa Aesar; sodium thiosulfate pentahydrate (99.5%). Potassium iodide, starch, concentrated sulphuric acid, 37% aqueous formaldehyde and methanol, sodium borohydride were purchased from Sigma-Aldrich. Tetrahydrofuran was supplied by Sigma-Aldrich and used freshly distilled. HPLC grade methanol (99.99%) from J.T. Baker; H_2, O_2 and CO_2 (99.999% mol/mol purity) from AGA. Methanol for Karl Fischer titration, Hydranal composite 2 and ammonium molybdate tetrahydrate were purchased from Fluka.
The reference catalyst is a standard 1 wt.% Pd/C reduced (Alfa Aesar), used as received.
A $K_2Cr_2O_7$ solution (0.7 mM) was used for the standardization of $Na_2S_2O_3$ solution.
Divinylbenzene (DVB, 80% technical reagent grade), tetrahydrofuran (THF), azobisisobutyronitrile (AIBN), sulfuric acid, 1,2-dichloroethane, 37% formaldehyde solution are used as received by Sigma-Aldrich without further purification.

Synthesis

Metalation of Pd materials

All the samples were prepared with a palladium loading of 1%. Whereas $[Pd(NH_3)_4]SO_4$ and $Pd(NO_3)_2$ are soluble in water, $Pd(OAc)_2$ are only soluble in less polar solvents and therefore two protocols of metalation are employed, the former in water, the latter in THF.

Typically 2 g of K2621 was suspended in 10 ml of distilled water for 2 hours and an aqueous solutions prepared from 0.188 mmol of palladium precursor was added (Table 2). The suspension was let to react overnight under mechanical stirring and then it was recovered by filtration and carefully washed with distilled water (3 x 10ml) on the filter. The second protocol, used for the metalation with $Pd(OAc)_2$, is similar to the former one, but replacing water for THF.

Table 1

Samples	Reductant	Metal Precursor	Pd found (wt. %)
1Pd/K2621H	H_2	$[Pd(NH_3)_4]SO_4$	1.01
1Pd/K2621N	H_2	$Pd(NO_3)_2$	1.03
1Pd/K2621A	H_2	$Pd(OAc)_2$	1.03
1Pd/K2621F	HCHO	$[Pd(NH_3)_4]SO_4$	1.00
1Pd/K2621M	MeOH	$[Pd(NH_3)_4]SO_4$	1.00
1Pd/K2621B	$NaBH_4$	$[Pd(NH_3)_4]SO_4$	1.02
1Pd/K2621HpT	H_2	$[Pd(NH_3)_4]SO_4$	1.02

Metalation of Pt-Pd materials

In typical experiment 2.0 g of K2621 were suspended in 10 ml of distilled water and left standing for 2 hours. Then aqueous solutions of $[Pd(NH_3)_4]SO_4$ and of $[Pt(NH_3)_4](NO_3)_2$. were added to the suspension. Whereas the total amount of the $[Pd(NH_3)_4]SO_4$ was always the same (0.188 mmol) and such to have 1 % (w/w) palladium in the final catalysts, the amount of $[Pt(NH_3)_4](NO_3)_2$ was varied from one experiment to the other in order to achieve 0.1, 0.25, 0.5 and 1 % (w/W) nominal Pt loadings (Table 2). After

adding the metal solutions the suspension was let to react overnight under mechanical stirring (swirling plate). After filtration it was carefully washed on the filter with distilled water (3 x 10ml). The mother liquor (filtrate and water from washing) was analyzed for the unreacted metal by ICP-MS. The residual amount of metals after the ion-exchange was less than 0.01 % (Pd) and 0.03% (Pt) of their respective starting amounts. The mass balance of the metals shows that their uptake was always complete and the experimental metal loading equal to the nominal one for each sample.

Table 2. Reagent amounts in the metalation of K2621 with Pd (fixed nominal loading: 1 %, w/w) and Pt.

Final catalyst	K2621 (g)	$[Pd(NH_3)_4]SO_4$ (g)	$[Pt(NH_3)_4](NO_3)_2$ (g)	Nominal Pt loading (%, w/w)	Pt/(Pd+Pt) (mol/mol)
1Pd/K2621	2.0173	0.0517	-	-	0
1Pd0.1Pt/K2621	1.2130	0.0314	0.0026	0.1	0.05
1Pd0.25Pt/K2621	1.0327	0.0267	0.0052	0.25	0.12
1Pd0.5Pt/K2621	1.0385	0.0258	0.0101	0.5	0.22
1Pd1Pt/K2621	1.0680	0.0271	0.0205	1	0.36

Metalation of Au-Pd materials

Before introducing the metals, K2621 was transformed into its neutral sodium form (K2621Na) by flowing a 0.1 M NaOH solution (ca. 200 ml in 4 h) though a glass column where 20 g of the resin had been packed into. K2621Na was recovered by vacuum filtration on a sintered silica filter, carefully washed with distilled water until neutral pH of the eluate and dried overnight in an oven at 110 °C. In typical experiment 2.0 g of K2621Na were suspended in 10 ml of distilled water and left standing for 2 hours. Then aqueous solutions of $[Pd(NH_3)_4]SO_4$ and of $[Au(en)_2]Cl_3$ (en = 1,2-diaminoethane) were added to the suspension. Whereas the total amount of the $[Pd(NH_3)_4]SO_4$ was always the same (0.188 mmol) and such to have 1 % (w/w) palladium in the final catalysts, the amount of $[Au(en)_2]Cl_3$ was varied from one experiment to the other in order to achieve 0.25, 0.5 and 1 % (w/w) nominal Au loadings (Table 3). After adding the metal solutions the suspension was let to react overnight under mechanical stirring (swirling plate). After filtration it was carefully washed on the filter with distilled water (3 x 10ml). The mother liquor (filtrate and

water from washing) was analyzed for the unreacted metal by ICP-MS. The residual amount of metals after the ion-exchange was less than 0.01 % (Pd) and 0.01% (Au) of their respective starting amounts. The mass balance of the metals shows that their uptake was always complete and the experimental metal loading equal to the nominal one for each sample.

Table 3: Au/Pd materials with a constant 1 wt.% Pd loading

Final catalyst	K2621 (g)	$[Pd(NH_3)_4]SO_4$ (g)	$[Au(en)_2]Cl_3$ (g)	Nominal Au loading (%, w/w)	Au/(Pd+Au) (mol/mol)
1Pd0.25Au/K2621	1.0104	0.0256	0.0060	0.25	0.12
1Pd0.5Au/K2621	1.0120	0.0260	0.0108	0.5	0.22
1Pd1Au/K2621	1.0026	0.0262	0.0222	1	0.36

Reduction with hydrogen

The solid was suspended with 50 ml of THF and undergone with a flux of H_2 at room temperature and pressure, for 5 hours (Table 1, coded with “H”). It was filtered and washed carefully with THF. The solid is dried in oven at 110°C overnight.

Reduction with formaldehyde

The beige material, already swollen in distilled water, was suspended in 50 ml of 37% aqueous formaldehyde solution and let to react under reflux condition for 5 hours (Table 1, F, coded with “F”). The black product was recovered by vacuum filtration and carefully washed on the filter with distilled water (3 x 10ml). The solid is dried in oven at 110°C overnight.

Reduction with methanol

The beige solid, already swollen in distilled water, was suspended in 20 ml of 1:1 methanol/water solution and let to react under reflux condition for 3 hours (Table 1, M, coded with “M”). The black product was recovered by vacuum filtration and carefully washed on the filter with distilled water (3 x 10ml). The solid is dried in oven at 110°C overnight.

Reduction with sodium borohydride

The material, already swollen in distilled water, was suspended in 10 ml of water. A solution of 0.58 g of $NaBH_4$ in 15 ml of water is added to the beige suspension under moderate stirring. The solid immediately acquires a dark grey colour. After two hours, the black product was recovered by vacuum filtration and carefully washed on the filter with distilled water (5 x 10ml).

The solid is dried in oven at 110°C overnight (Table 1, B, coded with "B").

Reduction in autoclave with 5 bars of hydrogen at 60°C

The beige solid was suspended with 50 ml of THF in the glass vessel, and, after purged three times with H_2, the autoclave was filled with hydrogen and the reduction was carried at 5 bar of hydrogen and 60°C for 5 hours. The black product was recovered by vacuum filtration and carefully washed on the filter with THF(3 x 10ml). The solid is dried in oven at 110°C overnight (Table 1, HpT, coded with "HpT").

Preparation of pDVB materials

Porous polymer monoliths were prepared as described by Feng-Shou and co-workers [163], under essentially identical conditions. In a typical experiment, a clear, homogeneous mixture of 6.0 g (6.6 cm^3) of divinylbenzene (tech. grade 80 %), 60 cm^3 of tetrahydrofurane (THF), 6 cm^3 of water and 165 mg of 2,2' azobis(2-methylpropionitrile) (AIBN) as the initiator (AIBN/DVB/H_2O/THF in molar ratio 0.025 : 1 : 9 : 20) was kept for 48 hours at 100 °C in a closed autoclave under autogenic pressure (2.1 bar). After cooling to room temperature a white, opaque cylinder of relatively soft polymer was removed and left to dry at room temperature for 10 days. The dried polymer turned out to be stiffer and more brittle. The polymer (referred to as pDVB1) was then ground with mortar and pestle and dried at 100 °C overnight. A second sample (referred to as pDVB2) was prepared with a double amount of DVB and AIBN as initiator, that is 12.0 g (13.2 cm^3) and 330 mg, respectively (AIBN/DVB/H_2O/THF in molar ratio 0.05 : 2 : 9 : 20), and under otherwise the same

conditions applied for pDVB2. A third sample, pDVB1b5 was obtained from the same composition of the reaction mixture of pDVB1 in a 100 ml glass autoclave under nitrogen at the final pressure of 5 bar (autogenic pressure = 2.1 bar).

The sulfonation of the materials was carried out as reported in [Irene Paolo art.]. Typically 1 g of dried pDVB1 is swollen in 6 ml of 1,2-dichloroethane and then 40 ml of 98% H_2SO_4 are slowly added. The mixture is heated at 80°C for three hours under moderate stirring. Finally the suspension is filtered and the solid is washed with 200 ml of water and 100 ml of THF. The brown product (hereafter coded as pDVB1S) is dried at 70°C for 3 days.

The metalation of pDVB1S with palladium (1 wt.%) was carried as reported [172]. Typically 1 g of pDVB1S is suspended in 20 ml of distilled water for 2 hours. An aqueous solutions of $[Pd(NH_3)_4]SO_4$ (25.8 mg in 5 ml of distilled water) is added. The suspension is let to react overnight under mechanical stirring and then the solid material is recovered by filtration and carefully washed with distilled water (3 x 10ml) on the filter. The material, which is still swollen by distilled water, is suspended in 50 ml of 37% aqueous formaldehyde solution and let to react at reflux temperature for 5 hours. The brown solid is recovered by vacuum filtration and carefully washed on the filter with distilled water (3 x 10ml). The solid is dried in oven at 110°C overnight.

Characterization methods

The determination of metal loading has been done with a ICP-MS instrument, PerkinElmer Sciex ICP Mass Spectrometer 6100 DRC Plus. The calibration solutions have been prepared from commercial single element solution for Pd, diluted into standard serial from 1 ppb to 100 ppb. Samples were prepared upon diluting the mother liquor from the metalation experiments (aqueous solutions of the unreacted metal precursor, see section 2.2) up to a known fixed volume.

Karl Fisher titrations were carried out with a Metrohm 736 GP Titrino with 728 stirrer.

TEM analysis were carried out with a JEOL JEM3010 operating at a 300 kV acceleration voltage and point- to-point resolution of 0.17 nm at Scherzer defocus. For TEM analysis, a few milligrams of the powdered samples were mixed with high purity isopropyl alcohol. The suspension was sonicated for 30 s in order to disrupt possible agglomerates. A 5 ml droplet of suspension was transferred onto holey-carbon film coated Cu grids and then put into the microscope.

The morphology of the dried polymers was assessed with nitrogen adsorption/desorption measurements at liquid nitrogen temperature using a computerized apparatus ASAP 2010 and the associated software (Micromeritics, USA). The size distribution of pore was estimated using the BHJ formula applied to the adsorption or desorption curve. The characterization of the swollen-state morphology of the materials was performed by ISEC with THF as the mobile phase using standard HPLC equipment connected to a computer data acquisition system programmed for precise evaluation of the elution volumes. The polymers were ground and sieved to separate the particles smaller than 0.2 mm. They were further purified from fines by decantation and packed inside a chromatographic column of known volume. Solutes with known effective molecular size (from 320 nm for polystyrene, MW = 10,000 KDa, down to 0.55 nm for n-pentane) were the eluted through the filled column where the polymer acted as the stationary phase. Their elution volumes were used as the basis for a mathematical treatment, based on an algorithm described in [168], which provided a description of the swollen polymer morphology. The latter was modeled as a set of discrete pore fractions, each characterized by single size of pores of simple geometrical shape. The cylindrical pore model was used in this case. Details on the experimental procedure and data treatment can be found elsewhere [164].

The acid exchange capacity of pDVB1S was estimated with an acid-base back titration

using 0.1 M NaOH and 0.1 M HCl standard solutions. Thermogravimetric analysis (TGA) and differential scanning calorimetry (DSC) were performed with a TA Instruments SDT 2960 equipped with a simultaneous TGA/DSC system.

SEM is a Jeol JSM- 6490.

Solid-state CP-MAS ^{13}CNMR spectra were recorded at room temperature on a Bruker AMX300 spectrometer (75.46 MHz for ^{13}C) by using high power decoupling and standard cross-polarization techniques. The magic angle was calibrated with KBr side bands and the samples were spun at 5 kHz in 4 mm diameter zirconia rotors equipped with Kel-F caps [130].

TEM analysis were carried out with a JEOL JEM3010 operating at a 300 kV acceleration voltage and point- to-point resolution of 0.17 nm at Scherzer defocus. Samples were prepared by suspending a few milligrams of the powdered materials in high purity isopropyl alcohol. After sonication (30 s) a small droplet (5 µl) of the suspension was transferred onto a holey-carbon film coated Cu grids, which was eventually introduced into the microscope.

Catalytic tests

EXPLOSION AND FIRE HAZARDS. H_2 and O_2 mixtures are explosive in the 4-96% range; in the presence of methanol the mixtures can be flammable even outside of the H_2/O_2 explosion range. For safe operations the H_2/O_2/MeOH mixtures must be kept outside of the explosion and flammability range upon dilution with an inert gas (CO_2 in this work). Deliberate or accidental failure in doing so can have very serious consequences.

Catalytic tests were carried out in a 600 mL stainless steel, tailor made batch reactor with a maximum working pressure of 200 bar., equipped aith a Heidolph RZR 2021 rotor (200-1000 rpm) and a K-type thermocouple, for continuous temperature detection. Further details can be found in ref. YY. [P. Biasi, N. Gemo, J. R. H. Carucci, K. Eranen, P. Canu, T. O. Salmi, *Ind. Eng. Chem. Res.* 51 (2012) 8903].

In a typical run after loading 0.15 g of the catalyst the reactor was closed, CO_2 (18.4 bar) and O_2 (6 bar) were fed directly from the cylinders at 25 °C and 420 ml (V_L) of methanol were fed with an HPLC pump. Then the stirrer and the HP-pump for the recirculation of the liquid phase were switched on (1000 rpm and 4 ml/min, respectively) After the stabilization of the pressure and the temperature (2 °C) both the stirrer and the pump were switched off and H_2 was fed until its partial pressure was set to the desired value. It was always the limiting reagent and its partial pressure was always below the explosion and flammability limit of the CO_2, O_2, H_2 and MeOH mixture. The number of moles of hydrogen introduced into the reactor ($n_{H2,0}$) was calculated from the volume of the head space of the filled reactor and the partial pressure of hydrogen in the gas phase. The amount of dissolved hydrogen, which was not known, was not taken into account. In the very moment when the delivery of the desired amount of H_2 was complete the stirrer and the pump were switched on again. This was taken as the reaction start-time. Unless otherwise stated the reaction was stopped after 3h. Portions of the liquid phase were periodically spilled from a side arm of the reactor for the analysis of hydrogen peroxide and water; their volume ($V_{spilled}$) was small enough to ensure that the amount of the catalyst per unit volume of the liquid phase was practically constant during the whole test. The concentration of the products in the spilled samples ([H_2O_2], [H_2O]'; mM) were determined by iodometric and Karl Fischer titrations. The initial concentration of water, $[H_2O]_0$, was also determined by the Karl Fischer titration of the solvent and used to calculate the concentration of water

effectively produced by the reaction, $[H_2O]$:

$[H_2O] = [H_2O]' - [H_2O]_0$

These data were used to monitor the progress of the reaction and its selectivity. The former was represented as the cumulative yield:

$CY(\%) = 100 \cdot \{[H_2O_2]_t + [H_2O_2]_t\} \cdot V_L / n_{H2,0}$

The number of hydrogen moles was determined from its partial pressure (the difference between the pressure values inside the reactor after and before the introduction of hydrogen) and the volume of the head space of the reactor filed with the liquid phase.

If not otherwise stated the selectivity towards hydrogen peroxide at time=*t* ($S_{H2O2,t}$) was calculated as:

$S(\%)_{H2O2,t} = 100 \cdot [H_2O_2]_t / \{[H_2O_2]_t + [H_2O_2]_t\}$

BIBLIOGRAPHY

[1] J.M. Campos-Martin, G. Blanck-Brieva, J.L.G. Fierro, *Angew. Chem. Int. Ed.*, 45 (2006) 6962

[2] G. Strukul in: G. Strukul (Ed.), *Catalytic oxidations with hydrogen peroxide as oxidant*, Kluver, Dordrecht, 1992, pp. 1-11

[3] G. Goor in: G. Strukul (Ed.), *Catalytic oxidations with hydrogen peroxide as oxidant*, Kluver, Dordrecht, 1992, pp. 13-43

[4] L.J. Thenard, *Ann. Chim. Phys.*, 8 (1818) 306

[5] H. Henkel, W. Weber, W., US Patent 1108752 (1914)

[6] C. Samanta, *Appl. Catal., A* 350 (2008) 133

[7] D.P. Dissanayake, J.H. Lunsford, *J. Catal.* 206 (2002) 173

[8] D.P. Dissanayake, J.H. Lunsford, *J. Catal.* 214 (2003) 113

[9] P. Landon,P.J. Collier, A.F. Carley, D. Chadwick, A.J. Papworth, A. Burrows,C.J. Kiely, G.J. Hutchings, *Phys. Chem. Chem. Phys.* 5 (2003) 1917

[10] G. Li, J. Edwards, A.F. Carley, G.J. Hutchings, *Catal. Commun.* 8 (2007) 247

[11] P.P. Olivera, E.M. Patrito, H. Sellers, *Surf. Sci.* 313 (1994) 25

[12] G. Li, J.K. Edwards, A.F. Carley, G.J. Hutchings, *Catal. Today* 114 (2006) 369

[13] J.K. Edwards, A. Thomas, A.F. Carley, A.A. Herzing, C.J. Kiely, G.J. Hutchings, *Green Chem.* 10 (2008) 388

[14] G. Li, J.K. Edwards, A.F. Carley, G.J. Hutchings, *Catal. Today* 122 (2007) 361

[15] Q. Liu, J.C. Bauer, R.E. Schaak, J.H. Lunsford, *Appl. Catal.*, A 339 (2008) 130

[16] S. Abate, S. Melada, G. Centi, S. Perathoner, F. Pinna, G. Strukul, *Catal. Today* 117 (2006) 193

[17] G. Bernardotto, F. Menegazzo, F. Pinna, M. Signoretto, G. Cruciani, G. Strukul, *Appl. Catal., A* 358 (2009) 129

[18] D. Hâncu, E.J. Beckman, *Green Chem.* 3 (2001) 80

[19] R. Burch, P.R. Ellis, *Appl. Catal., B* 42 (2003) 203

[20] Q. Liu, K. Gath, J. Bauer, R. Schaak, J. Lunsford, *Catal. Lett.* 132 (2009) 342

[21] S. Melada, R. Rioda, F. Menegazzo, F. Pinna, G. Strukul, *J. Catal.* 239 (2006) 422

[22] T. Ishihara, Y. Ohura, S. Yoshida, Y. Hata, H. Nishiguchi, Y. Takita, *Appl. Catal., A* 291 (2005) 215

[23] B.E. Solsona, J.K. Edwards, P. Landon, A.F. Carley, A.A. Herzing, C.J. Kiely, G.J. Hutchings, *J. Catal.* 236 (2005) 69

[24] B.E. Solsona, J.K. Edwards, P. Landon, A.F. Carley, A.A. Herzing, C.J. Kiely, G.J. Hutchings, *Chem. Mater.* 18 (2006) 2689

[25] J.K. Edwards, A.F. Carley, G.J. Hutchings, *J. Mater. Chem.* 15 (2005) 4595

[26] J.K. Edwards, A. Thomas, B.E. Solsona, P. Landon, A.F. Carley, G.J. Hutchings, *Catal. Today* 122 (2007) 397

[27] E. Ntainjua, J.K. Edwards, A.F. Carley, J.A. Lopez-Sanchez, J.A. Moulijn, A.A. Herzing, C.J. Kiely, G.J. Hutchings, *Green Chem.* 10 (2008) 1162

[28] F. Menegazzo, P. Burti, M. Signoretto, M. Manzoli, S. Vankova, F. Boccuzzi, F. Pinna, G. Strukul, *J. Catal.* 257 (2008) 369

[29] S. Park,S.-H. Baeck,T.J. Kim, Y.-M. Chung, S.-H. Oh, I.K. Song, *J. Mol. Catal. A: Chem.* 319 (2010) 98

[30] G. Blanco-Brieva, M.P. de Frutos Escrig, J.M. Campos-Martin, J.L.G. Fierro, *Green Chem.* 12 (2010) 1163

[31] G. Blanco-Brieva, E. Cano-Serrano, J.M. Campos-Martin, J.L.G. Fierro, *Chem. Commun.* (2004) 1184

[32] C. Burato, S. Campestrini, Yi-Fan Han, P. Canton, P. Centomo, B. Corain, *Appl. Catal., A* 358 (2009) 224

[33] C. Burato, P. Centomo, M. Rizzoli, A. Biffis, S. Campestrini, B. Corain, *Adv. Synth. Catal.* 348 (2006) 255

[34] T.A. Pospelova, N.I. Kobozev, E.N. Eremin, *Russ. J. Phys. Chem.* 35 (1961) 143

[35] V.R. Choudhary, C. Samanta, *J. Catal.* 238 (2006) 28

[36] Q. Liu, J.H. Lunsford, *J. Catal.* 239 (2006) 237

[37] V.R. Choudhary, C. Samanta, P. Jana, *Ind. Eng. Chem. Res.* 46 (2007) 3237

[38] E.N. Ntainjua, M. Piccinini, J. Pritchard, Q. He, J.K. Edwards, A.F. Carley, J.A. Moulijn, C.J. Kiely, G.J. Hutchings, *ChemCatChem* 1 (2009) 479

[39] E.N. Ntainjua, M. Piccinini, J. Pritchard, J.K. Edwards, A.F. Carley, J.A. Moulijn, G.J. Hutchings, *ChemSusChem* 2 (2009) 575

[40] Y.-F. Han, J.H. Lunsford, *J. Catal.* (2005) 230 313

[41] J.K. Edwards, B. Solsona, E.N. Ntainjua, A.F. Carley, A.A. Herzing, C.J. Kiely, G.J. Hutchings, *Science* 323 (2009) 1037

[42] J. Edwards, E.N. Ntainjua, A.F. Carley, A.A. Herzing, C.J. Kiely, G.J. Hutchings, *Angew. Chem. Int. Ed.* 48 (2009) 8512

[43] V.V. Krishnan, A.G. Dokoutchaev, M.E. Thompson, *J. Catal.* 196 (2000) 366

[44] M. Piccinini, J. K. Edwards, J. A. Moulijn, G. J. Hutchings, *Catal. Sci. Technol.*, 2 (2012) 1908

[45] S. Liu, J. Xiao, *J. Mol. Catal. A: Chem.* 270 (2007) 1

[46] J.R. Hyde, M. Poliakoff, *Chem. Commun.* 13 (2004) 1482

[47] D. Hâncu, J. Green, E.J. Beckman, *Acc. Chem. Res.* 35 (2002) 757

[48] Q. Chen, E.J. Beckman, *Green Chem.* 9 (2007) 802

[49] G. Schmdt, *Polyhedron,* 7 (1988) 2321

[50] L.N. Lewis, *Chem. Rev.*, 93 (1993) 2693

[51] N. Toshima, *Macromol. Symp.*, 105 (1996) 111

[52] A. Henglein, *Chem. Rev.*, 89 (1989) 1861

[53] H. Weller, *Angew. Chem.*, 105 (1993) 43

[54] H. Weller, *Adv. Mater.*, 5 (1993) 88

[55] C. Flyzanis, D.L. Richard, P. Roussignol, *Opt. Lett.*, 10 (1985) 511

[56] J.-O. Malm, G. Schmdt, B. Morun, *Angew. Chem. Int. Ed.*, 28 (1989) 778

[57] G.A. Braun, H. Bönnemann, *Chem. Eur. J.*, 3 (1997) 1200

[58] G.S. Bradley, D. De Caro, *Langmuir,* 13 (1997) 3067

[59] R.H. Holm, J.F. You, P. Papaefthymiou, *J. Am. Chem. Soc.*, 114 (1992) 2697

[60] H. Gleiter, *Adv. Mater.,* 4 (1992) 474

[61] H. Bönnemann, K. S. Nagabhushana by *Metal nanoclusters in catalysis and materials science: the issue of size control*, B. Corain, G. Schmid, N. Toshima eds., Elsevier, 2008, p. 21

[62] R.M. Richards,H. Bönnemann, *Eur. J. Inorg. Chem*., (2001) 2455

[63] G. Schmid by *Metal nanoclusters in catalysis and materials science: the issue of size control,* B. Corain, G. Schmid, N. Toshima eds., Elsevier, 2008, p. 10

[64] G. Schmid, *Chem. Rev.*, 92 (1992) 1709

[65] M. José-Yacamán, M. Marín-Almazo, J. A. Ascencio, *J. Mol. Catal. A: Chem.*,173 (2001) 61

[66] H. Bönnemann, K. S. Nagabhushana by *Metal nanoclusters in catalysis and materials science: the issue of size control*, B. Corain, G. Schmid, N. Toshima eds., Elsevier, 2008, p. 26

[67] G. Dyker, S. Hara, H. Shioyama, J. Walter, J. Heiermann, *J. Catal.*, 189 (2000) 449

[68] G. Schmid, *Endevour New Series,* 14 (1990) 172

[69] A. Lehnert, G. Schmdt, *Angew. Chem. Int. Ed.*, 28 (1989) 780

[70] A. Baiker, P.R. van Rheenen, D.G. Du, *J. Solid State Chem.*, 67 (1987) 151

[71] J. Hillier, J. Turkevich, P.C. Stevenson, *Discuss. Faraday Soc.,* 11 (1951) 55

[72] G. Kim, J. Turkevich, *Science*, 169 (1970) 873

[73] J. Turkevich, *Gold Bull.*, 18 (1985) 86

[74] J.H. El Nakat, I. G. Dance, K. J. Fisher, G. D. Willet, *Inorg. Chem.* 30 (1991) 2957

[75] R.G. Finke,C. Besson,E.E. Finney, *J. Am. Chem. Soc.*, 127 (2005) 8179

[76] G. Schmid, *Clusters and Colloids: From Theory to Application*, VCH, Weinheim, 1994

[77] N. Toshima, Y. Shiraishi, *Catalysis by metallic colloids,* in A. T. Hubbard (ed.) Encyclopedia of Surface and Colloid Science, Marcel Dekker, New York, 2002, 879

[78] T. Teranishi, N. Toshima, in A. Wieckowski, E. R. Savinova, C. G. Vayenas (eds.) *Catalysis and Electrocatalysis at Nanoparticle Surfaces*, Marcel Dekker Inc., New York, 2003

[79] N. Toshima, H. Yan, Y. Shiraishi by *Metal nanoclusters in catalysis and materials science: the issue of size control,* B. Corain, G. Schmid, N. Toshima eds., Elsevier, 2008, p. 49

[80] S. Luidold, H. Antrekowitsch, *JOM* 59 (2007) 20

[81] B. Zhou, S. Hermans, G.A. Somorjai by *Nanotechnology in catalysis,* D.J. Lockwood ed., Kluwer Academic, New York, 2004

[82] T. Yonezawa, N. Toshima, *New J. Chem.,* (1998) 1179

[83] M. Zecca, P. Centomo, B. Corain, by *Metal nanoclusters in catalysis and materials science: the issue of size control,* B. Corain, G. Schmid, N. Toshima eds., Elsevier, 2008, p. 201

[84] H. Hirai, Y. Nakao, N. Toshima, K. Adachi, *Chem. Lett.* 5 (1976) 905.

[85] G. Schmid editor. *Nanoparticles: From Theory to Application*. Wiley-VCH, Weinheim, 2004.

[86] B. Corain, G. Schmid, *Eur. J. Inorg. Chem.,* 17 (2003) 3081

[87] D. Astruc, F. Lu, J. R. Aranzaes, *Angew. Chem. Int. Ed.* 44 (2005) 7852

[88] H. Bönnemann, K. S. Nagabhushana, R. M. Richards, in: D. Astruc (ed.) *Nanoparticles and Catalysis,* Chapter 2, Wiley-VCH, Weinheim, 2007, 49

[89] J. Pollmann, J. Hormes, H. Bönnemann, W. Brijoux, R. Franke, J. Rothe, *J. Am. Chem. Soc.*, 118 (1996) 12090

[90] C. Amiens, B. Chaudret, O. Vidoni, K. Philippot, *Angew. Chem. Int. Ed.,* 38 (1999) 3736

[91] T. Motohiro, I. Konomi, S. Hyodo, *J. Catal.,* 192 (2000) 11

[92] M.M. Maye, W. Theng, *Langmuir,* 16 (2000) 490

[93] T. Sato, S. Yamada, Y. Niidome, A. Hori, *Chem. Lett.,* 29 (2000) 310

[94] Z. J. Jiang, C. Y. Liu, *J. Phys. Chem. B* 107 (2003) 12411

[95] W. Wang, S. A. Asher, *J. Am. Chem. Soc.* 123 (2001) 12528

[96] D. Wang, V. S. Maceira, L. M. L. Marzan, F. Caruso, *Adv. Mater.* 14 (2002) 908

[97] M. Králik, A. Biffis, *J. Mol. Catal. A: Chem.* 177 (2001) 113

[98] B. Corain, M. Zecca, K. Jeràbek, *J. Mol. Catal. A: Chem.* 177 (2001) 3.

[99] D. C. Sherrington, P. Hodge (ed.s) *Synthesis and Separations using Functional Polymer,* 1988, Wiley, New York

[100] Macromolecular Division-IUPAC Raccomendetion 2004

[101] Fruchtel J. S., Jung G., *Angew. Chem., Int. Ed.*, 35 (1996) 17

[102] Kempe M., Barany G. *J., Am. Chem. Soc.,* 118 (1996) 7083

[103] Hodge P., *Chem. Soc. Rev.* 26 (1997) 417

[104] Li W. H., Stover H. D. H., Hamielec A. E., *J. Polym. Sci., Part A, Polym. Chem*. 32 (1994) 2029

[105] Svec F., Frechet J. M. J., *Science* 273 (1996) 205

[106] Chambers T. K., Fritz J. S., *J. Chromatogr. A* 797 (1998) 139

[107] Lewandowski K., Svec F., Frechet J. M. J., *J. Appl. Polym. Sci.* 67 (1998) 597

[108] Takenaga M., Serizawa Y., Azechi Y., Ochiai A., Kosaka Y., Igarashi R., Mizushima Y., *J. Controlled Release* 52 (1998) 81

[109] Abraham S., Rajan P. K., Sreekumar K., *J. Appl. Polym. Sci.* 65 (1997) 1169

[110] Klampfl C. W., Buchberger W., Rieder G., Bonn G. K., *J. Chromatogr. A* 770 (1997) 23

[111] Steinke J. H. G., Sherrington D. C., Dunkin I. R., *Adv. Polym. Sci.* 23 (1995) 81

[112] Mayes A. G., Mosbach K., Trends *Anal. Chem.* 16 (1997) 321

[113] Sellergen B., Dauwe C., Schneider T., *Macromolecules* 30 (1997) 2454

[114] Chen G., Guan Z., Chen C.-T., Fu L., Sundaresan V., Arnold F. H., *Nature Biotech.* 15 (1997) 354

[115] W. O. Haag, D. D. Whitehurst (Mobil Oil) EP 1800371 (1969); W. O. Haag, D. D. Whitehurst (Mobil Oil) EP 1800379 (1969)

[116] J. Wöllner, W. Neier EP 1260454 (1969)

[117] J. Tulla-Puche, F. Albericio (ed.s) *The Power of Functional Resins in Organic Synthesis,* 2008, Wiley

[118] Guyot from D. C. Sherrington, P. Hodge (ed.s) *Synthesis and Separations using Functional Polymer* , 1988, Wiley, New York

[119] B. Corain, P. Centomo, S. Lora, M. Kralik *J. Mol. Cat. A. Chem,* 204-205 (2003) 755

[120] C. Burato, P. Centomo, G. Pace, M. Favaro, L. Prati, B. Corain, *J. Mol. Catal. A: Chem.,* 238 (2005) 26

[121] R. Arshady, *Adv. Mater.,* 3 (1991) 182

[122] A. Biffis, B. Corain, M. Zecca, C. Corvaja, K. Jerábek, *J. Am. Chem. Soc.,* 117 (1995) 1603

[123] H. Jacobelli, M. Bartholin, A. Guyot, *J. Appl. Polym. Sci.* 23 (1979) 927

[124] D. Horak, Z. Pelzbauer, M. Bleha, M. Ilavsky, F. Svec, J. Kalal, *J. Appl. Polym. Sci.* 26 (1981) 411

[125] A. Biffis, A. A. D'Archivio, K. Jerábek , G. Schmid, B. Corain, *Adv. Mater.*, 12 (2000) 1909

[126] B. Corain, A. A. D'Archivio, L. Galantini, S. Lora, A. A. Isse, F. Maran, *Chem. Eur. J.*, 13 (2007) 2392

[127] M. Zecca, A. Biffis, G. Palma, C. Corvaja, S. Lora, K. Jerábek, B. Corain, *Macromolecules,* 29 (1996) 4655

[128] B. Corain, M. Kralik, *J. Mol. Catal. A: Chem.*, 159 (2000) 153

[129] B. Corain, M. Zecca, K. Jerábek, *J. Mol. Catal. A: Chem.,* 177 (2001) 3

[130] F. Pozzar, A. Sassi, G. Pace, S. Lora, A. A. D'Archivio, K. Jerábek, A. Grassi, B. Corain, *Chem. Eur. J.*, 11 (2005) 7395

[131] B. Corain, M. Kralik, *J. Mol. Catal. A: Chem,* 173 (2001) 61

[132] A. Guyot, M. Bartholin, *Progr. Polym. Sci.* 8 (1982) 277

[133] Yuan H. G., Kalfas G., Ray W. H., *J. Macromol. Sci., Rev. Macromol. Chem. Phys.* C31 (1991) 215

[134] Vivaldo-Lima E., Wood P. E., Hamielec A. E., Penlidis A., *Ind. Eng. Chem. Res.* 36 (1997) 939

[135] Jo Y. D., Park K. S., Ahn J. H., Ihm S. K., *Eur. Polym. J.* 32 (1996) 967

[136] Coutinho F. M. B., Neves M. A. F. S., Dias M. L., *J. Appl. Polym. Sci.* 65 (1997) 1257

[137] Benda D., Snuparek J., Cermak V., *J. Dispersion. Sci. Technol.* 18 (1997) 115

[138] Wang G. J., Li M., Chen X. F., *J. Appl. Polym. Sci.* 65 (1997) 789

[139] Liang Y. C., Svec F., Frechet J. M. J., *J. Polym. Sci., Part A, Polym. Chem.* 35 (1997) 2631

[140] T. Brunelet, M. Bartholin, A. Guyot, *Angew. Makromol. Chem.*, 106 (1982) 79

[141] R. van Ballmos, D. H. Harris, J. S. Magee, in G. Ertl, H. Knotzinger, J. Weit. Kamp (Eds.), *Handbook of Heterogeneus Catalysis*, vol. 4, Wiley Weinheim (1997), 1955.

[142] B. Coq, in N. Russo, D.R. Salahub (Eds.), *Metal-Ligand Interaction in Chemistry, Physics and Biology*, vols. 49-71, Kluwer Academic Publishers, Dordrecht, 2000

[143] G. J. Hutchings, *Catal. Lett.,* 75 (2001) 1

[144] A. Biffis, R. Ricoveri, S. Campestrini, M. Kralik, K. Jerabek, B. Corain, *Chem. Eur. J.,* 8 (2002) 13.

[145] R. H. Grubbs, *CHEMTECH,* 7 (1977) 512

[146] *Metal nanoclusters in catalysis and materials science: the issue of size control,* B. Corain, G. Schmid, N. Toshima eds., Elsevier, 2008, p. 129

[147] B. Corain, K. Jerabek, P. Centomo, P. Canton, *Angew. Chem. Int. Ed.* 43 (2004) 959

[148] K. Jerábek, K.J. Shea, D.Y. Sasaki, G.J. Stoddard, *J. Polym. Sci., Part A, Polym. Chem*. 30 (1992) 605

[149] Lanxess Lewatit K2621 data sheet, http://www.lewatit.co.kr/pop/pdf/K%202621.pdf

[150] P. Centomo, M. Zecca, M. Kralik, D. Gasparovicova, K. Jerabek, P. Canton, B. Corain, *J. Mol. Catal. A: Chem.* 300 (2009) 48

[151] S. Simonato, Degree Thesis, 2009

[152] S. Abate, S. Perathoner, G. Centi, *Catalysis Today,* 179 (2012) 170

[153] Q. Liu, J.C. Bauer, R.E. Schaak, J.H. Lunsford, *Angew. Chem. Int. Ed.*, 47 (2008) 6221

[154] Q. Liu, J.H. Lunsford, *Appl. Catal. A: Gen.,* 314 (2006) 94

[155] T. Ishihara, R. Nakashima, Y. Nomura, *Catal. Sci. Technol.* (2012) 2, 961

[156] L.W. Gosser, US Patent 4,681,751 (1987);

L.W. Gosser, J.T. Schwartz, US Patent 4,772,485 (1988);

G. Paparatto, R. D'Aloisio, G. De Alberti, R. Buzzoni, US Patent 6,630,118 (2003)

[157] V.R. Choudhary, C. Samanta, T.V. Choudhary, *Appl. Catal. A: Gen.* 308 (2006) 128

[158] V. A. Davankov, M. P. Tsyurupa, *React. Polym.* 13, (1990) 27

[159] M. P. Tsyurupa, V. A. Davankov, *React. Func. Polym.* 53, (2002) 193

[160] K. Ando, T. Ito, H. Teshima, H. Kusano, in *Ion Exchange for Industry*, M. Streat Ed., Ellis Horwood Ltd., Chichester 1988, p.232

[161] K. Aleksieva, Jing Xu, Li min Wang, A. Sassi, Z. Pientka, Zhengpu Zhang, K. Jeřábek, *Polymer* 47 (2006) 6544

[162] J. Rouquerol, D. Avnir, C. W. Fairbridge, D. H. Everett, J. H. Haynes, N. Pernicone, J. D. F. Ramsay, kK S. W. Sing, K. K. Unger, *Pure & Appl. Chern.*, 66(8) (1994) 1739

[163] Y. Zhang, S. Wei, F. Liu, Y. Du, S. Liu, Y. Ji, T. Yokoi, T. Tatsumi, F.-S. Xiao, *Nano Today,* 4 (2009) 135

[164] K. Jeřábek: In: *Cross-Evaluation of Strategies in Size-Exclusion Chromatography,* ACS Symposium Series 635, p. 211 - 224, M. Potschka, P. L. Dubin (Eds.), American Chemical

Society, Washington 1996

[165] F. Liu, X. Meng,Y. Zhang,L.Ren,F. Nawaz, F. Xiao, *J. Catal.* 271 (2010) 52

[166] G. Jura, W.D. Harkins, *J. Amer. Chem. Soc*., 66 (1944) 1856

[167] M. P. Tsyurupa, V. A. Davankov, *React. Func. Polym.* 66 (2006) 768

[168] K. Jeřábek, *Anal. Chem*. 57 (1985) 1598

[169] A. G. Ogston, *Trans. Faraday Soc.* 54 (1958) 1754

[170] T. Gitli, M. S. Silverstein, *Soft Matter,* 4 (2008) 2475

[171] Centomo, P., Jeřábek, K., Canova, D., Zoleo, A., Maniero, A.L., Sassi, A., Canton, P., Corain, B., Zecca, M., *Chemistry - A European Journal* 18 (2012) 6632

[172] Centomo, P., Zecca, M., Kralik, M., Gasparovicova, D., Jerabek, K., Canton, P., Corain, B., 2009. *Journal of Molecular Catalysis A: Chemical* 300, 48

[173] B.P. Block, J.C. Bailar Jr, *J. Am. Chem. Soc*., 73 (1952) 4722